CNIC-00810
CNDC-0013
INDC(CPR)-031/L

COMMUNICATION OF NUCLEAR DATA PROGRESS

No. 10 (1993)

China Nuclear Information Center
Chinese Nuclear Data Center
Atomic Energy Press

CNIC-00810
CNDC-0013
INDC(CPR)-031 / L

COMMUNICATION OF NUCLEAR DATA PROGRESS

No. 10 (1993)

Chinese Nuclear Data Center

China Nuclear Information Centre

Atomic Energy Press

Beijing, December 1993

EDITORIAL NOTE

This is the tenth issue of *Communication of Nuclear Data Progress* (CNDP), in which the achievements in nuclear data field since the last year in China are carried. It includes the measurements of $^{54}Fe(d,\alpha)$, $^{56}Fe(d,2n)$, $^{58}Ni(d,\alpha)$, $(d,\alpha n)$, $(d,x)^{57}Ni$, $^{182\sim 184}W(d,2n)$, $^{186}W(d,p)$, $(d,2n)$ and $^{58}Ni(n,\alpha)$ reactions; theoretical calculations on $n+^{16}O$ and ^{197}Au, $^{10}B(n,n)$ and (n,n') reactions, channel theory of fission with diffusive dynamics; the evaluations of intermediate energy nuclear data for ^{56}Fe, ^{63}Cu, $^{65}Cu(p,n)$ monitor reactions, and of ^{180}Hf, $^{181}Ta(n,2n)$ reactions, revision on recommended data of ^{235}U and ^{238}U for CENDL–2; fission barrier parameters sublibrary, a PC software of EXFOR compilation, some reports on atomic and molecular data and covariance research.

We hope that our readers and colleagues will not spare their comments, in order to improve the publication.

Please write to Drs. Liu Tingjin and Zhuang Youxiang
Mailing Address : Chinese Nuclear Data Center
China Institute of Atomic Energy
P. O. BOX 275 (41), Beijing 102413
People's Republic of China
Telephone : 9357729 or 9357830
Telex : 222373 IAE CN
Facsimile : 86–1–935 7008
E–mail : CIAEDNP@VXIHEP.IHEP.CERN.CH

CONTENTS

I EXPERIMENTAL MEASUREMENT

The Absolute Cross Sections on W, Ni and Fe by Deuteron–Induced Reactions

Tao Zhenlan Zhu Fuying Wang Gongqing Qiu Huiyuan
Wang Zhenxia He Jianhua Cheng Xiaowu

(Institute of Nuclear Research, Academia Sinica, Shanghai)

Abstract

The excitation functions for $^{182\sim186}W(d,2n)^{182\sim186}Re$, $^{186}W(d,p)^{187}W$, $^{58}Ni(d,\alpha)^{56}Co$, $^{58}Ni(d,\alpha n)^{55}Co$, $^{58}Ni(d,x)^{57}Ni$, $^{54}Fe(d,\alpha)^{52}Mn$ and $^{56}Fe(d,2n)^{56}Co$ reactions were measured in incident energy bellow 16 MeV with activation method. Those of the reactions of (d,2n), (d,αn) and (d,α) were calculated by using the code Alice, the calculated results reproduce the shapes of the experimental excitation functions well but the absolute cross sections are overestimated by a factor of 0.14～0.73, respectively.

Introduction

The Fe, Ni, and W(d,2n), (d,p), (d,α) reaction cross sections are important for nuclear science and technology. In order to investigate the self–diffusion in single–crystal tungsten and the diffusion of rhenium tracer in single–crystal tungsten, R. L. Andelin[1] measured first the excitation functions of $^{184}W(d,p)^{185}W$, $^{186}W(d,p)^{187}W$ and $^{184}W(d,2n)^{184}Re$. But the cross section and the excitation functions of $^{182}W(d,2n)^{182}Re$, $^{183}W(d,2n)^{183}Re$ and $^{184}W(d,2n)^{184m}Re$ have not yet been reported so far except that of $^{186}W(d,2n)^{186}Re$[2, 3].

Only a few excitation functions for the production of radioactive nuclides by deuteron induced reaction on Ni[4, 5] and Fe[6～8] have been reported, and the

discrepancies among them are evidently beyond the experimental uncertainty.

In the present work, experimental excitation functions are reported for $^{182\sim186}W(d,2n)^{182\sim186}Re$, $^{186}W(d,p)^{187}W$, $^{58}Ni(d,\alpha)^{56}Co$, $^{58}Ni(d,\alpha n)^{55}Co$, $^{58}Ni(d,x)^{57}Ni$, $^{54}Fe(d,\alpha)^{52}Mn$, $^{56}Fe(d,2n)^{56}Co$ reactions. Both the present results and previously published data are compared with the calculated values.

1 Experimental Measurement

Present work was carried out by stack foils target activation method and Ge(Li) spectrometer to measure the activities of samples. The experimental arrangement and method were described in our previous work[9].

(1) Irradiation of the Samples

The targets with a purity of 99.9% were made by evaporation in vacuum on aluminium foils. Each aluminium foil (pure 99.99%) was punched to the same area (15 mm in dia.), cleaned and weighed on balance to within 10 μg before making targets. Using infra–red spectroscopy and Rutherford backscattering analysis, the tungsten target was determined to be WO_3 molecular structure. All others were atom structure. The natural targets (10mm in dia.) range in thickness from 5.24 to 6.78 mg / cm^2 for WO_3, 4.10 to 4.56 mg / cm^2 for Ni and 2.45 to 3.54 mg / cm^2 for Fe with accuracies of about 2%. Each face of targets was covered tightly with aluminium foil to avoid recoiling products escaping. The stacked natural targets were bombarded with deuteron beam at the Cyclotron of Shanghai Institute of Nuclear Research. The deuteron beam were focused in 6 mm dia. spots in the center of the targets.

The targets were interspaced with Al absorbers to degrade the energy of d^+ beam. The d^+ beam energies in each target foil in the stack were calculated from a range–energy relationship[10, 11].

The d^+ beam intensity was determined by a Faraday cup connected to a current integrator. The uncertainty of integrator was about 5%. The secondary electrons induced by deuteron bombarding targets and Faraday cup were suppressed by −300 V voltage bias.

An individual foil was bombarded and used as standard to obtain other absolute cross sections of the stacked foils.

(2) Detection of Activities

γ–ray energy and intensity measurements were performed with a Canberra closed–end type Ge(Li) detector whose efficiency compared with 3″ × 3″ NaI(Tl) is 23.6%. Ge(Li) detector was placed in a lead chamber (diameter 70 cm, height 75 cm, and wall thickness 10 cm). The present Ge(Li) spectrometer system consists of a Canberra 120 cm^3 coaxial Ge(Li) detector, a preamplifier,

a spectroscopy amplifier, a multichannel analyzer with 8192 channel ADC and a minicomputer. The energy resolution (FWHM) and the ratio peak / Compton of the spectrometer was 1.9 keV and 50, respectively, for the 1332 keV γ–ray of ^{60}Co. The absolute full energy peak efficiency of this spectrometer was calibrated in the energy range 60 ~ 3500 keV using the standard sources ^{115m}In and ^{60}Co, and multi–γ–ray calibration sources ^{75}Se, ^{152}Eu and ^{56}Co, which are very useful as a relative intensity calibration source. The distance between the detector case and the source was 10 cm or 0 cm. These sources were placed at the detector axes. Source spot is about 3 mm in dia. The radioactivity concentration of the solution of ^{115m}In and ^{60}Co was determined by means of the $4\pi\beta$ and $4\pi\beta-\gamma$ coincidence method, respectively. The coincidence measurement was performed with a box–type 4π counter and two 3″ × 3″ NaI(Tl) detectors. The reliability of this system was already established by the international intercomparison measurement. Careful measurements and data analyses were performed, especially for γ–ray absorption, the distance between the source and the detector case, the position of the source on the source holder plate, the dead time of the electronic systems, the effect of coincidence summing and of random summing and the background subtraction.

It is a general practice in γ–ray spectrometry to establish a calibration curve for the energy–dependent full–energy peak efficiency of the Ge(Li) detector system for interpolation purposes. In most cases an empirical or semi–empirical analytical function[12] is fitted to experimental calibration data by means of the least–squares method. The number of free parameters is kept small in order to achieve a reasonable computational speed and to avoid oscillations in the calibration curve if polynomials are used. The full–energy peak efficiency at a specific energy value is then calculated from the fit function and the associated standard deviation may be obtained from the parameters' covariance matrix by error propagation rules. The detector efficiency was obtained from the integrated peak counts of the calibration sources, the standard source strengths, the evaluated intensities[13, 14] per decays, the sum correction and the normalization factors given by cubic spline interpolation at various overlap points. The full–energy peak efficiencies of 33 spline knots are listed in table 1. The efficiency curves were determined with error of 1.0~2.3%.

γ–ray energies were determined by recording the spectra of radioactive foil simultaneously with the spectra from suitable calibration sources whose γ–ray energies are precisely known. High separation among the spectra was achieved by operating the 4096–channel pulse height analyzer at its maximum conversion and using a different ADC bias and gain for each run. Then the γ spectra

of individual foils were measured by multichannel pulse height analyzer and transferred directly to a computer for which a program was available to calculate characteristic peak area. The absolute detector efficiency and decay scheme data were used to convert peak intensity to the intensity of each radioisotope. These data together with foil thickness and beam current measurement were used to calculate the cross sections for all nuclides observed in each target.

2 Analysis and Treatment

The decay while the targets were irradiated was negligible for longer half–life of nucleus, then the cross section was simplified as follow:

$$\sigma = \frac{1.6 \times 10^{-19} M}{n Q N \chi \alpha \lambda \varepsilon p} A(t) e^{\lambda t} \quad (1)$$

where M is atomic or molecular mass; n is the number of target atom in a molecule; ε is the detector efficiency of γ–ray; Q is the integrated irradiation current in Coulomb; N is Avogadro number 6.0225×10^{23} molecules per gram–molecule; χ is the weight of target material in mg / cm^2; α is the isotopic abundance of the isotope concerned; λ is the decay constant of species; p is the branch ratio of the characteristic γ–ray per disintegration; $A(t)$ is activities counts measured at a time t after termination of the bombardment.

The following cross section formula were used for shorter half–life of the species

$$\sigma = \frac{M A(t)}{N \chi \alpha \lambda \varepsilon p} \left[\sum_i \frac{Q_i}{1.6 \times 10^{-19}} e^{-\lambda (t - t_i)} \right]^{-1} \quad (2)$$

in which t_i is the time interval from ith end of the bombardment to the measurement. Q_i is the integrated beam current of ith in Coulomb. All the measurements described above were repeated.

The uncertainties of absolute cross sections are estimated as follows: 5% for beam current measurement uncertainty, 1.0～3.0% for the absolute detector efficiency uncertainty, 2% for the target uniformity and as 1～8% for the statistical error of activity measurements, depending on the specific radionuclide.

3 Results and Discussion

The characteristic γ–ray energies of active nuclides were selected carefully. The identifications of active nuclides were based on the half–lives and characteristic radiations. The data of active nuclides produced on W+d, Ni+d and Fe+d reactions are taken from Ref. [15]. The results of the absolute cross section for W+d, Ni+d and Fe+d reactions are listed in tables 2～4 and shown in Figs. 1～11, respectively.

The measurements of ^{189}Re and ^{184}Re were started after about 174 days of the irradiation end. Although both ^{184m}Re and ^{184m}Re emitted 0.792 MeV γ–ray energy, according to the calculation, the γ–ray energy of ^{184m}Re was much smaller than ^{184}Re's so that influence of ^{184m}Re in 0.792 MeV γ–ray energy was negligible. ^{184}Re, ^{189}Re and ^{182}Re were also produced by W(d,n) and W(d,3n) at the end of lower and higher incident energies, respectively. The contribution of (d,n), (d,3n) reactions were subtracted with the cross sections obtained from semi–empirical approach method[16].

The experimental excitation functions were compared with calculations based on the theory of the compound nucleus in statistical equilibrium and pre–equilibrium reactions. By way of the code Alice[17] the excitation functions are calculated in 0.5 MeV energy step up to 16 MeV. The choice of the parameters used in the calculation are made as follows. The evaporation calculations were performed according to Weisskopf and Ewing[18]. The nuclear masses are calculated from the Meyers and Swiatecki mass formula[19], including shell corrections and pairing effects. The level density parameters are taken from the work of Chatterjee et al.[20] according to the renormalized Fermi gas model. The inverse cross sections are calculated by using the optical model subroutine of Alice. For the pre–equilibrium reactions the hybrid model option[21, 22] is chosen. The mean free path multiplier k introduced by Blann[21] is a free parameter in Alice. In our calculation $k = 1$ is taken, as is suggested in Refs. [21, 23]. Shown in Figs. 2, 4, 5～8, 10 and 11 are the calculated results for $^{182\sim186}$W(d,2n)$^{182\sim186}$Re, ^{58}Ni(d,α)^{56}Co, ^{58}Ni(d,2n)^{55}Co, ^{54}Fe(d,α)^{52}Mn and ^{56}Fe(d,2n)^{56}Co. They are in good agreement with the experimental data by a normalization factor of 0.14～0.73.

Pure evaporation calculations are also performed for $^{182\sim186}$W(d,2n)$^{182\sim186}$Re and shown together with the Alice calculations in Fig. 2 and 4～6.

Generally the calculations including the pre–equilibrium reactions reproduce the experimental excitation functions better than that of the pure equilibrium. It means that even in the energy range below 20 MeV it is still necessary to take into account the pre–equilibrium contributions for some reactions such as $^{182, 184}$W(d,2n).

The authors would like to thank Yan Cifu and Zhang Xin for preparing some of samples and drawing.

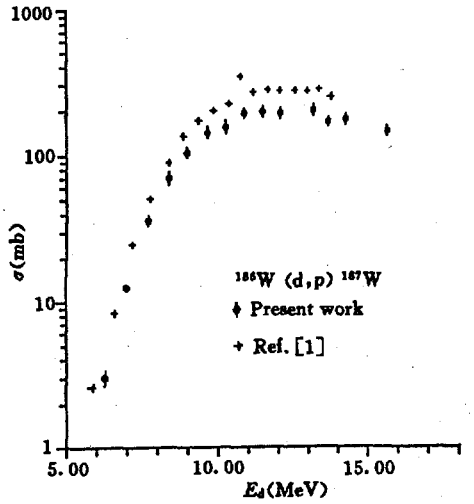

Fig. 1 The cross section of the reaction $^{186}W(d,p)^{187}W$

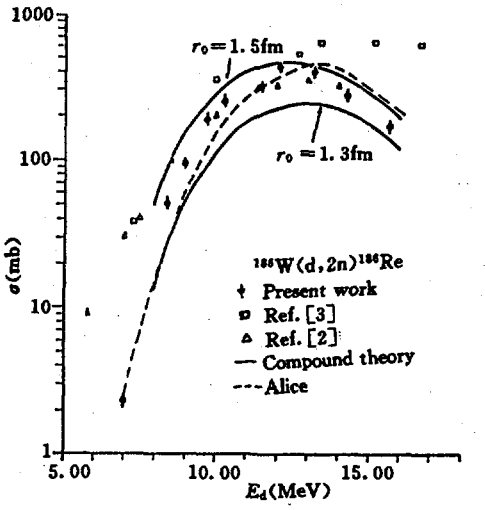

Fig. 2 The cross section of the reaction $^{186}W(d,2n)^{186}Re$

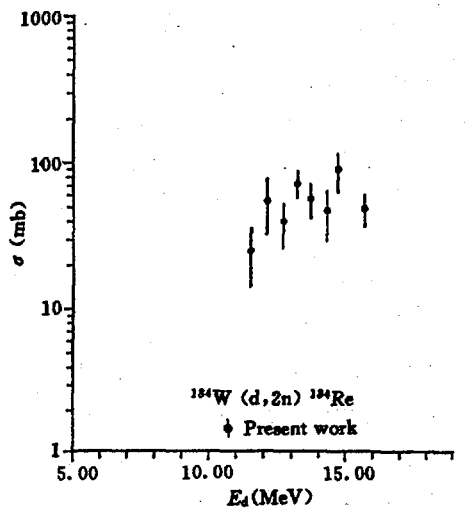

Fig. 3 The cross section of the reaction $^{184}W(d,2n)^{184m}Re$

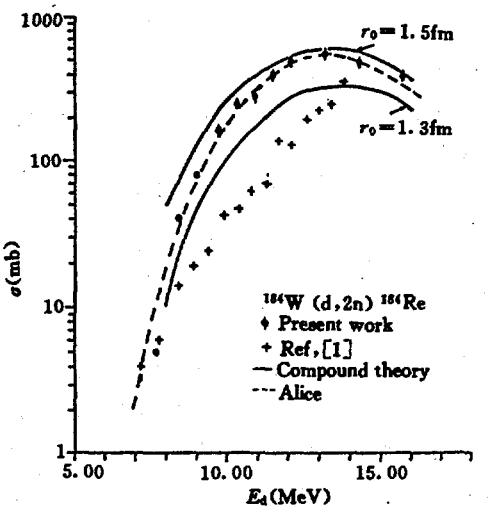

Fig. 4 The cross section of the reaction $^{184}W(d,2n)^{184}Re$

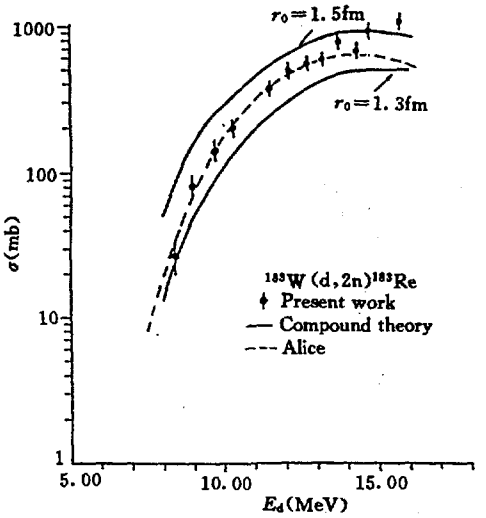

Fig. 5 The cross section of the reaction $^{183}W(d,2n)^{183}Re$

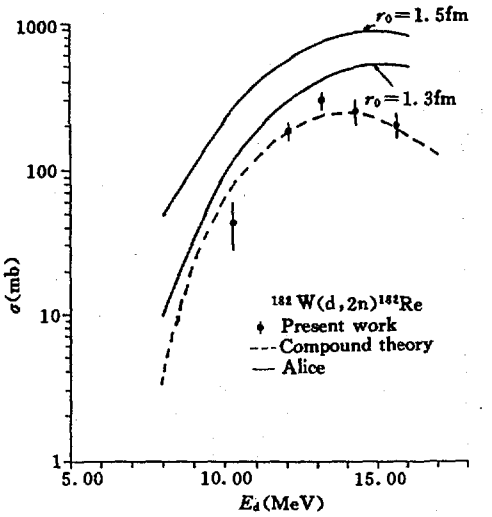

Fig. 6 The cross section of the reaction $^{182}W(d,2n)^{182}Re$

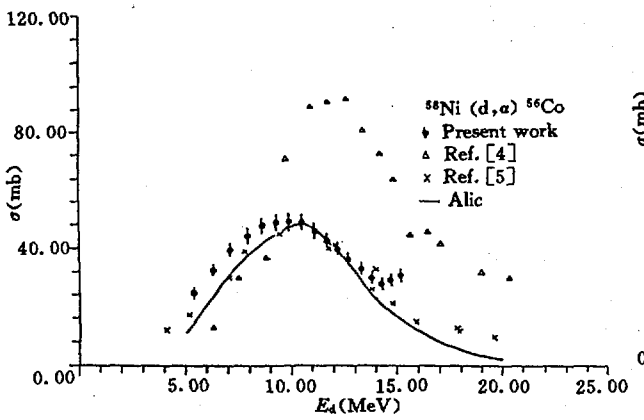

Fig. 7 The cross section of the reaction $^{58}Ni(d,\alpha)^{55}Co$

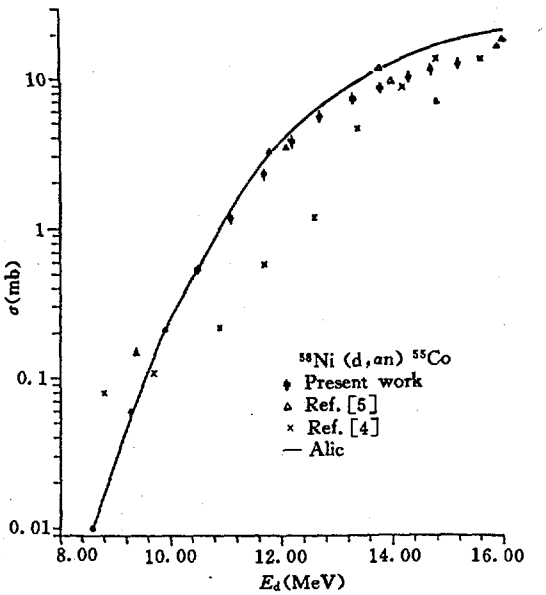

Fig. 8 The cross section of the reaction $^{58}Ni(d,\alpha n)^{55}Co$

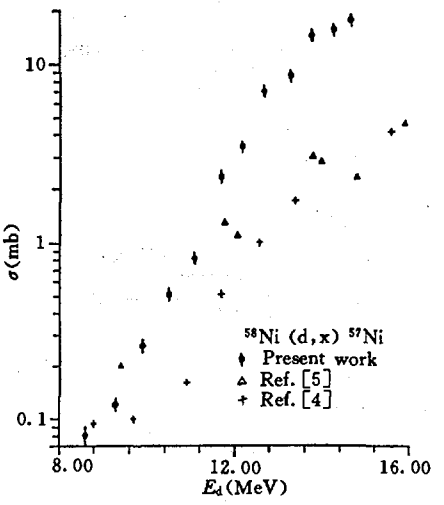

Fig. 9 The cross section of the reaction $^{58}Ni(d,x)^{57}Ni$

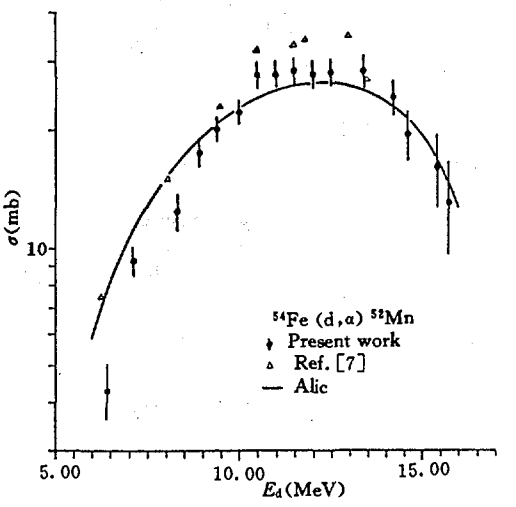

Fig. 10 The cross section of the reaction $^{54}Fe(d,\alpha)^{52}Mn$

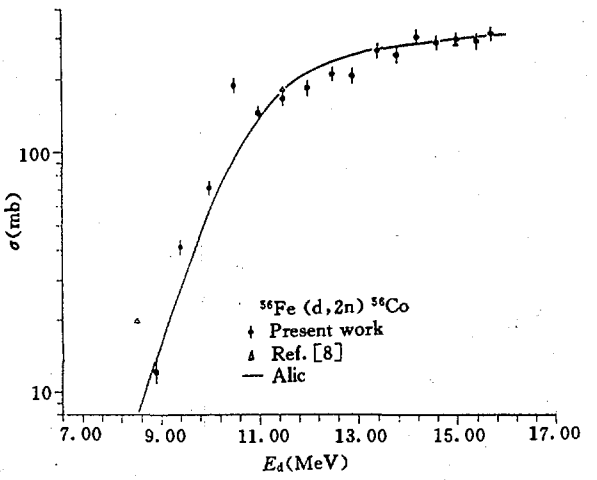

Fig. 11 The cross section of the reaction $^{56}Fe(d,2n)^{56}Co$

Table 1 The absolute full-energy peak efficiency $\varepsilon(\gamma)$ and its relative error $d\varepsilon$ for cubic spline interpolation

E_γ (keV)	$\varepsilon(\gamma)$ (10^{-9})	$d\varepsilon$
66.06	4.288	0.034
96.73	7.552	0.032
121.12	7.711	0.022
136.00	7.658	0.018
198.60	6.592	0.026
264.66	5.028	0.015
279.54	4.867	0.018
303.92	4.524	0.021
344.27	4.081	0.015
367.80	3.924	0.016
391.69	3.790	0.012
400.66	3.740	0.017
411.11	3.557	0.024
488.87	2.980	0.033
778.87	1.998	0.015
846.77	1.762	0.0096
867.37	1.657	0.020
964.04	1.610	0.016
977.37	1.595	0.030
1173.20	1.316	0.0089
1238.29	1.257	0.011
1332.49	1.179	0.012
1408.02	1.167	0.014
1771.34	0.913	0.012
1810.75	0.870	0.027
2015.19	0.782	0.013
2113.11	0.769	0.027
2598.46	0.632	0.0099
3009.59	0.568	0.020
3201.95	0.529	0.010
3253.43	0.523	0.011
3273.01	0.473	0.022
3451.15	0.449	0.025

Table 2 Experimental cross sections for deuteron induced reactions on tungsten

E_d (MeV)	$^{186}W(d,p)^{187}W$ (mb)	$^{186}W(d,2n)^{186}Re$ (mb)	$^{184}W(d,2n)^{184m}Re$ (mb)	$^{184}W(d,2n)^{184}Re$ (mb)	$^{183}W(d,2n)^{183}Re$ (mb)	$^{182}W(d,2n)^{182}Re$ (mb)
15.7	145 ± 9	170 ± 14	49 ± 13	383 ± 23	(1190 ± 140)	205 ± 15
14.7			89 ± 27		(1060 ± 120)	
14.3	175 ± 14	277 ± 19	47 ± 18	474 ± 28	(762 ± 91)	243 ± 51
13.7	170 ± 10		57 ± 15		761 ± 91	
13.2	204 ± 14	405 ± 24	72 ± 15	545 ± 31	583 ± 70	291 ± 35
12.7			40 ± 14		543 ± 65	
12.1	194 ± 14	434 ± 26	55 ± 23	480 ± 27	487 ± 58	182 ± 27
11.5	198 ± 14	317 ± 19	25 ± 11	393 ± 24	373 ± 48	
10.9	193 ± 10			277 ± 21		
10.3	154 ± 11	251 ± 15		247 ± 15	(221 ± 28)	43 ± 16
9.7	141 ± 10	190 ± 11		162 ± 10	(160 ± 17)	
9.0	104 ± 6	97.1 ± 5.8		(86.6 ± 5.4)	(106 ± 17)	
8.4	69.4 ± 6.7	50.6 ± 4.0		(46.9 ± 3.2)	(27 ± 9)	
7.7	35.5 ± 2.1			(6.0 ± 1.6)		
7.0	12.5 ± 7.5	2.3 ± 0.2				
6.3	3.0 ± 0.3					

The value in parentheses is the composite cross sections of (d,n) and (d,2n), or (d,2n) and (d,3n).

Table 3 Experimental values of nickel cross sections by deuteron beam

E_d (MeV)	$^{58}Ni(d,\alpha)^{56}Co$ (mb)	$^{58}Ni(d,\alpha n)^{55}Co$ (mb)	$^{58}Ni(d,x)^{57}Ni$ (mb)
15.2	(30.7±2.1)*	13.1 ±1.0	
14.7	(29.0±2.0)*	11.7 ±0.9	17.3 ±1.2
14.3	27.8±1.9	10.5 ±0.8	15.3 ±1.0
13.8	29.8±2.0	8.8 ±0.7	14.2 ±1.0
13.7	32.9±2.2	7.4 ±0.6	8.4 ±0.6
12.7	36.3±2.4	5.6 ±0.4	6.9 ±0.5
12.2	39.6±2.6	3.8 ±0.3	3.4 ±0.2
11.7	42.3±2.7	2.3 ±0.2	2.3 ±0.2
11.1	45.7±3.0	1.2 ±0.1	0.81±0.05
10.5	48.5±3.2	0.54±0.04	0.51±0.04
9.9	49.0±3.2	0.21±~0	0.26±0.02
9.3	48.8±3.2	0.06±~0	0.12±0.01
8.6	47.7±3.1	0.01±~0	0.08±0.01
7.9	44.3±2.9		0.11±0.01
7.1	39.3±2.6		0.12±0.01
6.3	32.6±2.1	0.02±~0	0.11±0.01
5.4	24.5±1.6	0.01+~0	0.10±0.01

* The value in parentheses is the sum of $^{58}Ni(d,\alpha)^{56}Co$ and $^{60}Ni(d,\alpha 2n)^{56}Co$ cross sections.

Table 4 Experimental values of iron cross sections by deuteron beam

E_d (MeV)	$^{54}Fe(d,\alpha)^{52}Mn$ (mb)	$^{56}Fe(d,2n)^{56}Co$ (mb)
15.7	13.0 ± 3.4	315 ± 23
15.4	16.0 ± 3.4	293 ± 21
15.0		298 ± 21
14.6	19.4 ± 2.8	289 ± 20
14.2	24.3 ± 2.5	305 ± 21
13.8	10.8 ± 1.8	256 ± 18
13.4	28.3 ± 2.7	266 ± 18
12.9		209 ± 15
12.5	28.1 ± 2.2	212 ± 14
12.0	27.7 ± 2.2	186 ± 13
11.5	28.3 ± 2.1	167 ± 11
11.0	27.7 ± 2.1	147 ± 10
10.5	27.7 ± 2.2	190 ± 13
10.0	22.2 ± 1.6	72.0 ± 5.0
9.4	20.1 ± 1.6	41.4 ± 3.0
8.9	17.5 ± 1.5	12.2 ± 1.2
8.3	12.4 ± 1.3	
7.1	9.3 ± 0.8	
6.4	4.3 ± 0.7	

References

[1] R. L. Andelin, LA–2880 (1963)

[2] F. W. Pement et al., Nucl. Phys., 86, 429(1966)

[3] S. J. Nassiff et al., Radiochimica Acta, 19, 97(1973)

[4] M. Blann et al., Phys. Rev., 131, 764(1963)

[5] C. K. Cline, Nucl. Phys., A174, 73(1971)

[6] J. W. Clark et al., Phys. Rev., 179, 1104(1969)

[7] N. A. Flasov, et el., Atomnaya Energy (Soviet), 2, 169(1957)

[8] W. H. Burgus et al., Phys. Rev., 95, 750(1954)

[9] Tao Zhenlan et al., Chinese J. of Nucl. Phys., 3, 242(1981)

[10] F. E. Chukreev, IAEA–NDS–146, (1992)

[11] P. Kafalas, Phys. Rev., 104, 703(1956)

[12] K. Debertin et al., γ– & X–Ray Spectrometry with Semiconductor Detectors (Elsevier, Amsterdam, 1988)

[13] Wang Gongqing et al., Nucl. Instr. & Meth., A272, 791(1988)

[14] IAEA–TECDOC–619 . X–ray & γ–ray standards for detector calibration (1991)

[15] E. Browne et al., Table of Radioactive Isotopes (John Wiley & Sons, Inc., New York 1986), some updata are from Nucl. Data Sheets, after 1986

[16] K. A. Keller, Estimation Functions, Landolt–Bornstein: Numerical Data and Functional Relationships in Science and Technology, New Series I / 5, part C, Springer, (1974)

[17] M. Blann et al., CODE ALICE / LIVERMORE 82

[18] V. F. Weisskopf et al., Phys. Rev., 57, 472(1940)

[19] W. D. Meyers et al., Nucl. Phys., 81, 1(1966)

[20] A. Chatterjee et al., Tables of Nuclear Level, Density Parameters, INDC(IND)–20 / U (1976)

[21] M. Blann, Phys. Rev. Lett., 27, 337(1971)1550 (errata)

[22] M. Blann et al., Nucl. Phys., A186, 245(1972)

[23] R. Michel et al., Nucl. Phys., A322, 40(1979)

Measurement of Angular Distribution at 5.13 MeV for Reaction of $^{58}Ni(n,\alpha)^{55}Fe$

Tang Guoyou Bai Xinhua Shi Zhaomin Chen Jinxiang

(Peking University)

Yd. Gledenov Huuhanhuu

(Joint Institute for Nuclear Research, Dubna 141980, Russia)

Abstract

α particle angular distribution of $^{58}Ni(n,\alpha)^{55}Fe$ reaction has been measured at incident neutron energy of 5.13 MeV using a gridded–ionization chamber. Neutron fluence was determined by a fission chamber. Preliminary results of total cross section and angular distribution have been obtained.

Introduction

Nickel is an important component element of alloy and is widely used as reactor material. It is therefor very important to measure the cross section and the angular distribution of $^{58}Ni(n,\alpha)^{55}Fe$ accurately for determining the radiation resistant ability of metals.

Up to now, because of experimental difficulties only a few reports have touched upon the angular distribution measurements of $^{58}Ni(n,\alpha)^{55}Fe$. Recently A. A. Говерповский et al.[1] presented an experimental measurement at incident neutron energy of 5.0 MeV. Their experimental result is largely discrepant with theoretical calculation of the compound model. Therefor, further experiment would be worthy to examine that whether $^{58}Ni(n,\alpha)^{55}Fe$ angular distribution can be explained by compound model. We carried out the measurement of $^{58}Ni(n,\alpha)^{55}Fe$ angular distribution using a gridded–ionization chamber at incident neutron energy of 5.0 MeV. The chamber was made in Neutron Laboratory of Joint Institute of Nuclear Research (NL, JINR), Dubna, Russia. So this work is in cooperation with NL, JINR. Our preliminary results show that the angular distribution slants forward in laboratory system and the cross sec-

tion is in agreement with other measurements.

1 Set up of the Experiment and Measurement

A. Gridded–Ionization Chamber (GIC) and Target

The structure of GIC is the same as that described in reference[2], but in this experiment we only used one grid. The distance is 7 cm between the anode and the cathode, and 5.0 cm between the grid and cathode. During the experiment GIC was filled by gas of 98.3% Kr and 1.7% CO_2 at the pressure of 2.2 atm. We have measured the relations between FWHM (energy resolution) and $(V_a - V_g) / (V_g - V_c)$ and the relations between pulse height and $(V_a - V_g) / (V_g - V_c)$ by a Pu–α source. From these relations, we obtained the best working conditions of GIC: V_c (cathode voltage) = − 3800 V, V_g(grid voltage) = −1700 V, V_a (anode voltage) = 0 V. Target sample was a metallic disk with a diameter of 4.0± 0.1 cm and a thickness of 1.047± 0.002 mg / cm^2 that consist of 99.9% ^{58}Ni isotope component. Target was backed on cathode which was made of aluminum. Target was located at 8.2 ° with respect to the neutron source.

B. Fission Chamber of ^{238}U

Neutron fluence was determined by fission chamber of ^{238}U. This chamber was made by copper of 0.18～0.11 mm thickness. Sample of ^{238}U (abundance: 99.997%) was electrodeposited on stainless steel plate (thickness: 0.05 mm). The diameter of sample is 20 mm. Total weight of the sample is 547.2 (1 ± 1.3%) g. The distance between anode and cathode was 7 mm. During the experiment run, angles subtended for neutron source by target of ^{58}Ni and sample ^{238}U were the same.

C. Measurement

The block diagram of experimental equipment is shown in Fig. 1.

The measurement was carried out using 4.5 MeV Van–de–Graff accelerator in the Institute of Heavy Ion Physics, Peking University (IHIPPU). The 5.13 MeV neutrons from D(d,n)^{3}He reaction was used in the measurement, 1.90 MeV deuteron beam was supplied by the 4.5 MeV Van– de –Graff accelerator. Total energy spread of neutrons is 0.2 MeV.

Experiment was done in four runs: (1) measuring event+ background at

forward direction of beam. (2) measuring background at forward direction of beam. (3) measuring event+ background at backward direction of beam. (4) measuring background at backward direction of beam. Total running time was about 100 hour.

2 Result and Discussion

A. Angular Distribution

For backward directions (90 ° ~ 180 °), the two dimensional picture of anode and cathode signal is shown in Fig. 2A and background spectrum is shown in Fig. 2B. For forward directions (0 ° ~ 90 °), the situation is similar to backward direction. The information of angular distribution is derived in the same way as that given in Ref. [2]. For our present conditions of GIC, shield coefficient (σ) is 0.0287. Anode signal have been revised by this shield coefficient.

Fig. 3 and Fig. 4 show anode signal spectra of forward and backward directions, respectively.

Fig. 5 shows the preliminary result of angular distribution.

B. Total Cross Section

Using the recommended data of ENDF / B–6 file for $^{238}U(n,f)$ cross section we got the absolute neutron fluence rate, then total cross section can be derived from the angular distribution data.

The preliminary result of total cross section is 42.4 ± 4.6 mb.

Comparing present results with the data measured by C. Badtz–Jorgensen[3], our results are in agreement with data extrapolated by their data at 5.0 MeV to 10.0 MeV range, ENDF / B6 data are little higher than our experimental data (see Fig. 6).

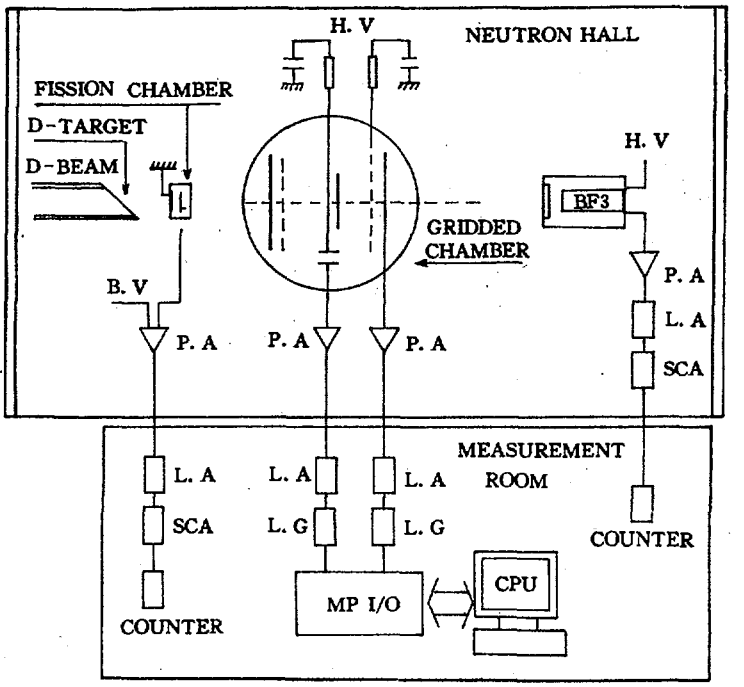

Fig. 1 The block diagram of experimental equipment

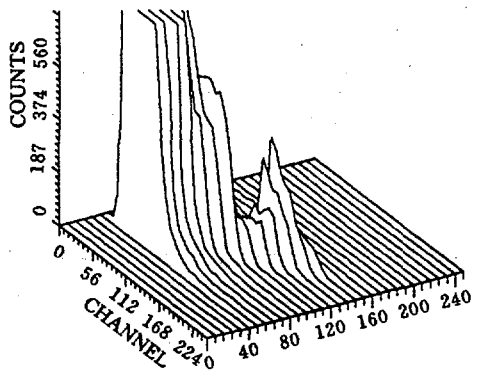

Fig. 2A The two dimensional picture of anode and cathode signal (backward)

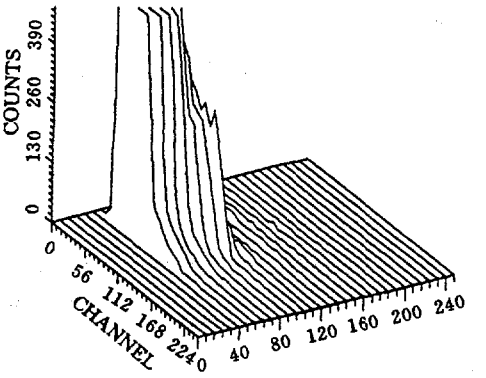

Fig. 2B The two dimensional picture of anode and cathode background (backward)

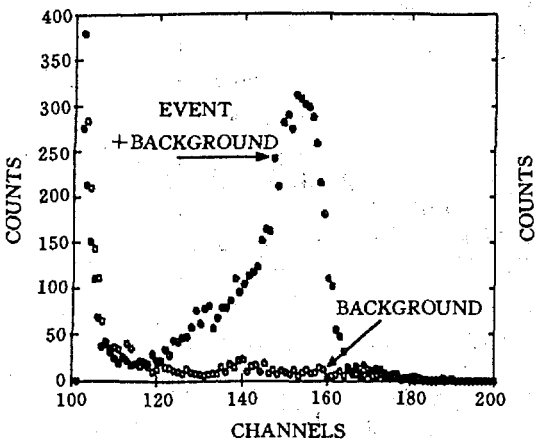

Fig. 3 Anode signal spectrum (forward)

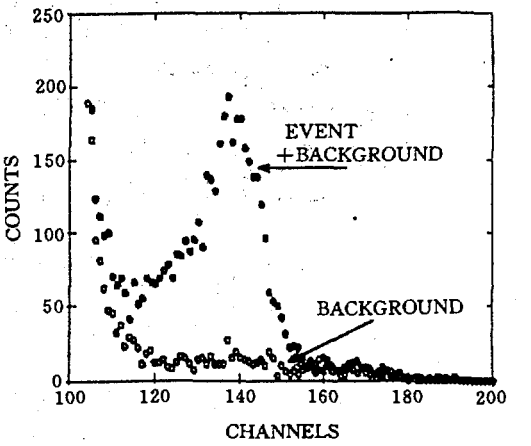

Fig. 4 Anode signal spectrum (backward)

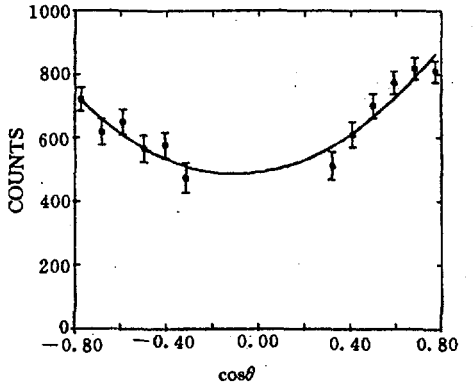

Fig. 5 The experimental and fitted angular distribution of $^{58}Ni(n,\alpha)^{55}Fe$

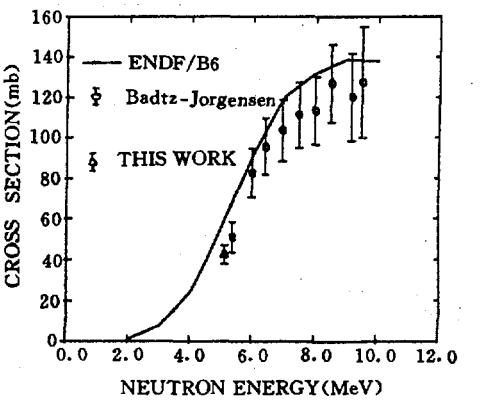

Fig. 6 The comparison between our preluminary results and of ENDF / B-6

References

[1] A. A. Говерповский et al., FEI-2242, 1992

[2] Tang Guoyou et al., INDC(CPR)-029 / L, p. 7, 1992

[3] C. Budtz-Jorgensen et al., Nucl. Instr. & Meth., 223, 295(1984)

Development of a Multitelescope System for the Measurement of Differential (n,charged particle) Reaction

Ye Bangjiao Fan Yangmei Wang Zhongmin Han Rongdian
Mei Wen Yu Xiaoqi Yang Yanming Han Renyu Du Huaijiang

(Dept. of Modern Physics, Univ. of Scin. & Tech. of China, Hefei, Anhui)

Xiao Zhenxi

(Institute of Management, Univ. of Sci. & Tech. of China, Beijing)

Abstract

A multitelescope system for measurement of energy and angular distribution of charged particles from neutron induced nuclear reactions is described. The system consists of two ΔE detectors and an E energy detector. The electronics system for acquiring five-parameters was established. The system was calibrated carefully. The system allows simultaneously measuring the energy of charged particles at all reaction angles.

Introduction

The measurements of the energy spectra and angular distributions of emitted particle from the fast-neutron (n,charged particle) reactions are rather scarce even around 14 MeV, because of the small values of cross sections and high background. This measurement has so far been done mostly by means of counter telescopes and requires very long measuring time due to the extremely low event rates and background problems. In order to improve this situation, a lot of new detectors were developed[1~4]. Further for this aim, an USTC multitelescope system has been designed. In the following the design and performance of this system is included in detail.

1 The Multitelescope System

1.1 Construction of the System

A multitelescope system was designed and installed as shown in Fig. 1. It consists of three parts: cylinder multiwire proportional chamber (MWPC), the central energy detector and gas pressure steady parts. The target to be investigated is laid in a semicircle target holder. Charged particle from neutron induced reactions traverses first the outer ring–shaped MWPC consisting of 32 separate proportional counters and then traverses the inner ring–shaped consisting of 16 separate proportional counters, at last, stops in the central CsI(Tl) scintillator. Each of the proportional counters in conjunction with the central scintillator acted as a normal counter telescope allows measuring particle energy and particle identification. The different telescopes correspond to different reaction angles and allow simultaneously measuring charged particle spectra at 16 reaction angles. The second half of the chamber not covered by the target is used for simultaneously measuring the background.

The cylinder multiwire proportional counter consists of the ground–plate and the top–plate (both made of Al). Two disks made of tungsten cover the

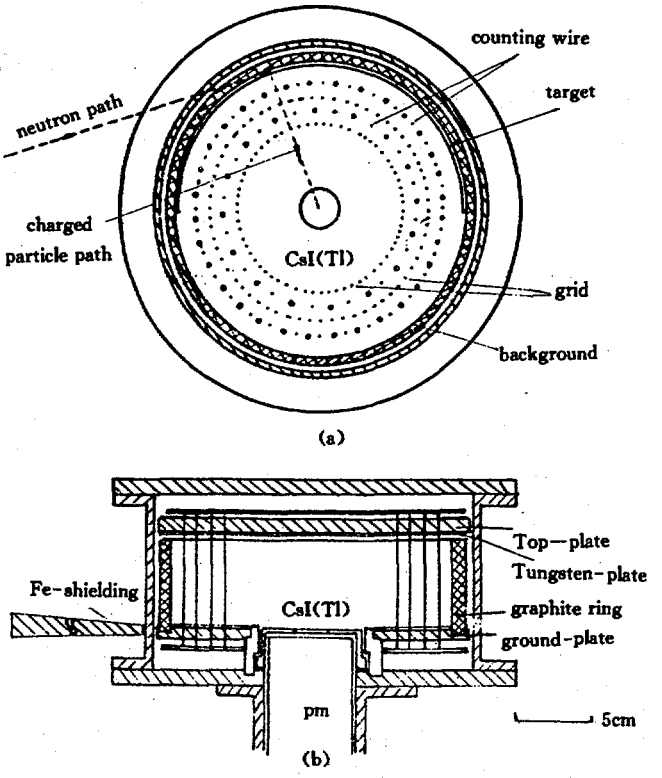

Fig. 1 The multitelescope system (schematic) (a): top view, (b): side view

inner surface of the plates, because the tungsten has very low (n,p) and (n,α) cross sections. The gold–coated tungsten wires (sense wires and grid wires are both 50 μm) are soldered at the print plates with a tension of 140 g. The wire between each two sense wires was used as segregate–wire with a same voltage as that of grid. This construction has proved very successful during the experimental runs.

A CsI(TI) crystal of Φ 25 mm and 1 mm height coupled to photomultiplier was chosen as the central energy detector, as both Cs and I have very low (n,p) and (n,α) cross sections and in addition CsI(TI) has excellent pulse–shape property which allows α–p–γ discrimination down to about 2 MeV proton. For 1 mm thickness, protons emitted from the target foil with energy up to 18 MeV can be stopped. Selecting the suitable photomultiplier, the energy resolution of CsI detector is 8% for ^{241}Am α–source ($E_\alpha = 5.486$ MeV). The CsI detector is shielded against the neutron source by 20 cm of Fe.

95% Ar + 5% CO_2 mixture gas was used in this system. The system was operated at low gas pressure (100 mb) and in the gas flow mode. A graphite ring was used as the target holder. In the graphite there is practically no proton production because of the large negative Q–value for the ^{12}C(n,p) reaction.

1.2 Geometry of the System

Fig. 2 shows the geometry relative to neutron source, target ring and central energy detector. For application of this system to measure double–differential cross section (DDCS) of charged particles, the solid angles per telescope, the average distance from target ring to central detector and the reaction angle function for each telescope must be known. These quantities were determined with Monte Carlo calculation.

The average path length for charged particle travel through the gas was determined as $S = 97.1 \pm 0.02$ mm. With this one can calculate the energy loss of charged particles in MWPC and revise the energy of charged particles. The solid angle per telescope was calculated numerically to be 14.7 ± 0.3 msr.

The reaction angle is calculated according to relation

$$\theta = \arccos [X Y / (| X | | Y |)] \qquad (1)$$

X and Y being vectors with components

$$X = (A + R \cos \alpha, R \sin \alpha, h)$$

$$Y=(\ R\ \cos\ \beta-\gamma\ \cos\ \gamma,\ R\ \sin\ \beta-\gamma\ \sin\ \gamma,\ h\ ) \tag{2}$$

The target foil corresponding to each counter and the crystal surface are both decomposed into a large number of elements. For each combination of elements the reaction angle was calculated. The reaction angle function $W(\alpha)$ is the reaction angle distribution of each telescope. The calculation results are shown in Fig. 3, the average reaction angle varies from 33° for the first to 159° for the last telescope, the angular resolution (FWHM of the reaction angle functions) amounts to 11.5°~15° except for the first and second telescopes which have a FWHM of 18.3° and 16.8°.

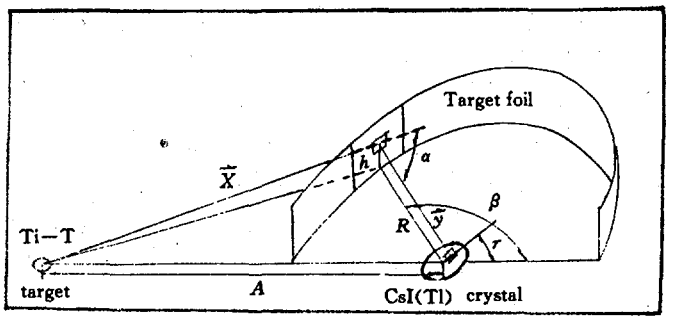

Fig. 2 Geometry of the multitelescope system

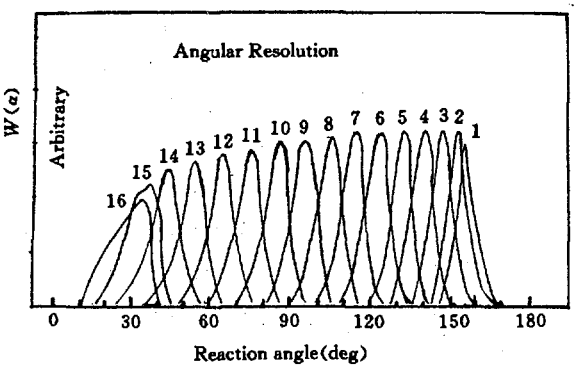

Fig. 3 Reaction angle functions of the various telescope

2 Electronics and Data Handling

The electronics system includes two parts: the electronic signals readout

circuits and CAMAC data collection system. The block diagram of the associated electronics is shown in Fig. 4. For each (n,xp) reaction event, the five parameters were recorded sequentially on disc in an on–line computer: the energy loss signal (ΔE) of the charged particle in the outer proportional counter, the wire address signal (ADDR) which gives out the reaction angle, the time difference signal (TIME) between the proportional counter and the E–detector, the energy signal (E) and the pulse shape distinguish signal (PSD) produced by the CsI(TI) crystal.

Charged particle produced by neutron–induced reaction at target foil has to traverse the outer proportional counters and produce an analog and a logical signals (address readout)[5]. The logical signals are fed to an address logic which transforms them to a 5 bit address code characterizing the different counting wires. The analog pulses from the proportional counters are at first amplified, and then, combined in summing amplifiers summing four preamplifier outputs each. The outputs of these summing amplifiers are fed into the eight–channel linear gates, which are opened in a case of coincidence corresponding inner wire signals with the E–detector signals and eventually all proportional counter signals are combined in a final summing amplifier. By this method, four times higher count rate can be admitted to the proportional counter than in case of direct summing of all proportional counters signals in one summing amplifier.

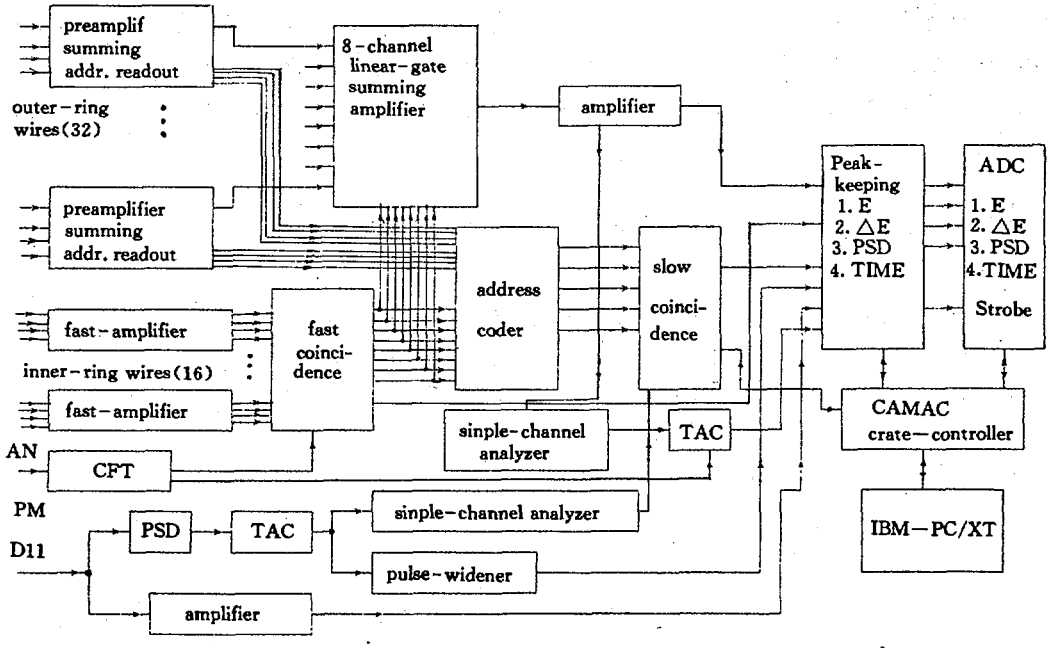

Fig. 4 Block diagram of system electronics (schematic)

The CsI scintillator is used to produce an energy signal and a pulse shape signal. The decay time of fluorescence for the α, proton and γ particle produced in CsI(TI) crystal are about $T_\alpha = 0.65\ \mu s$, $T_p = 0.75\ \mu s$ and $T_\gamma = 0.9\ \mu s$, respectively. Using this property, a circuit of the pulse shape discrimination (PSD) was designed. The PSD signal outputed from this circuit is fed to the slow–coincidence circuit. The slow–coincidence signal is used as stroking signal to open all ADC gates.

For controlling the ADC circuits and communicating with on–line computer, a new intelligent CAMAC crate controller[6] was designed and it not only adopts a high function CPU to manage its actions, but also includes a large memory to store the data and the controlling programs. The data is recorded in buffer–region of the CAMAC crate controller. When the buffer–region is full or the collection is finished, the data is readout and stored on disc from it by the host computer.

A number of computer programs was developed to analyze the five–parameter data and derive absolute double differential particle production cross sections $\frac{d^2\sigma}{(\ dEd\Omega\ )}$. In first step the chance–coincidence count was deleted with PSD and time spectra. The particles were identified with PSD and $E\Delta E$ spectra. In this way excellent particle identification is obtained. In the second step the net particle–emission energy spectrum is derived by subtraction of the count of the background from the corresponding foreground spectra. The double differential cross sections are calculated from these net spectra.

3 Calibration of the System

For measuring absolute double–differential charged particle production cross ssections, the system must be calibrated. The calibration of the system includes three parts: energy calibration, neutron flux calibration and detection efficiency calibration.

3.1 Energy Calibration of the System

Energy calibration of the system was performed in two steps: First, because energy respond of CsI(TI) is nonlinear for α–particles, energy calibration of the CsI crystal was done experimentally by means of various energy α–particles and

protons, which were produced from the reactions of $^{6}Li(d,p)^{7}Li$, D(d,p)T and $^{6}Li(d,\alpha)^{4}He$ in 150 kV Cockcroft–Walton accelerator and particles all of these pass through a variety of thickness of Al–foil. The CsI detector was laid at 90° with respect to the deuteron beam direction. During the calibration, the ^{22}Na and ^{239}Pu were used as standards for the range. The calibration curve is shown in Fig. 5, the dotted line was the calibration result of CsI by N. R. Dixion[7].

Second, because signal amplitude respond of electronics system is linear, the energy zero–point was calibrated using ^{241}Am α–source in the different voltage of the photomultiplier and in the different gas pressure of the proportional counters. The result is given as[8]:

$$E_p = (0.51 \pm 0.02) + (0.0652 \pm 0.0004)\, X \quad (\text{MeV}) \qquad (3)$$

E_p is energy of the proton emitting from the target, X is the energy channel of the CAMAC–ADC.

3.2 Neutron Flux Distribution Along Target Ring

Neutron flux distribution was calibrated by using the "Associated Particle Method" (APM) and the activation method. First a α–particle detector was mounted at 90° with respect to the deuteron beam direction, then at a given point out telescope system the neutron flux per associated α–particle was determined. Second the neutron flux distribution along the target ring was determined relative to the given point by measuring relative ^{24}Na activities of Al–foil corresponding to each telescope. These foils were placed at target ring and the given point, and irradiated by neutron beam under same measuring condition for $^{93}Nb(n,xp)$ reaction.

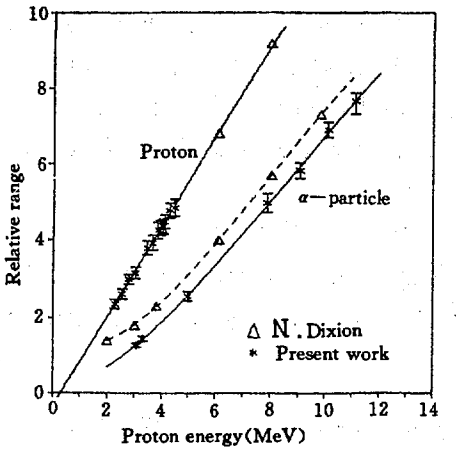

Fig. 5 Calibration curves of the energy response of the CsI(TI) crystal

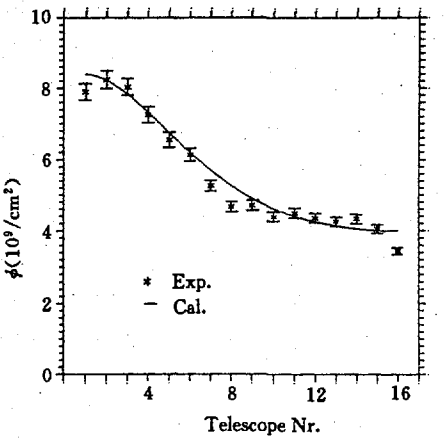

Fig. 6 Neutron flux distribution along the target foil

The result is given in Fig. 6. The curve corresponding to the flux distribution was calculated according to distance between neutron source and each target foil. There are the deviations between experimental data and calculated curve at forward and 90° angles. The intensity at forward angles, which is somewhat too low, was probably due to neutrons absorbed by Fe–shielder; while at 90° angles was probably due to neutrons absorbed by Al–ring wall and graphite ring.

3.3 Detection Efficiency Calibration of the System

The efficiency of the system was depended on working conditions of MWPC and CsI detector and the various electronics thresholds. The proton detection efficiency was obtained by means of determining ^{241}Am α–particle detection efficiency, but under separate working conditions. For example, working voltage of MWPC was 500 V for detection α–particle and 750 V for detection proton. For this purpose, the 32 ^{241}Am α–sources (2×3 mm^2) with very weak intention were mounted in the target–holder corresponding to each outer sense wires.

First the pulse amplitudes of 32 outer sense wires were adjusted to a same value. Then the various electronics thresholds were chosen to a proper value. The detection efficiency of the system is determined with a value of (97.0 ± 1.0)%. This result was checked under neutron irradiation using a weak ^{241}Am

α–source and a polyethylene foil which was laid at the forward angle telescope (33°).

4 Summary

The multitelescope system described in this paper was allowed to measure double–differential proton and α production cross sections in neutron induced reactions. The advantages of the system can be summarized as follows.

The system allows simultaneously to measure 16 reaction angles from 33 ~ 160° and simultaneously to measure foreground and background spectra. The energy range of the charged particles which is measured are from 3 to 20 MeV for proton, and from 4 to 30 MeV for α particle. The triple–coincidence was used to decrease chance coincidence. An excellent particle identification was obtained by PSD spectrum. The event–rate is high (about 0.4 / s) for the thick target.

With this system, the energy spectrum and the angular distributions have been measured for protons emitted from the ^{93}Nb(n,xp) reaction at 14.6 MeV[8]. The results are in fair agreement with the results of theoretical calculations.

Acknowledgments

This work was supported in part by the National Natural Science Foundation and the National Nuclear Industry Corporation of China.

References

[1] N. Koori et al., Nucl. Instr. Meth., 206, 413(1983)
[2] C. Derndorfer et al., Nucl. Instr. Meth., 187, 423(1981)
[3] S. M. Grimes et al., Nucl. Sci. & 62, 187(1977)
[4] W. R. McMurray et al., Nucl. Instr. Meth., A288, 421(1990)
[5] Mei Wen et al., Nucl. Ele. & Tech., (in Chinese) Vol. 11, No. 5, 270(1991)
[6] Jin Ge et al., Nucl. Ele. & Tech., (in Chinese) Vol. 11, No. 3, 146(1991)
[7] N. R. Dixion et al., Nucl. Phys., 42, 27(1963)
[8] Ye Bangjiao, Ph. D Thesis, Univ. of Sci. & Tech. of China (1992)

II THEORETICAL CALCULATION

Program NDCP–1 and Theoretical Calculations on n+^{16}O

Liu Jianfeng

(Department of Physics, Zhengzhou University, Zhengzhou)

Liu Tingjin Su Zongdi

(Chinese Nuclear Data Center, IAE)

Abstract

The program NDCP–1 of neutron data calculation is developed, in which the optical model and simplified pre–equilibrium correction for the statistical theory of compound nucleus reaction are included. The particle emission processes are described by means of the exciton model in which only less than five excitons are involved and the corresponding radiative capture processes are calculated by use of the direct–semidirect capture mechanisms but the nuclear reaction processes for the exciton number equal to or greater than five are still described by the statistical theory of the compound nucleus reactions. Using this program the neutron reaction data of ^{16}O are calculated and compared with the experimental ones in the incident neutron energy region from 5 MeV to 20 MeV. The aim of the present work is to examine the potentiality of using the optical model and statistical theory of the nuclear reactions for light nuclei.

Introduction

The theoretical calculation of the neutron reaction data of ^{16}O is very significant. As well known ^{16}O widely exists in the nuclear constructional and

shielding materials, its complete neutron nuclear reaction data are very important for fission reactor design, fusion research and nuclear shielding calculation. More exact calculations of the neutron reaction data are all done by means of the optical model, the statistical theory of the compound nucleus reactions and the exciton model which has been developed to describe the pre–equilibrium emission processes. Up to now, these calculations are mostly done for medium–heavy nuclei with $A > 40$. For light nuclei such as ^{16}O, it is difficult to calculate the data, and only a few systematical calculation have been done. Therefore, the potentiality of the use of the optical model and the statistical theory to calculate the nuclear reaction data for light nuclei is still a problem to be studied. Besides, the level density parameters and the photo–nuclear reaction giant dipole resonance parameters which are indispensable for the theoretical calculations have been less studied in the light nucleus region. For the nucleus with neutron number or proton number less than 10, there are no recommendations[1] for level density parameters and no experimental data[2] of the photo–nuclear reaction giant dipole resonance parameters. Therefore it is worth to do some work in these respects.

The theoretical and experimental results[3,4] show that the contributions of the pre–equilibrium γ emissions to the (n,γ) reaction cross sections increase with the decrease of the mass number. For light nuclei such as ^{16}O, the cross section from the pre–equilibrium γ emission is much larger than the one of the γ emission from the statistical equilibrium states. Because the γ deexcitation process is a cascade process, with increasing the incident energy, the (n,γ) cross section from compound nucleus will decrease further due to the competitions with the particle channels. Thus, the pre–equilibrium γ emissions which are mainly the primary transitions to the low excited states become more important. Meanwhile, these primary transitions to the low excited states correspond to some discrete lines with large intensity and high energy in the γ spectrum. Therefore it is very necessary for practical application and improving the agreement between the theoretical calculations and the experimental data to consider the contributions of this process reasonably.

The early exciton model did not consider the γ emission in the calculations of the particle emission process. Though the research on the pre–equilibrium γ emission has been done over the years[5], it is still not available for the calculations of the nuclear data. Since the direct–semidirect capture mechanisms [6,7] can describe the γ emission processes for one and three exciton states quite well, in this paper the pre–equilibrium correction for the statistical theory of the compound nucleus reactions is introduced. The particle emission processes are described by means of the exciton model, in which the exciton states with less

than five excitons are only involved, and the corresponding radiative capture processes are calculated by use of the direct–semidirect capture mechanisms but the nuclear reaction processes with the exciton number equal to or greater than five are still described by the statistical theory of the compound nucleus reactions. The program NDCP–1 of neutron data calculation has been developed and applied to calculate neutron data and analyse the experimental results. As a example, the complete neutron reaction data of ^{16}O have been calculated in the incident neutron energy region from 5 MeV to 20 MeV. In section 2, the physical model and the functions of the program NDCP–1 are introduced and the main formulas are listed. In section 3, the optical potential parameters, level density parameters, giant resonance parameters and the discrete low–lying levels are listed and some calculated results as well as the comparisons with the experimental data are given. In section 4, the calculation results are discussed briefly.

1 The Calculation Program and the Formulas

The neutron data calculation program NDCP–1 was developed for the theoretical calculations of the complete neutron data in the energy region up to 20 MeV. It can give not only the neutron data (files 3 to 5), but also the γ–ray production data (files 12 to 15). In addition, the program can also give the isomeric cross sections of each residual nucleus.

It is the most important feature of the program NDCP–1 that the theoretical calculations of γ–ray production data are described more carefully. In this program different theoretical model and calculation formula are used for different energy regions and the energy regions are divided according to the (n,γ) reaction mechanisms. In the thermal and resonance region, the cross sections of various reaction channels are calculated by using the resonance parameters. For the (n,γ) reaction in this region, besides the compound nucleus process, the non–statistical effects are described by the potential capture[8], the valence capture[9] and the interference effects between them. In the continuous region of the nuclear reactions and when the neutron incident energy is less than 5 MeV, the cross sections of various channels are calculated by using the Hauser–Fechbach theory with the width fluctuation correction[10], and the non–statistical effects of the (n,γ) reaction in this region are the captures process in the shape–elastic channels and the compound elastic channels[11]. When the incident neutron energy is higher than 5 MeV, as has been pointed out in the introduction, the pre–equilibrium correction for the compound nucleus theory is introduced and the direct–semidirect capture mechanisms are intro-

duced to describe the pre–equilibrium γ–ray emissions.

The reaction channels considered in the program NDCP–1 are shown in Fig. 1. Where $\gamma_0 \sim \gamma_{10}$ represent the γ–ray emissions of the (n,γ) reaction and the corresponding residual nuclei after emitting particles respectively. Since the calculations of the energy spectra and the angular distributions of the particles are done by adopting the well known calculation formulas of optical model and the statistical theory of the nuclear reactions and these formulas can be found in the relative Refs. [12, 13], in this paper the calculation methods and the calculation formulas on the (n,γ) reactions and the (n,xγ) reactions are introduced briefly only. The reaction cross sections of the corresponding reaction type, the γ–ray production cross sections and the γ–ray spectra are given by means of these formulas.

If E_m represents the highest excitation energy of the system, compound or residual nucleus, then the region from E_m to E_c is the continuous one, where E_c is its inferior limit. Below E_c there are N discrete levels from the ground state denoted by (E_1, J_1, π_1), (E_2, J_2, π_2), $\cdots$, (E_N, J_N, π_N) respectively. The continuous region is described usually by means of the level density $\rho(E, J, \pi)$, and $\sigma_c(E, J, \pi)$ is defined as the total excitation cross section in a unit energy interval with spin J, parity π and energy E in the whole process, which includes the excitation coming from the particle emissions of the parent nucleus and from the cascade γ de–excitations. $\sigma_{c0}(E, J, \pi)$ is its initial value. For the compound nucleus, it is the excitation coming from direct–semidirect capture and the primary γ transitions after the statistical equilibrium. For the residual nucleus, it is the excitation coming from the particle emissions of the parent nucleus. Let σ_i be the total excitation cross section of ith discrete level in the whole process and σ_{i0} is its initial value. Then the cascade γ de–excitation processes can be described by the following integral equations:

$$\sigma_c(E,J,\pi) = \sigma_{c0}(E,J,\pi) + \int_E^{E_m} \sum_{J'\pi'} \sigma_c(E',J',\pi') \frac{T_\gamma^{E',J',\pi',E,J,\pi}}{T^{E',J',\pi'}} \rho(E,J,\pi)\, dE' \tag{1}$$

$$\sigma_i = \sigma_{i0} + \sum_{j=i+1}^{N} \sigma_j \frac{T_\gamma^j}{T^j} S^{ji} + \int_{E_c}^{E_m} \sum_{J'\pi'} \sigma_c(E',J',\pi')$$

$$\frac{T_\gamma^{E',J',\pi',E_l,J_l,\pi_l}}{T^{E',J',\pi'}}\,dE' \tag{2}$$

$$\frac{d\sigma^\gamma}{dE_\gamma} = \sum_{i=1}^{N}\sum_{j=i+1}^{N}\sigma_j\frac{T_\gamma^j}{T^j}S^{j\,i}\,\delta\,(E_\gamma+E_i-E_j)$$

$$+\sum_{i=1}^{N}\sum_{J'\pi'}\sigma_c\,(E_i+E_\gamma,J',\pi')$$

$$\times\frac{T_\gamma^{E_i+E_\gamma,J',\pi',E_l,J_l,\pi_l}}{T^{E_i+E_\gamma,J',\pi'}}+\int_{E_c+E_\gamma}^{E_m}\sum_{J\pi J'\pi'}\sigma_c\,(E',J',\pi')$$

$$\times\frac{T_\gamma^{E',J',\pi',E'-E_\gamma,J,\pi}}{T^{E',J',\pi'}}\,\rho\,(E'-E_\gamma,J,\pi)\,dE' \tag{3}$$

Where $T^{E,J,\pi}$ is the total transmission coefficient. $T_\gamma^{E,J,\pi,E',J',\pi'}$ is the γ transmission coefficient from the level (E, J, π) to the level (E', J', π'). T^j is the total transmission coefficient of the discrete level. T_γ^j is its γ transmission coefficient. $S^{j\,i}$ is the γ transition branching ratio among the discrete levels. $\frac{d\sigma^\gamma}{dE_\gamma}$ is the γ energy spectrum and the γ production cross section is:

$$\sigma^\gamma = \int_0^{E_{\gamma\,max}}\frac{d\sigma^\gamma}{dE_\gamma}\,dE_\gamma \tag{4}$$

The cross sections of the corresponding reaction types can be given according to the following different ways:

(1) The integrated cross section of the given reaction type

$$\sigma(E) = \sigma_1 \tag{5}$$

(2) The cross sections of the discrete levels and the cross section of the continuous region

$$\sigma_i(E) = \sigma_{i0} \frac{T_\gamma^i}{T^i} \tag{6}$$

$$\sigma_c(E) = \sigma_1 - \sum_{i=1}^{N} \sigma_i(E) \tag{7}$$

For each nucleus of the decay chain shown in Fig 1, in order to solve the Eq. (1) ~ (3), the corresponding σ_{i0} and $\sigma_{c0}(E,J,\pi)$ must be calculated out first. For the (n,γ) reaction

$$\sigma_{i0} = \sum_f \sigma_{fi} + \sum_{J\pi} \sigma_a^{J\pi} \frac{\lambda_{(3)}^{J\pi}}{\lambda_{(3)}^{J\pi} + L_{(3)}^{J\pi}} \frac{T_\gamma^{J\pi,i}}{T^{J\pi}} \tag{8}$$

$$\sigma_{c0}(E',J',\pi') = \sum_{J\pi} \sigma_a^{J\pi} \frac{\lambda_{(3)}^{J\pi}}{\lambda_{(3)}^{J\pi} + L_{(3)}^{J\pi}} \times \frac{T_\gamma^{J\pi,E',J',\pi'}}{T^{J\pi}} \rho(E',J',\pi') \tag{9}$$

Where $\sigma_a^{J\pi}$ is absorption cross section. $\lambda_{(3)}^{J\pi}$ is the transition ratio of three exciton states to five exciton states. $L_{(3)}^{J\pi}$ is the particle emission ratio of three exciton states. The calculation formulas of $\lambda_{(3)}^{J\pi}$ and $L_{(3)}^{J\pi}$ can be found in the reference [14]. σ_{fi} is the contribution of the direct–semidirect capture and its calculation formulas can be found in the Ref. [15]. The symbol $\sum_f$ represents the summation for the different single particle states (l_f, j_f). In the formula (9), the pre–equilibrium emissions, i. e the contributions of the direct–semidirect capture, are not considered because this process is mainly the primary transitions to the low excited levels. For the six residual nuclei obtained after the first particle emissions, we have

$$\sigma_{i0} = \sum_{J\pi l' f} \sigma_a^{J\pi}$$

$$\left[\frac{W^{il'j'}_{\beta(3)}}{\lambda^{J\pi}_{(3)} + L^{J\pi}_{(3)}} + \frac{\lambda^{J\pi}_{(3)}}{\lambda^{J\pi}_{(3)} + L^{J\pi}_{(3)}} \frac{T^{il'j'}_{\beta}}{T^{J\pi}} \right] \tag{10}$$

$$\sigma_{c0}\ (\ E',J',\pi'\ ) = \sum_{J\pi l'j'} \sigma^{J\pi}_{a}$$

$$\times \left[\frac{W^{E'l'j'}_{\beta(3)}}{\lambda^{J\pi}_{(3)} + L^{J\pi}_{(3)}} + \frac{\lambda^{J\pi}_{(3)}}{\lambda^{J\pi}_{(3)} + L^{J\pi}_{(3)}} \frac{T^{E'l'j'}_{\beta}}{T^{J\pi}} \rho\ (\ E',J',\pi'\ ) \right] \tag{11}$$

Where $W^{il'j'}_{\beta(3)}$ represents the emission ratio of the β particle with energy $E_n + B_n - B_\beta - E_i$ and angular momentum l', j' in the three exciton states. B_n and B_β represent the neutron and the β particle separation energies, respectively. The difference between $W^{E'l'j'}_{\beta(3)}$ and $W^{il'j'}_{\beta(3)}$ is that the former is the emission ratio of the particles with energy $E_n + B_n - B_\beta - E'$ in a unit energy interval. Their calculation formulas can be found in the Ref. [14].

For the calculations of σ_{i0} and $\sigma_{c0}\ (\ E,J,\pi\ )$ of the residual nuclei obtained after the second or the third particle emissions, it can be exactly carried out by means of the compound nucleus theory.

2 Parameters and Calculation Results

Using the program NDCP–1, the neutron reaction data of ^{16}O were calculated in the neutron incident energy region from 5 MeV to 20 MeV. Ref. [14] has been consulted to calculate the exciton state density in the pre–equilibrium correction. The level densities of the compound nucleus and the residual nuclei were calculated by use of Gilbert–Cameron formula[1] and the method of selecting level density parameters is that the parameters are estimated according to the corresponding ones of the nucleus with Z and N larger than 10 first and then adjusted according to the comparisons of the calculated results with the experimental values. The photo–nuclear reaction giant dipole resonance parameters were estimated by means of the empirical formulas.

In the calculation the optical potential parameters of the incident channels were adjusted first to make the total cross sections, the elastic scattering cross sections as well as the angular distributions of the elastic scattering agreeing with the experimental data as better as possible. Then the optical potential parameters of the other particle channels, the giant dipole resonance parameters

and, if necessary, the level density parameters were adjusted to make the calculated results agreeing with the available experimental results as well as possible. The optical potential parameters of the neutron channel, the proton channel and the α channel used in the final calculation are listed in table 1. The level density parameters and the giant dipole resonance parameters of the compound nucleus and the residual nuclei are shown in table 2.

Fig. 2 shows the calculation results of total cross sections and their comparisons with the experimental data which are taken from S. Cierjack (1968) and are averaged over some energy region[16]. Figs. 3~5 are the calculation results and their comparisons with the experimental data of the elastic scattering cross sections as well as the angular distributions of the elastic scattering at the energies 5 MeV and 14.14 MeV respectively. Fig. 6 shows the comparisons of the calculated values of (n,p) reaction cross section with the experimental results. Near $E = 12$ MeV, there is a sharp peak which could not be reproduced by the theoretical calculations and is not drawn out. Fig. 7 shows the comparison of (n,α) cross section, the curve I gives the calculation results of the (n,α) cross section, the curve II and experimental data points are the sums of (n,α) cross sections and the (n,n'α) cross sections. Fig. 8 gives the calculated results of the non-elastic cross sections, the evaluated results of JENDL-3 and the experimental results. Fig. 9 shows the calculated results of γ production cross sections of the inelastic scattering processes and their comparisons with the evaluated data of ENDF / B-6 etc. Fig. 10 shows the calculated (n,γ) reaction cross sections and there are no experimental data in the computation energy region. The experimental data quoted in this paper are evaluated ones, and are recommended by Liu[16].

3 Discussions

3.1 It can be seen from the comparisons that in the incident neutron energy region from 5 MeV to 20 MeV, by adjusting the parameters properly, the average behaviors of the various cross sections of the neutron nuclear reactions on ^{16}O can be described better by means of the optical model and the statistical theory of the nuclear reactions.

3.2 In the present work, not only neutron data (file 3 to file 5) but also γ production data were given out (file 12 t file 15) which are the first calculations in China for CENDL.The data have already been used for the evaluations of the complete neutron data of ^{16}O in CENDL-2[16].

3.3 It can be seen from the Fig. 8 that when $E > 12$ MeV, the calculated values of the non–elastic scattering cross sections are a little lower than the experimental ones. This is to make the calculated elastic cross sections agree with the experimental values as well as possible. The experimental data are not consistent in this energy region. From the theoretical point of view, this is possibly related to the physical model adopted in the calculations because only the simplified pre–equilibrium correction of the three exciton states was considered in the calculations of the pre–equilibrium emissions of the particles and the contributions from the direct reaction process were not taken into account.

3.4 Fig. 7 shows that the sums of (n,α) and (n,n'α) cross sections, the curve II, are larger than the experimental data in $E > 10$ MeV region. Because of the competition with (n,n') channels, it causes the decrease of the inelastic cross section and its γ production cross section, as is shown in Fig. 9. Therefore by adjusting the optical potentials of α channels in (n,α) and (n,n'α) reactions further, the calculated results will be improved. In addition, when $E_n > 18$ MeV, the sums of (n,α) and (n,n'α) cross sections are obviously larger than the experimental data. This is because when E_n is greater than about 15 MeV, the (n,n'2α) channel are open energetically but they are not separated from (n, n'α) channel in the present calculation. It causes (n,n'α) cross section larger.

3.5 Fig. 10 shows the calculated (n,γ) cross sections. The contribution of the pre–equilibrium γ emission, i. e., the contributions of the direct and semidirect capture, is the main parts and account for about 90 percent, and, when $E_n > 15$ MeV this ratio will increase further. In present calculations the experimental values of (n,γ) reactions in the energy region from 0.2 MeV to 1 MeV for ^{18}O and in the energy region from 0.5 MeV to 2 MeV and from 0.01 MeV to 20 MeV for ^{19}F and ^{23}Na respectively were used for reference and, in addition, according to the fact that the giant resonance of the photo–nuclear reactions of ^{17}O taken place in the energy region from 22 MeV to 26 MeV, one can infer that the order of magnitude and the trend of the calculation results are reasonable.

Table 1 The optical potential parameters of n, p and α

	V_R	r_R	a_R	W_v	$r_{I'}$	$a_{I'}$	W_{SF}	r_I	a_I	V_{so}	r_{so}	a_{so}	r_c
n	−47.686 +0.304E	1.255	0.615	0			−3.0 −0.25E	1.478	0.321	−3.392	1.0086	0.545	
p	−58.32 +0.08E	1.1	0.208	0			−3.5 −0.2E	1.05	0.47	−7.5	1.1	0.47	1.55
α	−239.4 +0.54E	1.2	0.56	−0.5 −0.507E	1.0	0.35	0						1.32

Table 2 The level density parameters and the giant resonance parameters

	Level density parameters					Giant resonance parameters		
	E_x, MeV	T, MeV	E_o, MeV	P_Z+P_N, MeV	a, MeV^{-1}	σ_g, b	Γ_g, MeV	E_g, MeV
^{16}O	15.00	2.68	2.00	7.00	1.85	0.0416	4.5	24.45
^{16}N	11.80	2.50	−3.88	0.0	2.42	0.0416	4.5	24.45
^{13}C	10.64	3.65	−1.64	4.00	2.5335	0.0338	4.5	26.07
^{15}N	16.00	3.43	−0.60	3.5	2.12	0.0390	4.5	24.94
^{14}N	13.21	4.13	−4.07	0.0	1.67	0.0364	4.5	25.48
^{14}C	20.71	2.85	2.46	7.5	2.48	0.0364	4.5	25.48
^{15}O	16.00	3.14	−0.796	3.5	2.40	0.0390	4.5	24.94
^{12}C	18.00	4.61	1.40	3.0	1.27	0.0312	4.5	26.73
^{17}O	14.83	2.39	−0.784	3.5	3.44	0.0422	4.5	24.00

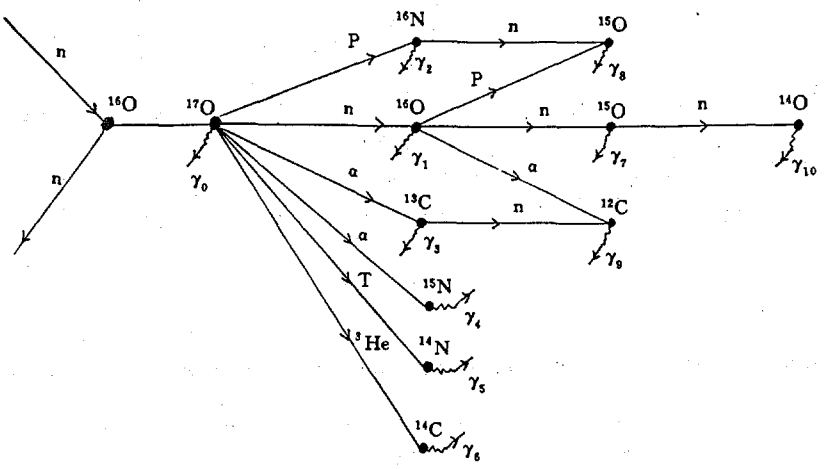

Fig. 1 The reaction channels considered in the calculations

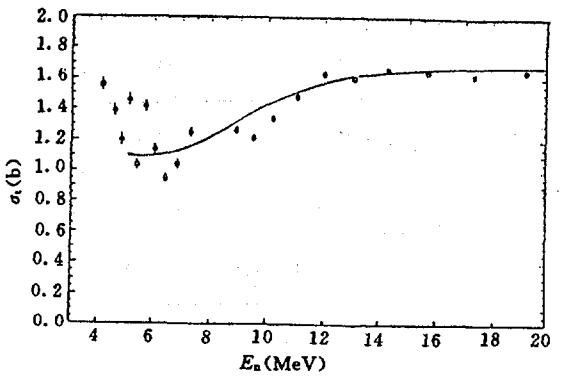

Fig. 2 Total cross sections

♦ S. Cierjacks (GERKFE), 1968,

—— theoretical calculated data.

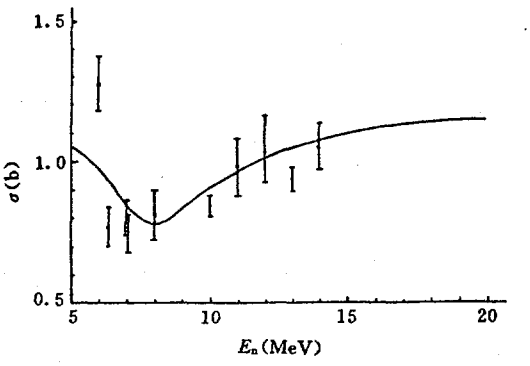

Fig. 3 Elastic scattering cross section : comparison between calculation results and experimental values

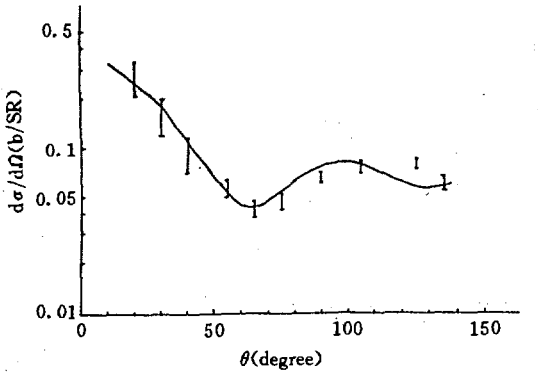

Fig. 4 The elastic scattering angular distribution at 5 MeV : comparison between calculation results and experimental values

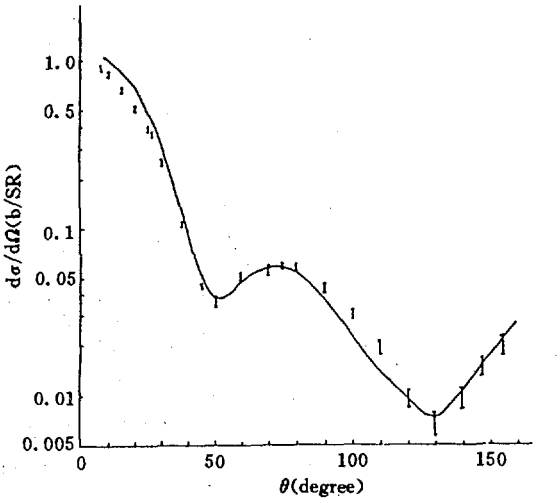

Fig. 5 The same as Fig. 4 but at 14.14 MeV

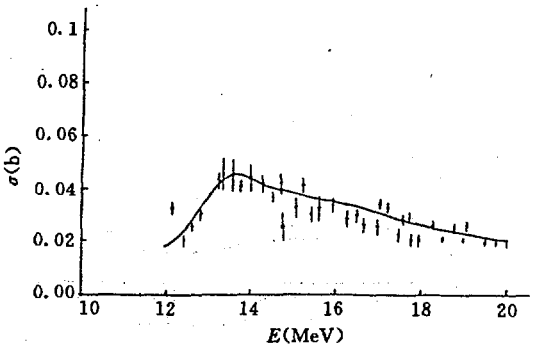

Fig. 6 (n,p) cross section : comparison between calculation results and experimental values

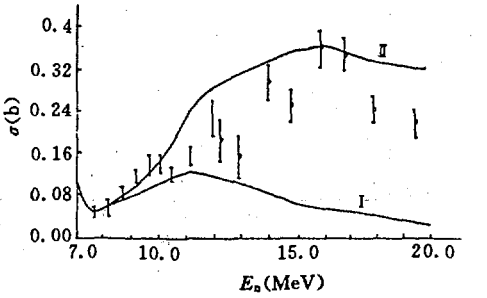

Fig. 7 (n,α) and (n,nα) cross sections and the comparisons with experiments
I (n,α), II (n,α)+(n,nα)

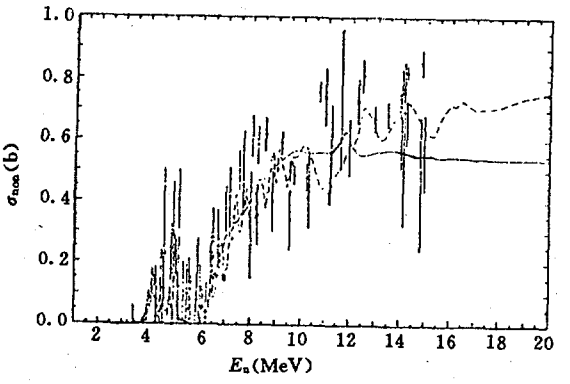

Fig. 8 Nonelastic cross section

—— This work, – – – JENDL–3, Others : experimental points.

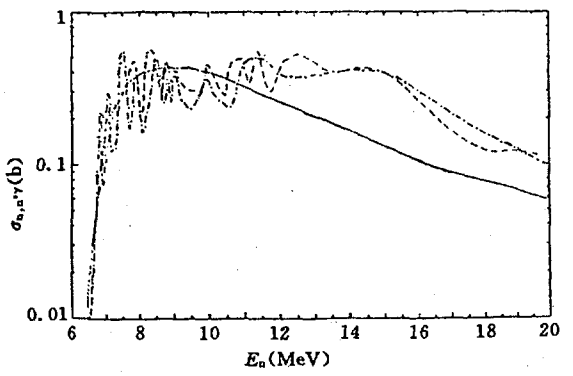

Fig. 9 Inelastic γ–production cross section

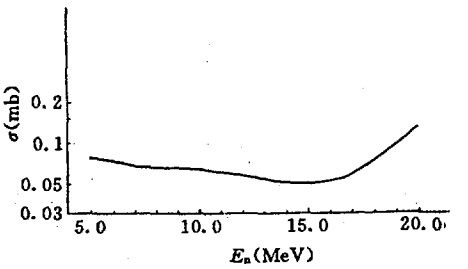

Fig. 10 Calculated results of (n,γ) cross section

— This work, – – ENDF / B–6, —· BROND–2.

References

[1] A. Gilbert et al., Can. J. Phys., 43, 1446(1965)
[2] S. S. Dietrich et al., Atomic Data & Nuclear Data Tables, 38, 199(1988)
[3] Huo Yukun et al., High Energy Physics & Nuclear Physics, 5, 465(1989)
[4] Liu Jianfeng et al., High Energy Physics & Nuclear Physics, 4, 349(1991)
[5] P. Oblozisky, Phys. Rev. C4, 1652(1990)
[6] G. E. Brown, Nucl. Phys., 57, 339(1964)
[7] C. F. Clement, Nucl. Phys., 66, 273(1965)
[8] A. M. Lane et al., Nucl. Phys., 11, 646(1959)
[9] J. E. Lynn, The Theory of Neutron Resonance Reaction, (Clarendon Oxford, 1968)
[10] Su Zongdi, High Energy Physics & Nuclear Physics, 3, 80(1979)
[11] Y. K. Ho et al., Nucl. Phys., A406, 1(1983)
[12] Hu Jimin et al., Nuclear Theory, Atomic Energy Press, (1987)
[13] Su Zongdi et al.,Nuclear Science & Technology, 4, 445(1979)
[14] Shi Xiangjun et al., Nucl. Phys., A466, 333(1987)
[15] Liu Jianfeng et al., Chinese Journal of Nuclear Physics, 2, 127(1992)
[16] Liu Tingjin et al., Communication of Nuclear Data Progress, 6, 3(1992)

Channel Theory of Fission with Diffusive Dynamics

Wang Shunuan

(Chinese Nuclear Data Center, IAE)

Abstract

The channel theory of fission with diffusive dynamics is proposed based on Bohr channel theory of fission and Fokker–Planck equation.

Introduction

As we know that the fission properties of excited states can be observed only if the fission probability is not too small compared to that of the other modes of decay. This can be fulfilled for excitation energies comparable to or higher

than the fission barrier height, for example 5 to 6 MeV for actinides. At this excitation energy, the compound nucleus states have extremely complex wave function and the density of these states is high with spacing of the order of ev[1]. Such a great complexity of the compound nucleus states makes it possible to study fission properties on the basis of statistical theory. A. Bohr[2] proposed a concept of fission exit channels by considering that the passage from saddle point to scission is so rapid that the properties of fission are nevertheless influenced by those of the transition states at the saddle point (collective transition states). Thus, these transition states act as exit open channels expressed in terms of fission saddle point configurations to fission[2, 3].

Within the framework of the Bohr channel theory, and the assumption of that the fission barrier is single–humped as predicted by liquid drop model calculations and that the shape of fission barrier is well approximated by a parabola, the fission width formula with quantum penetration of fission barrier presented by D. L. Hill and J. A. Wheeler[4] reads

$$\Gamma_f(E) = \frac{1}{2\pi\rho_c(E)} \int_0^\infty \frac{\rho_f(\varepsilon)}{1+\exp\left[\frac{2\pi}{h\omega}(V_f+\varepsilon-E)\right]}\,d\varepsilon \qquad (1)$$

Here, V_f, $h\omega$ are the parameters of fission barrier, ρ_c is the level density of the compound nucleus, ρ_f is the level density on saddle point. This theory has been applied to analysis of fission cross section and other fission–related quantities for many years.

In Eq. (1), it is the essential assumption that both the internal motion and the collective deforming motion degrees of freedom are completely in equilibrium inside the saddle point of the excited nucleus. The fission collective coordinate x is treated explicitly and all the other internal degrees of freedom are treated statistically. The detail of the fission process for the nucleus deforming from its ground state to saddle point is not taken into account. In the present paper we consider that the collective deforming motion during the process from its ground state to saddle point undergoes the stage from non–equilibrium to equilibrium process. Because the relaxation time of collective deforming variable in nuclear fission process is much longer than that for nucleonic degrees of freedom[5], it can be assumed that the single particle motion degrees of freedom is in equilibrium inside the saddle point of the excited nucleus, but the collective deforming variable in nuclear fission process is not in equilibrium inside the saddle point. Therefore the Fokker–Planck equation can be used to describe the collective deforming motion at other degrees of freedom

(single particle motion) acting as a heat bath with temperature T. It means that the fission process from ground state to saddle point can be governed by Fokker–Planck equation for the distribution function of the collective coordinates and their conjugate momenta at any time t, as in many areas of nonequilibrium statistical mechanics and also in the domain of heavy ion physics,the Fokker–Planck equation is used for the description of dissipative phenomena. In Sec. 2 the channel theory of fission with diffusive dynamics are described in detail. In Sec. 3 the calculation and analysis are presented.

1 Description of Channel Theory of Fission with Diffusive Dynamics

The channel theory of fission with diffusive dynamics is described by Fokker–Planck equation from the point of view of Brownian motion as a diffusion process at other degrees of freedom as a heat bath with temperature T. It takes the form of

$$\frac{\partial W(x,u,t)}{\partial t} + u\frac{\partial W(x,u,t)}{\partial x} + \omega^2 x\frac{\partial W(x,u,t)}{\partial u}$$

$$= \beta W(x,u,t) + \beta u\frac{\partial W(x,u,t)}{\partial u} + q\nabla_u^2 W(x,u,t) \tag{2}$$

with

$$q = \frac{\beta kT}{m}$$

Here, $W(x,u,t)$ is the probability density in phase space as a function of time t. x is the collective motion deforming variable along the elongating coordinate. β is the friction coefficient and m is the mass of "Brownian motion particle".

The diffusion is caused by the coupling between the deforming variable and the other degrees of freedom of the system as a heat bath with temperature T to attain random or stochastic.

We define a dimensionless quantity W_{right} as the following

$$W_{\text{right}} = \int_0^\infty \mathrm{d}x \int_{-\infty}^\infty \mathrm{d}u \; W(x,u,t\to\infty) \tag{3}$$

We suppose a "Brownian motion particle" moving in one–dimensioned in-

version harmonic oscillator potential barrier from the left side (ground state of the compound nucleus) to the right side with initial condition of $\delta(x-x_0)\delta(u-u_0)$ seeing from Fig. 1 as introduced in Refs. [7, 8]. The analytical formula of W_{right} is derived by using the solution of Fokker–Planck equation[6] as described in detail in Ref. [8].

Thus, we have

$$W_{\text{right}}(E,\varepsilon,\beta)=\frac{1}{2}\ (\ 1+\text{erf}\ (Z)\ ) \tag{4}$$

with

$$Z=(\ x_0\mu_2-u_0\ )\ (\ \frac{\mu_1}{2q}\ )^{\frac{1}{2}} \tag{5}$$

$$u_0=(\ \frac{2(E-V_f-\varepsilon\ )}{m}\ )^{\frac{1}{2}} \tag{6}$$

$$\mu_1=-\frac{1}{2}\beta+(\ \frac{1}{4}\beta^2+\omega\ )^{\frac{1}{2}} \tag{7}$$

$$\mu_2=-\frac{1}{2}\beta-(\ \frac{1}{4}\beta^2+\omega\ )^{\frac{1}{2}} \tag{8}$$

The fission width formula based on channel theory of fission with diffusive dynamics can be written as

$$\Gamma_f(E,\beta)=\frac{1}{2\pi\rho_c(E)}\int_0^\infty \rho_f(\varepsilon)\ \ \frac{W_{\text{right}}(\ E,\varepsilon,\beta\ )}{1+\exp\ [\ \frac{2\pi}{\hbar\omega}\ (\ \varepsilon-E+V_f\ )\ ]}\ d\varepsilon \tag{9}$$

As discussed in Refs. [7, 8], it can be seen clearly from Eq. (4) that when $\beta\to 0$ or $kT\to 0$, we have $Z\to\infty$, $\text{erf}(Z)\to 1$, so $W_{\text{right}}\to 1$. This is just exactly the Hill–Wheeler formula as written in Eq. (1). It can be seen clearly also from Eq. (4) that as the following: If $T\to\infty$, then $Z\to 0$, $\text{erf}(Z)\to 0$, $W_{\text{right}}\to 1/2$. If $m\to 0$, then $Z\to 0$, $\text{erf}(Z)\to 0$, $W_{\text{right}}\to 1/2$. If $m\to\infty$, then $Z\to\infty$, $\text{erf}(Z)\to 1$, $W_{\text{right}}\to 1$. If $\omega\to 0$, then $Z\to 0$, $\text{erf}(Z)\to 0$, $W_{\text{right}}\to 1/2$. If $\omega\to\infty$, then $Z\to\infty$, $\text{erf}(Z)\to 1$, $W_{\text{right}}\to 1$. Hence, channel theory of fission with diffusive dynamics are sensibly influenced by all of changes of those quantities mentioned above.

2 Calculation and Analysis

We take n+^{238}U as an example to calculate Γ_f by using the channel theory of fission with diffusive dynamics in the range of incident neutron energy from 1 to 9 MeV. In the calculation, the form of Gilbert–Cameron[9] is taken for level densities ρ_c and ρ_f but for ρ_f, the level density parameter a_f decreasing as excitation energy increasing is considered as used in Ref. [10]; $V_f = 6.22$ MeV, $\hbar\omega = 1$ MeV are also adopted as used in Ref. [10]. The friction coefficient varies from 0 to 200×10^{20} s^{-1} and the temperature kT of the heat bath varies from 0.5 MeV to 2 MeV to see how their sensitivities are, although the varying ranges of the friction coefficient and the temperature are not reasonable as a matter of fact from the physical point of view. The calculated results are shown in Fig. 2. It is clear from Fig. 2 as the following: When $\beta = 0$ or $T = 0$, Γ_f is exactly the one given by Hill–Wheeler formula shown by Eq. (1), represented by solid line in Fig. 2. It is much different from the other ones with $\beta \neq 0$ and $T \neq 0$. The other ones with $\beta \neq 0$ and $T \neq 0$ are always lower than the one calculated by Hill–Wheeler formula, and the β or T are higher, the Γ_f are lower. When T = const. and β = const., Γ_f increases as energy E increases. When T = const. and E = const., Γ_f decreases as β increases. When β = const. and E = const., Γ_f decreases as T increases.

In summary, based on Bohr channel theory of fission and Fokker–Planck equation the Bohr channel theory of fission has been generalized to it with diffusive dynamics, in which the internal single particle motion degrees of freedom are in equilibrium but the collective motion degrees of freedom are not in equilibrium. n+^{238}U is taken as an example to analyze the calculated results. The main features of the theory proposed in the present paper are illustrated both in analytical and numerical ways. Since the model is physically insight, and consistent with Hill– Wheele formula when $T \to 0$ or $\beta \to 0$, and also rather easy to work with, it can be used in the analysis of fission cross section and many other applications. It is sure that the model with physical reasonable value of friction coefficient and considering the temperature of the heat bath as a function of the excitation energy according to the Fermi gas model works well for fission cross section calculations, especially in the slope range, where the fission cross section mostly is hardly to be calculated in good agreement with experimental data[10].

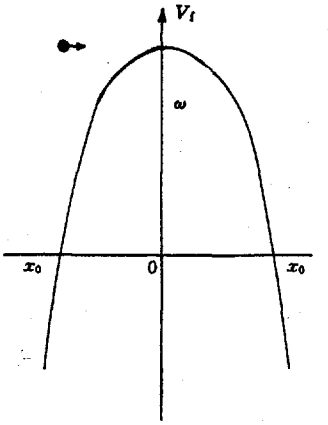

Fig. 1 Scheme of fission barrier

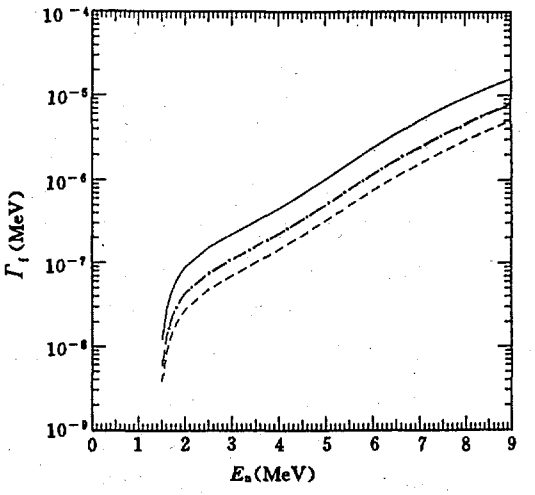

Fig. 2 Calculated fission width Γ_f as a function of incident neutron energy E_n, friction coefficient β and temperature T of the heat bath

—— for $\beta = 0$ or $kT = 0$,

—· for $\beta = 180 \times 10^{20}$ s^{-1} and $kT = 0.5$ MeV,

– – for $\beta = 180 \times 10^{20}$ s^{-1} and $kT = 2.0$ MeV.

References

[1] A. Michaudon, Nuclear Fission, Advances in Nucl. Phys., Edited by M. Baranger and E. Vogt, Vol. 6, 1(1973)

[2] A. Bohr, Proc. Int. Conf., Peaceful Uses of Atomic Energy (Geneva 1955), Vol. II , United Nations, New York, p. 220(1956)

[3] N. Bohr et al., Phys. Rev., 56, 426(1939)

[4] D. L. Hill et al., Phys. Rev., 89, 1102(1953)

[5] D. Brink, Nucl. Phys., A519, 3C (1990)

[6] S. Chandrasekhar, Rev. Mod. Phys. 15, 1(1943)

[7] Wang Shunuan et al., Commun. in Theor. Phys., Vol. 10, No. 3, 251(1988)

[8] Wang Shunuan et al., Chinese Jour. of Nucl. Phys., Vol. 10, No. 3, 216(1988)

[9] A. Gilbert et al., Can. J. Phys., 43, 1446(1965)

[10] Zhang Jingshang et al., hsj–78227(lljs); Atomic Energy Science & Tech., No. 3, 267(1976)

Theoretical Calculation of Neutron Elastic and Inelastic Scattering on First Excited State of ^{10}B

Zhang Yujun Zhu Yaoyin

(Jilin University, Changchun)

Abstract

The fast neutron elastic scattering on ^{10}B has been analysed by means of the optical model and the microscopic DWBA has been used to calculate the neutron inelastic scattering on ^{10}B at the excited state 0.717 MeV, $J^{\pi} = 1^{+}$. The theoretical calculations of the integral cross section and angular distribution of the elastic and inelastic scatterings are in good agreement with the experimental data.

Introduction

Boron is an important control material of reactor and is usually used to shield neutron. Therefore its data of the neutron nuclear reaction are very important. Because the experimental data are not enough, particularly in the energy range 15～20 MeV the experimental data of the integral scattering are less, the evaluation and application of these data are difficult. Therefore, the systematic theoretical analysis by means of the present experimental data and prediction of the data are very necessary.

Using the experimental data[1] of the fast neutron elastic scattering on ^{10}B the optical model analyses have been made and the better optical potential parameters have been got in this paper. For the neutron inelastic scattering on ^{10}B at the excited state 0.717 MeV, $J^{\pi} = 1^{+}$, the theoretical calculations have been made and the results are in better agreement with the experimental data.

1 The Optical Model Analysis

In the optical model analysis of the fast neutron elastic scattering on ^{10}B, the potential of Woods–Saxon form is used

$$V_{(r)} = -Uf(r, r_1, a_1) + i\,4Wa_2 \frac{d}{dr} f(r, r_2, a_2)$$

$$+ U_s \left(\frac{h}{m_\pi c}\right)^2 \frac{1}{r} \frac{d}{dr} f(r, r_3, a_3)\, \vec{\sigma}\, \vec{L}$$

$$f(r, r_j, a_j) = \left[1 + \exp\left(\frac{r - r_j A^{1/3}}{a_j}\right)\right]^{-1} \qquad (j = 1, 2, 3)$$

where U, W and U_s are the depth parameters of the real–well, imaginary potential and spin–orbit term respectively, r_j are the radius parameters and a_j are the surface–diffuseness parameters.

The key to the optical model analysis is to choose the suitable optical potential parameters. The usual method is to adjust the optical potential parameters by means of the existing experimental data. The measured results of the elastic scattering cross section and angular distribution of n+^{10}B reaction at $E_n = 8 \sim 14$ MeV have been given in the Ref. [1]. In order to avoid the influence of compound–elastic scattering, the experimental data of five high energy points at 9.96, 10.95, 11.95, 12.94 and 13.94 MeV were used in adjusting of

the optical potential parameters. According to previous method of the optical model analysis for the neutron elastic scattering from the light nuclei[2, 3], we regard the surface–diffuseness a_1 and the depth parameters of the imaginary potential as a linear function of incident neutron energy, other parameters are independent of the energy. Finally, the adjusted optical potential parameters are

U = 45.5200 MeV a_1 = (0.9869–0.0388E_c) fm r_1 = 1.3135 fm

W = (4.2894+0.3503E_c) MeV a_2 = 0.3297 fm r_2 = 1.4764 fm

U_s = 3.9796 MeV a_3 = 0.1359 fm r_3 = 1.3248 fm

The comparisons of the calculated results of total cross section σ_T with the experimental data are given in table 1. It is able to see from the table that the deviation of calculated results of total cross section from the experimental data isn't greater than 3%.

Table 1 The comparison of calculated and evaluated total cross sections

E_n (MeV)	10	11	12	13	14
σ_T^{eva} (mb)	1472	1488	1485	1480	1476
σ_T^{cal} (mb)	1500	1484	1469	1452	1435

The comparison of the calculations of the elastic scattering angular–distribution with the experimental data are given in Fig. 1. As illustrated in the Fig. 1, at angular range from 30° to 160° the calculations of the elastic scattering angular–distribution are in very good agreement with the experimental data, not only the shape of a curve but also the value. These show the obtained optical potential parameters are good. For the energy points where the experimental data are poor, the calculations using these parameters are reliable.

2 The Distorted–Wave Born Approximation

For the neutron inelastic scattering on ^{10}B at the excited state 0.717 MeV, $J^\pi = 1^+$, at the energy range corresponding with the optical model analysis of the elastic scattering, we carried out the calculations by means of a microscopic distorted–wave Born approximation (DWBA). We regard the

interaction as the sum of the constituent nucleon–nucleon interaction and use a finite–range interaction of the form

$$V = \sum_{i=1}^{A} V_{0i}$$

$$V_{0i} = -V_0 [W + MP^{r}_{0i} + BP^{\sigma}_{0i} - HP^{\tau}_{0i}] \exp (-\gamma r^{2}_{0i})$$

where W, B, H, and M are the strength of Wigner, Bartlett, Heisenberg and Majorana force, γ is a parameter of Gaussian potential, r_{0i} is the radial distance, V_0 is the depth of the potential well. The wave functions of shell model are used for the initial and final state function of ^{10}B. The all possible configurations of $1P$ shell have been considered and the state functions of ^{10}B are given in table 2.

Table 2 The state functions of ^{10}B

T	J^{π}	E_x	$P^4\,P'^2$ (03)	$P^4\,P'^2$ (01)	$P^3\,P'^3$ $(\frac{1}{2}\,\frac{5}{2})$	$P^3\,P'^3$ $(\frac{1}{2}\,\frac{1}{2})$	$P^3\,P'^3$ $(\frac{1}{2}\,\frac{3}{2})$	$P^3\,P'^3$ $(\frac{1}{2}\,\frac{7}{2})$
0	3^+	0	0.8450		−0.2320			−0.3595
0	1^+	0.707		−0.2544		0.0016	0.8495	

P^2 (10) P'^4 (13)	P^2 (01) P'^4 (02 $v=2$)	P^2 (01) P'^4 (02 $v=4$)	P^2 (01) P'^4 (04)	P^2 (10) P'^4 (11)	P^2 (01) P'^4 (00)
0.2936	−0.0048	0.0512	0.0797		
	0.1323	0.2480		0.2092	−0.1821

$P\,P'^5$ $(\frac{1}{2}\,\frac{5}{2})$	$P\,P'^5$ $(\frac{1}{2}\,\frac{7}{2})$	$P\,P'^5$ $(\frac{1}{2}\,\frac{1}{2})$	$P\,P'^5$ $(\frac{1}{2}\,\frac{3}{2})$	P'^6 (03)	P'^6 (01)
0.0277	0.0740			0.0388	
		−0.0098	0.2394		0.0143

In the above table E_x is excitation energy of ^{10}B, P' or P express the shell whose spin is $3/2$ or $1/2$, respectively. The wave functions of the harmonic oscillator are used as the radial parts of the state wave functions,

$$R_{nl}(r) = U_{nl}(r)$$

$$U_{nl} = [2V^{l+3/2}(n-1)!/\Gamma(n+l+1/2)]^{1/2}$$

$$r^{l+1}\exp(-Vr^2/2)L_{n-1}^{l+1/2}(Vr^2)$$

After the interaction potentials and wave functions are chosen, we can deduce the calculation formulas of the integral and differential cross sections for neutron inelastic scattering[4]. The adjustable parameters are V_0, γ, M, B, H and ν in the computation. According to previous method[3], the potential parameters V_0 and γ are regarded as energy–dependent.

Because the experimental data of the neutron inelastic scattering for ^{10}B of the first excited state are poor and the Ref. [1] only gave the measured results of the differential cross sections at the range of the big angular, therefore we referred to the data of ENDF / B–6, finally the obtained potential parameters are:

$$V_0 = 54.7798 + 6.3E_n \qquad \gamma = 0.7407 + 0.00139E_n$$
$$M = 0.3923 \qquad B = 0.127 \qquad H = 0.1 \qquad \nu = 0.787$$

The comparison of the calculations of the inelastic scattering angular–distribution of the excited state at 0.717 MeV, $J^\pi = 1^+$ with the experimental data are given in Fig. 2. As illustrated in the Fig. 2, the calculations are in better agreement with the experimental data.

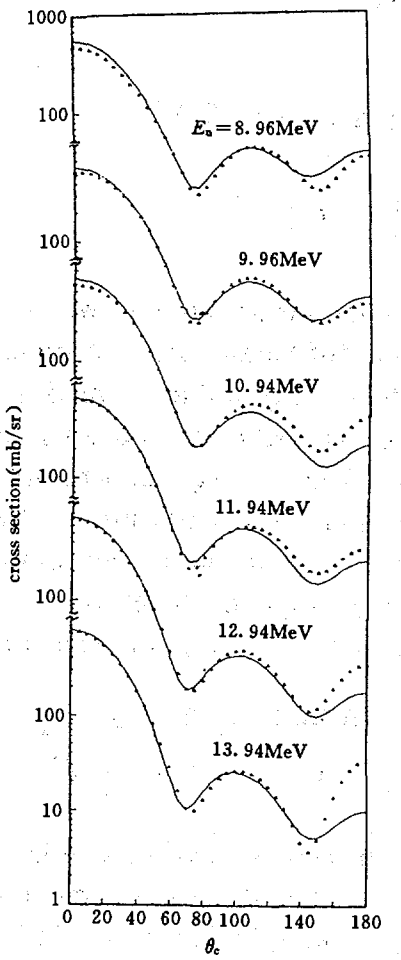

Fig. 1 Angular distributions of elastical scattering neutrons from ^{10}B

▲ S. G. Glendinning[1], — Present work,

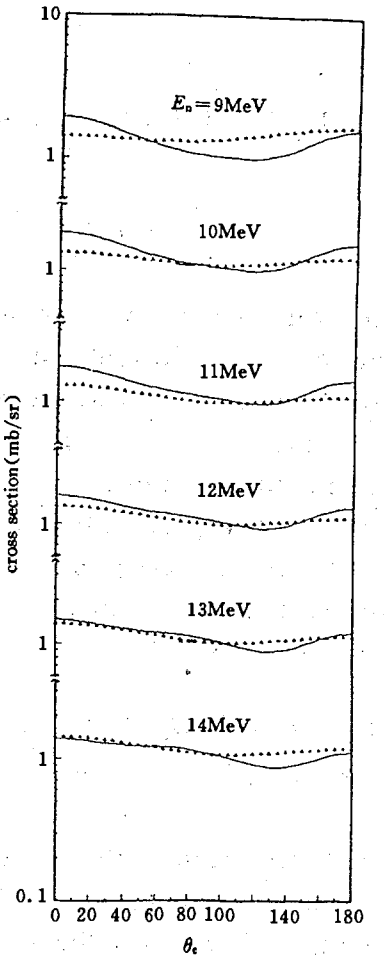

Fig. 2 Angular distributions of inelastical scattering neutrons from the first exited state of ^{10}B (Q = −0.717 MeV)

▲ ENDF / B−6, — Present work.

References

[1] S. G. Glendinning et al., Nucl. Sci. & Eng., 80, 256(1982)

[2] Zhu Yaoyin et al., Communication of Nuclear Data Progress No. 1, 29(1989)

[3] Zhu Yaoyin et al., Communication of Nuclear Data Progress No. 4, 7(1990)

[4] Zhu Yaoyin et al., CNDC, hsj−78217(11js)

Calculation of Cross Sections for Neutron Monitor Reactions of ^{197}Au in Energy Region 0.5～80 MeV

Shen Qingbiao Yu Baosheng Cai Dunjiu

(Chinese Nuclear Data Center, IAE)

Abstract

A set of neutron optical potential parameters for ^{197}Au in energies of 0.5～80 MeV was obtained with available experimental data. In higher energy region the calculated total cross sections have good fitting with the experimental data and the calculated nonelastic scattering cross sections are closed to the measured values of ^{208}Pb; in lower energy region the calculated (n,2n), (n,3n), and (n,4n) cross sections also have good fitting with the experimental data. Therefore, the predicted neutron monitor reaction (n,2n), (n,3n), and (n,4n) cross sections in higher energy region are reasonable and reliable.

Introduction

The need for a consistent set of evaluated neutron cross section data for standard and monitor reactions in the region above 20 MeV was especially stressed. The activation monitor reaction cross sections can be used as a reference standard for the measurements in high energy neutron fields. In the case of the neutron induced monitor reaction of ^{197}Au, the active isotopes ^{196}Au (half life is 6.18 day), ^{195}Au (half life is 186.1 day), and ^{194}Au (half life is 1.64 day) can be produced through (n,2n), (n,3n), and (n,4n) reactions, respectively. Some relative measurement data can be found in EXFOR data below 28 MeV, but now no experimental data for 3 reaction channels mentioned above can be found above 28 MeV. In order to meet the needs of them, the calculation of cross sections of neutron monitor reactions on ^{197}Au in energy region 0.5～80 MeV were performed.

In Sec. 1, the theories and parameters used in our calculation are described. The calculated results and analyses are given in Sec. 2. Finally, a summary is given in Sec. 3.

1 Theories and Parameters

The calculation was made with the program SPEC[1]. In this program, the optical model, evaporation model, and the master equation of exciton model[2] are included. The pre–equilibrium and direct reaction mechanisms of γ emission[3] are also included in this program. The direct inelastic scattering cross sections were obtained by the collective excitation distorted–wave Born approximation[4]. The compound–nucleus elastic scattering contributions were calculated by Hauser–Feshbach model.

Program SPEC includes the first to the sixth particle emission processes.

$$
\begin{aligned}
a + A \rightarrow b + B^{\star},\ & a = n,\ p,\ \alpha,\ d,\ t,\ {}^{3}He, \quad b = n,\ p,\ \alpha,\ d,\ t,\ {}^{3}He,\ \gamma \\
B^{\star} \rightarrow c + C^{\star},\ & c = n,\ p,\ \alpha,\ d,\ t,\ {}^{3}He,\ \gamma \\
C^{\star} \rightarrow d + D^{\star},\ & d = n,\ p,\ \alpha,\ d,\ t,\ {}^{3}He,\ \gamma \\
D^{\star} \rightarrow e + E^{\star},\ & e = n,\ p,\ \alpha,\ d,\ \gamma \\
E^{\star} \rightarrow f + F^{\star},\ & f = n,\ p,\ \gamma \\
F^{\star} \rightarrow g + G^{\star},\ & g = n,\ p,\ \gamma
\end{aligned}
$$

When a particle is emitted, the residual nucleus may emit another particle or γ ray continuously if the excited energy is large enough to overcome the binding energy. In generally speaking, the γ emission cross section is much less than neutron emission cross section when neutron emission channel is open, we assume that after γ ray is emitted the residual nucleus do not emit any particle except after the first γ ray emission process the particle or γ are allowed to be emitted. Thus, 7 channels can be opened for the first emission process, 49 channels for the second emission process, 252 channels for third emission process, 1080 channels for forth emission process, 2592 channels for fifth emission process, and 5184 channels for sixth emission process.

For composite particle emissions, the pick–up mechanism of cluster formation[5~7] was included in the first and second particle emission processes.

Firstly, based on various experimental data of ^{197}Au from EXFOR data a set of optimum neutron optical potential parameters in energy region 0.5~ 80 MeV was obtained as follows:

$$V = 53.69978 - 0.34752E + 0.0017724E^{2} - 24.0(N - Z)/A, \tag{1}$$

$$W_{S} = \min\ \{\ 0, 11.93632 - 0.24632E - 12.0(N - Z)/A\ \}, \tag{2}$$

$$W_{V} = \min\ \{\ 0, -0.845068 + 0.20648E - 0.0014107E^{2}\ \}, \tag{3}$$

$$U_{so} = 6.2, \tag{4}$$

$$r_r = 1.2093, \quad r_s = 1.2814, \quad r_v = 1.4104, \quad r_{so} = 1.2093, \tag{5}$$

$$a_r = 0.69607, \quad a_s = 0.36, \quad a_v = 0.32, \quad a_{so} = 0.69607, \tag{6}$$

Since the charged particle emission cross sections are much less than that of neutron for heavy nuclei ^{197}Au, we adjusted the charged particle optical potential parameters to fit the charged particle cross sections and they hardly affect the neutron emission cross sections.

The Gilbert–Cameron level density formula[8] is applied in our calculations, but some parameters were changed and read as the following

$$U_x = 3.1 + 310/A, \tag{7}$$

$$a = (\ 0.0053 \times S + 0.142\ )A, \tag{8}$$

where S is shell correction factor. At the same time, the exciton model constant K is taken as 2200 MeV^3.

2 Calculated Results and Analyses

Fig. 1 shows the comparison of neutron total cross sections between the calculated values and the experimental data in the energy region 0.5～80 MeV. The theoretical values are in good agreement with the experimental data, especially in higher energy region. Fig. 2 shows the calculated elastic scattering cross sections. The comparisons of calculated neutron elastic scattering angular distributions of ^{197}Au from 0.5 MeV to 14.6 MeV with the experimental data are given in Fig. 3. They are all in very good agreement. Fig. 4 shows the calculated neutron nonelastic cross sections. From Fig. 4 we can see that above 14 MeV there is no nonelastic scattering experimental data. As we know that the nonelastic scattering cross section plays the crucial role in determining the cross sections of the monitor reaction. We found that the measured nonelastic scattering cross sections of ^{208}Pb are 2.35 b and 2.00 b at 55 MeV and 80 MeV, respectively. The calculated nonelastic scattering cross sections of ^{197}Au at these two energy points are very close and less slightly to them. Since the mass number of ^{197}Au is less slightly than that of ^{208}Pb, the calculated results are reasonable. Based on these fitting situation shown in Figs. 1～4, a set of neutron optical potential parameters in the energy region 0.5～80 MeV were determined.

The calculated inelastic scattering cross sections (solid line) including the direct reaction contributions calculated with DWBA method, in which only the

first excited state was considered with $\beta=0.11$ (dashed line) are shown in Fig. 5. Fig. 6 shows the comparison of calculated and experimental (n,γ) cross sections. They are basically in agreement with each other. The (n,γ) cross sections at around 14 MeV are mainly from direct reaction of γ emission (dash line).

The (n,p) and (n,α) cross sections are shown in Fig. 7 and Fig. 8, respectively. The theoretical values are reasonable.

The calculated neutron monitor reaction (n,2n), (n,3n), and (n,4n) cross sections in energy region up to 80 MeV are shown in Figs. 9~ 11. They agree with the experimental data pretty well below 28 MeV energy region except at the threshold nearby.

3 Summary

Based on the available experimental data, a set of neutron optical potential parameters for ^{197}Au in energies of 0.5~ 80 MeV was obtained. Then adjusting some charged particle optical potential and level density parameters as well as taking larger exciton constant, various calculated nuclear data are good in comparison with the experimental data. Therefore, the predicted neutron monitor reaction (n,2n), (n,3n), and (n,4n) cross sections in higher energy region are reasonable and reliable.

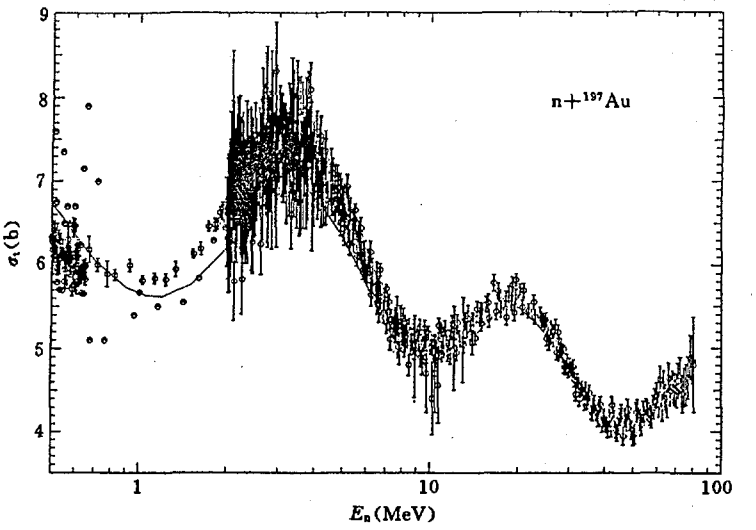

Fig. 1 Comparison of neutron total cross sections of ^{197}Au between the calculated values and the experimental data

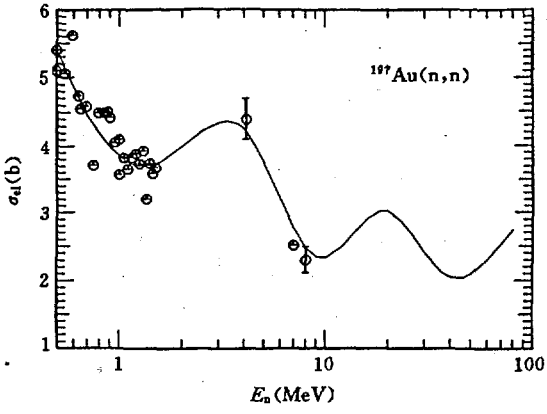

Fig. 2 The same as Fig. 1 but for elastic scattering cross sections

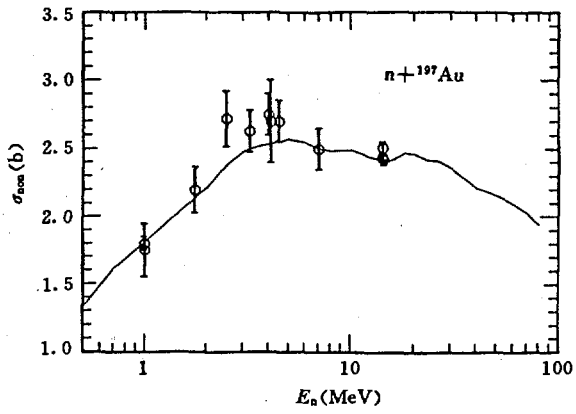

Fig. 4 The same as Fig. 1 but for non-elastic scattering cross sections

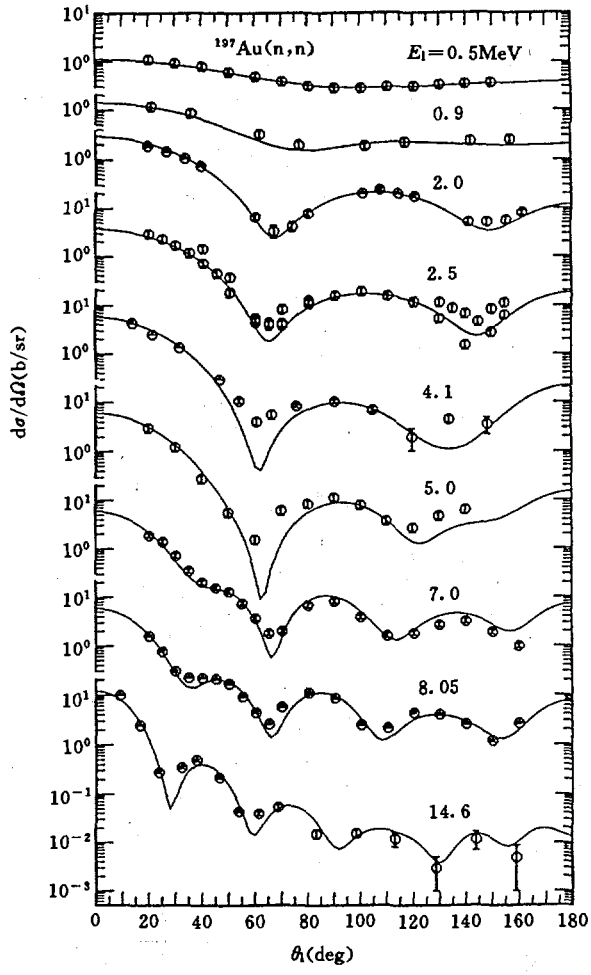

Fig. 3 Comparison of neutron elastic scattering angular distributions of ^{197}Au between the calculated values and the experimental data

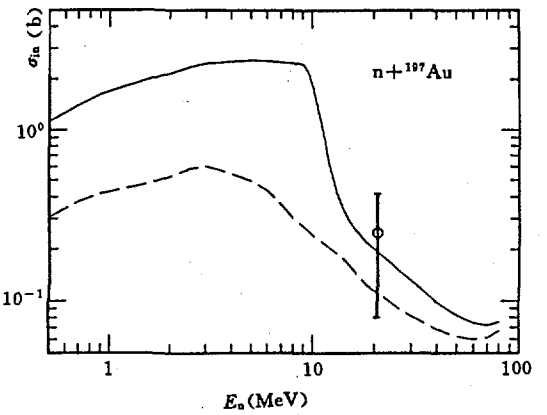

Fig. 5 Comparison of neutron inelastic cross sections of ^{197}Au between the calculated values and the experimental data. The dash line represents the direct reaction contributions

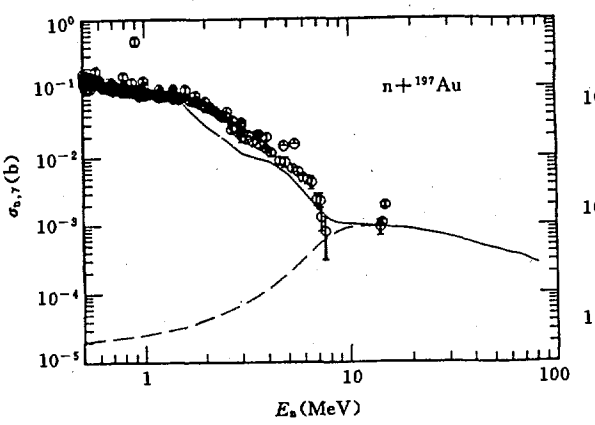

Fig. 6 The same as Fig. 5 but for (n,γ) cross sections

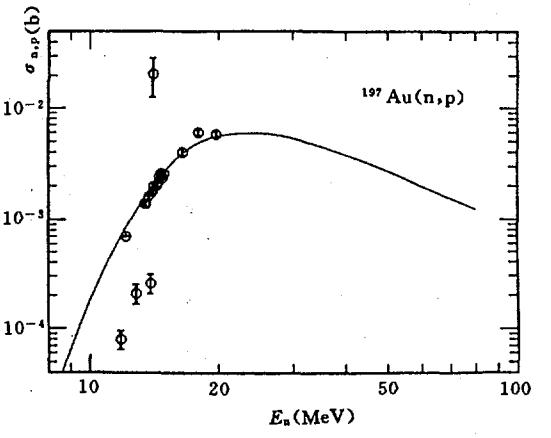

Fig. 7 The same as Fig. 1 but for (n,p) cross sections

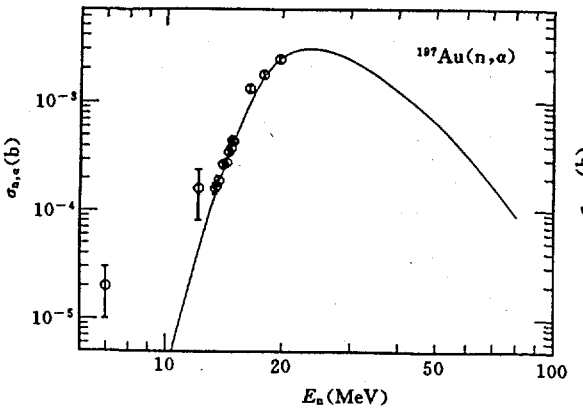

Fig. 8 The same as Fig. 1 but for (n,α) cross sections

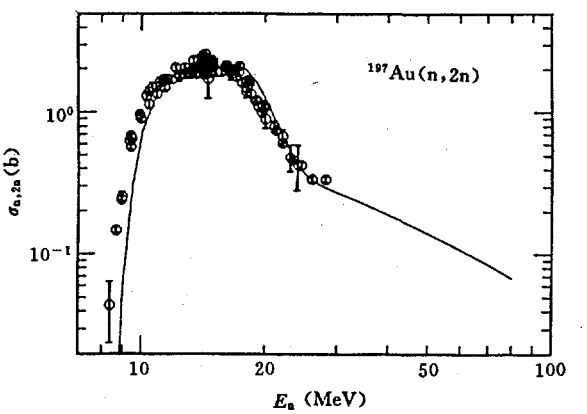

Fig. 9 The same as Fig. 1 but for (n,2n) cross sections

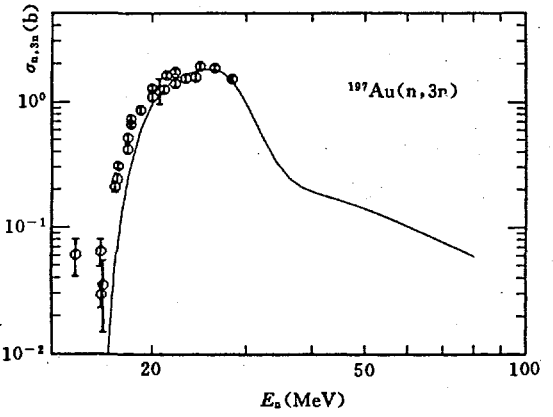

Fig. 10 The same as Fig. 1 but for (n,3n) cross sections

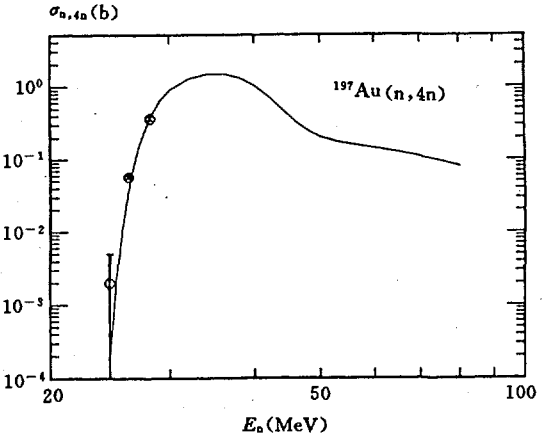

Fig. 11 The same as Fig. 1 but for (n,4n) cross sections

References

[1] Shen Qingbiao et al., unpublished

[2] M. Blann, Ann. Rev. Nucl. Sci., 25, 123(1975)

[3] J. M. Akkermans et al., Phys. Let., 157B, 95(1985)

[4] P. D. Kunz, "Distorted Wave Code DWUCK4", University of Colorado

[5] A. Iwamoto et al., Phys. Rev., C26, 1821(1982)

[6] K. Sato et al., Phys. Rev. C28, 1527(1983)

[7] Zhang Jingshang et al., Commun. in Theor. Phys., (Beijing, China), 10, 33(1988)

[8] A. Gilbert et al., Can. J. Phys., 43, 1446(1965)

III DATA EVALUATION

The Evaluation and Calculations of Intermediate Energy Nuclear Data for ^{56}Fe, ^{63}Cu and $^{65}Cu(p,n)$ Monitor Reactions

Zhuang Youxiang

(Chinese Nuclear Data Center, IAE)

Introduction

There is a considerable interest in medium energy proton reaction data because of applications to astrophysics, neutron source, radiation therapy, isotope production, radiation damage, accelerator shielding, neutral or charged particle beam spectroscopy, etc.[1].

The proton monitor reactions have been widely used in accelerator target flux and beam energy monitoring, medical radioisotope production, researches on radiation damage and activation analysis; and will be as a part of the united references of international nuclear data.

As reported in excitation function experiments, there exist, sometimes,discrepancies between different authors. One of the reasons of these discrepancies would come from the errors of beam intensity measurements. In this respect monitor reactions should be useful in stacked foil activation method. About the monitor to produce medical isotopes, copper, aluminium and iron targets are often used, being these substances also served as a energy degrader. It is necessary to start evaluation for some of the monitor reactions.

1 The Evaluations of Experimental Data and Calculations for ^{56}Fe, ^{63}Cu, $^{65}Cu(p,n)$ Reactions up to 1000 MeV

1.1 General Analyses

The excitation functions of ^{56}Fe, ^{63}Cu, $^{65}Cu(p,n)$ reactions were measured by means of activation method. Stacked target irradiation or energy degradation by foils, beam current integration, chemical separation, separate monitor–foil, coincidence technique, Ge–Li detector, NaI crystal, proportional counter, ionization chamber and G–M counter were used in these experiments.

The experimental data are quite enough for the evaluations up to 1000 MeV or still more.

(1) $^{56}Fe(p,n)^{56}Co$ reaction cross section

The main 10 measurements are as follows:

I. L. Jenkins[2],	2UK HAR(70),	$E_p = 4.8 \sim 39.0$ MeV;
L. P. Remsberg[3],	1USACOL(63),	$E_p = 370$ MeV;
R. Michel[4],	2GERGER(79),	$E_p = 13.43 \sim 44.53$ MeV;
G. V. S. Rayudu[5],	1USACAR(64),	$E_p = 130 \sim 396$ MeV;
E. Gadioli[6],	2ITYMIL(74),	$E_p = 11.1 \sim 44.6$ MeV;
S. Tanaka[7],	2JPNTOK(59),	$E_p = 6.0 \sim 13.7$ MeV;
J. B. J. Read[8],	1USALRL(68),	$E_p = 370$ MeV;
P. Dyer[9],	1USAWAU(81),	$E_p = 5.5 \sim 22.8$ MeV;
G. V. S. Rayudu[10],	1USACAR(68),	$E_p = 500$ MeV;
T. Asano[11],	2JPNTSU(83),	$E_p = 1200$ MeV.

All the experimental data are shown in Figs. 1～2. They coincide with each other within their errors. Thus, the recommended values can be obtained from fitting experimental data.

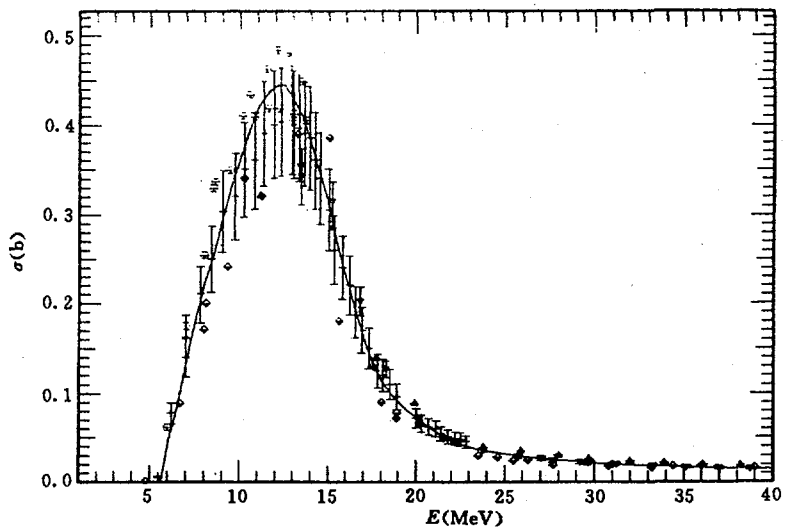

Fig.1 $^{56}Fe(p,n)^{56}Co$ reaction cross section for $E_p = 5.446 \sim 40$ MeV

—— Fitted curve, ◇ I. L. Jenkins(70), ▽ R. Michel et al.(79),

△ E. Gadioli(74), ○ S. tanaka(59), + P. Dyer et al.(81).

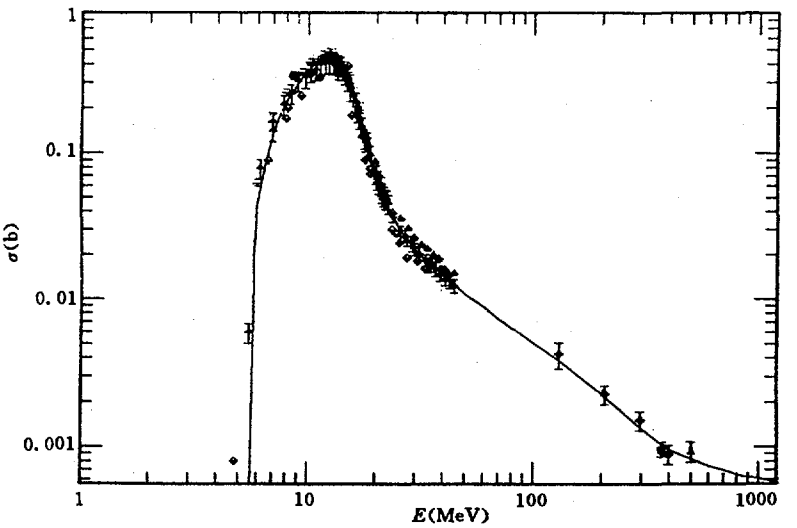

Fig.2 $^{56}Fe(p,n)^{56}Co$ reaction cross section for $E_p = 5.446 \sim$ 1200 MeV

—— Fitted curve, ◇ I. L. Jenkins(70), ▽ L. P. Remsberg(63),

× I. Asano et al.(83), † P. Dyer et al.(81), ⅄ G. V. S. Rayudu(68),

△ E. Gadioli(74), ○ S. tanaka(59), + J. B. J. Read(68),

* R. Michel et al.(79), ◆ G. V. S. Rayudu(64).

(2) $^{63}Cu(p,n)^{63}Zn$ reaction cross section

There are 16 measurements:

M. E. Sevior[12],	3AULAML(83),	E_p=4.246~4.833 MeV;
J.-P. Blaser[13],	2SWTETH(51),	E_p=4.22~6.30 MeV;
J. W. Meadows[14],	1USAHRV(53),	E_p=5.0~99.2 MeV;
M. Hille[15],	2GERMUN(72),	E_p=8.7~15.8 MeV;
R. M. Humes[16],	1USAOSU(63),	E_p=6.75 MeV;
D. J. Reuland[17],	1USACAR(69),	E_p=400 MeV;
J. Wing[18],	1USAORL(60),	E_p=4.5~10.5 MeV;
C. H. Johnson[19],	1USABRK(50),	E_p=4.240~5.780 MeV;
S. N. Ghoshal[20],	1USAANL(62),	E_p=3.9~22.1 MeV;
H. Taketani[21],	1USAROC(62),	E_p=4.20~6.56 MeV;
R. Colle[22],	1USACLA(58),	E_p=3.99~25.02 MeV;
H. A. Howe[23],	1USABNL(74),	E_p=4.5~11.4 MeV;
G. A. Jones[24],	2UK HAR(61),	E_p=9.85 MeV;
K. F. Chackett[25],	2UK BIR(62),	E_p=9.3 MeV;
L. F. Hansen[26],	1USALRL(62),	E_p=6.0~11.0 MeV;
E. P. Steinberg[27],	1USAANL(73),	E_p=1.5~11.5 GeV.

In Figs. 3~4, the measured data are shown. The agreement among them is good, except two early measurements in 1950 and 1953. However, dispersion at peak is still remarkable, and it stands in need of theoretical calculation.

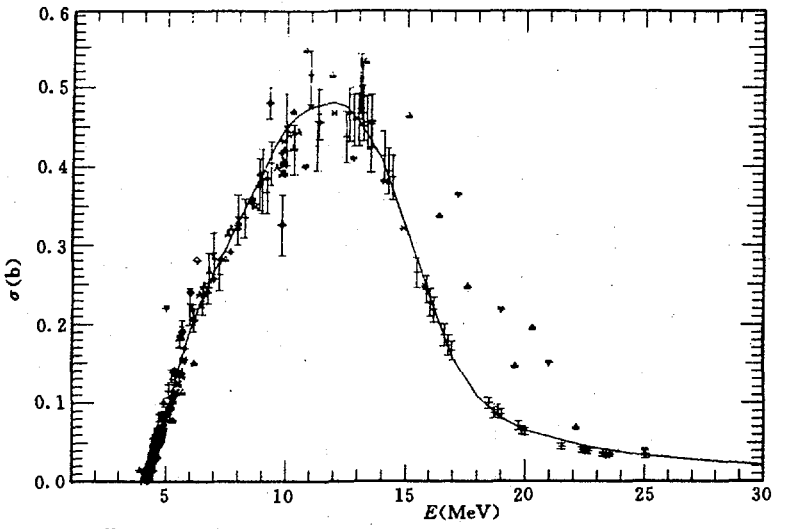

Fig. 3 $^{63}Cu(p,n)^{63}Zn$ reaction cross section for $E_p = 4.214 \sim 30$ MeV

—— Fitted curve, □ M. E. Sevior(83), ◇ J. −P. Blaser(51),
▽ J. W. Meadows(53), × M. Hille(72), † R. M. Humes(63), D. J. Reuland(69),
⅄ J. Wing(62), ✖ C. H. Johnson(60), ▲ S. N. Ghoshal(50),
○ H. Taketani(62), + R. Colle(74), * H. A. Howe(58),
◆ G. A. Jones(61), K. F. Chackett(62), Y L. F. Hansen(62).

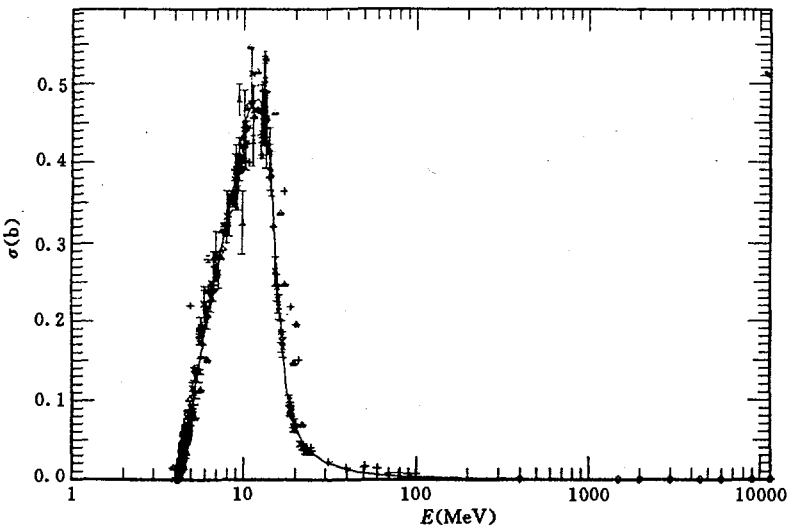

Fig. 4 $^{63}Cu(p,n)^{63}Zn$ reaction cross section for $E_p = 4.214 \sim 11500$ MeV

—— Fitted curve, □ M. E. Sevior(83), ◇ E. P. Steinberg(73),
▽ H. Haketani(62), × R. Colle(74), † H. A. Howe(58),
⅄ G. A. Jones(61), K. F. Chackett(62), ✖ L. F. Hansen(62), △ S. N. Ghoshal(50),
○ J. −P. Blaser(51), + J. W. Meadows(53), * M. Hille(72),
◇ R. M. Humes(63), D. J. Reuland(69), Y J. Wing(62), — C. H. Johnson(60).

(3) $^{65}Cu(p,n)^{65}Zn$ reaction cross section

Altogether 17 measurements from 1950 to 1985 were collected. There exist big discrepancies among reported excitation functions, see Figs. 5～ 6. They were divided into two groups. These experiments are as follows:

M. E. Sevior[12],	3AULAML(83),	E_p=2.180～3.217 MeV;
E. Gadioli[6],	2ITYMIL(74),	E_p=10.2～44.3 MeV;
J.–P. Blaser[13],	2SWTETH(51),	E_p=2.77～6.31 MeV;
H. A. Howe[23],	1USACLA(58),	E_p=6.4～11.4 MeV;
J. Wing[18],	1USAANL(62),	E_p=4.5～10.5 MeV;
C. H. Johnson[19],	1USAORL(60),	E_p=2.225～5.780 MeV;
G. Albouy[28],	2FR PAR(62),	E_p=45.5～142.0 MeV;
P. Kopecky[29],	3CSRUJV(85),	E_p=4.42～32.40 MeV;
C. H. Johnson[30],	1USAORL(58),	E_p=2.171～2.544 MeV;
R. Colle[22],	1USABNL(74),	E_p=2.86～25.02 MeV;
G. F. Dell[31],	1USAOSU(65),	E_p=6.75 MeV;
B. W. Shore[32],	1USAMIT(61),	E_p=7.5 MeV;
G. A. Jones[24],	2UK HAR(61),	E_p=9.85 MeV;
K. F. Chackett[25],	2UK BIR(62),	E_p=9.3 MeV;
L. F. Hansen[26],	1USALRL(62),	E_p=5.0～11.0 MeV;
M. W. Greene[33],	1USABNL(72),	E_p=16.0～32.8 MeV;
P. Pulfer[34],	2SWTUBE(79),	E_p=15.53～70.92 MeV.

It is necessary for $^{65}Cu(p,n)^{65}Zn$ reaction to do theoretical calculation and further evaluation, in order to get a correct judgement.

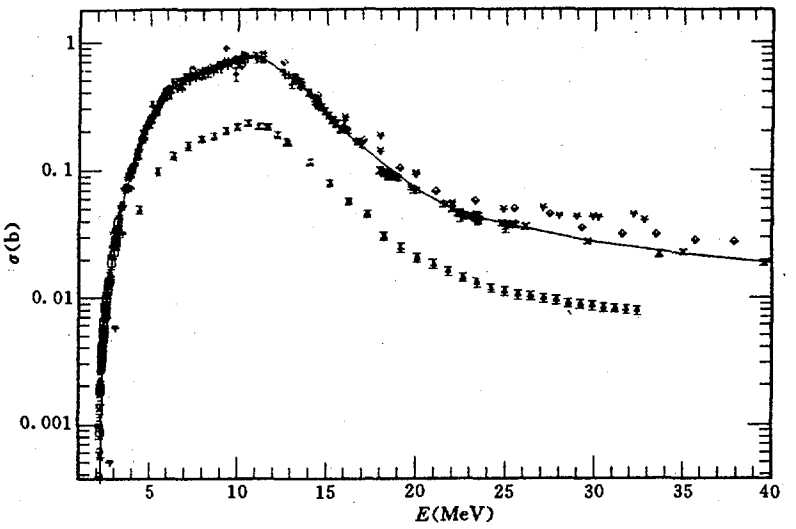

Fig. 5 $^{65}Cu(p,n)^{65}Zn$ reaction cross section for $E_p = 2.166 \sim 40$ MeV

—— Fitted curve, □ M. E. Sevior(83), ◇ E. Gadioli(74),
▽ J. -P. Blaser(51), × H. A. Howe(58), † J. Wing(62),
⅄ C. H. Johnson(60), ✱ P. Pulfer(79), ▲ P. Kopecky(85),
○ C. H. Johnson(58), + R. Colle(74), * Dell, Shore, Jones and Chackett,
◇ L. F. Hansen(62), Y M. W. Greene(72).

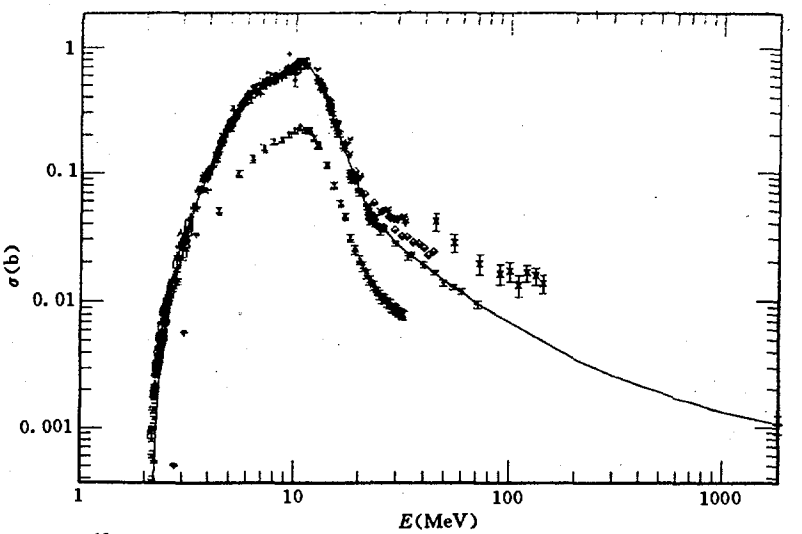

Fig. 6 $^{65}Cu(p,n)^{65}Zn$ reaction cross section for $E_p = 2.166 \sim 1820$ MeV

—— Fitted curve, □ M. E. Sevior(83), ◇ E. Gadioli(74),
▽ J. -P. Blaser(51), × H. A. Howe(58), † J. Wing(62),
⅄ C. H. Johnson(60), ✱ G. Albouy(62), ▲ P. Kopecky(85),
○ C. H. Johnson(58), + R. Colle(74), * Dell, Shore, Jones and Chackett,
◇ L. F. Hansen(62), Y M. W. Greene(72), — P. Pulfer(79).

1.2 Theoretical Calculation

(1) $^{63}Cu(p,n)^{63}Zn$ reaction

$^{63}Cu(p,n)^{63}Zn$ reaction cross sections for $E_p < 55$ MeV were calculated[35] with the aid of code CMUP2[36], which is based on optical model, H–F theory with width fluctuation correction and the unified treatment of exciton model and evaporation model. CMUP2 code is more suitable for $E_p < 55$ MeV than code ALICE.

The comparison for theoretical calculated results and experimental data of $^{63}Cu(p,n)^{63}Zn$ reaction cross section is given in Fig. 7. The calculated value at peak is about 480 mb at 12 MeV.

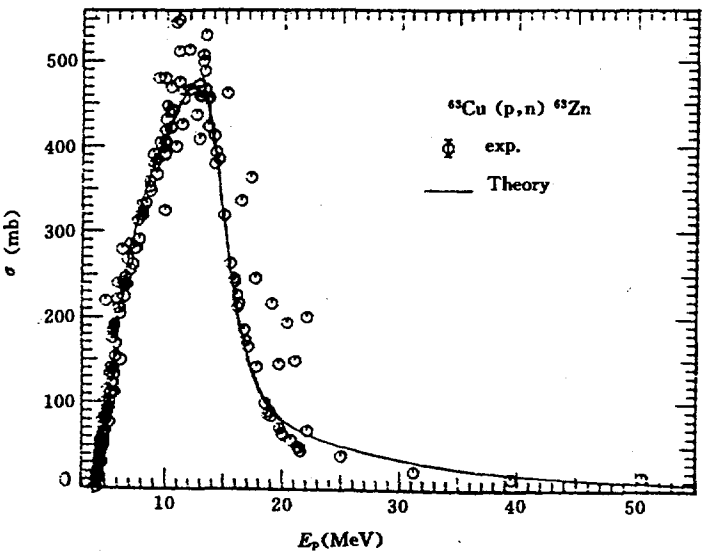

Fig. 7 Comparison of calculated $^{63}Cu(p,n)^{63}Zn$ reaction cross section by code CMUP2 with experimental data for $E_p = 5.446 \sim 55$ MeV

(2) $^{65}Cu(p,n)^{65}Zn$ reaction

The excitation function of $^{65}Cu(p,n)^{65}Zn$ reaction were calculated by the code ALICE91[37] up to $E_p = 200$ MeV. The evaporation calculations were

performed according to Weisskopf and Ewing. The nuclear masses were calculated from the Meyers and Swiatecki mass formula, including shell corrections and pairing effects. The level density parameters were taken from the work of Ignatyuk. The inverse cross sections were calculated by using the optical model. For the pre-equilibrium reactions the geometry dependent hybrid model option was chosen.

It is understood that theoretical results are inclined to the higher group data, see Fig. 8.

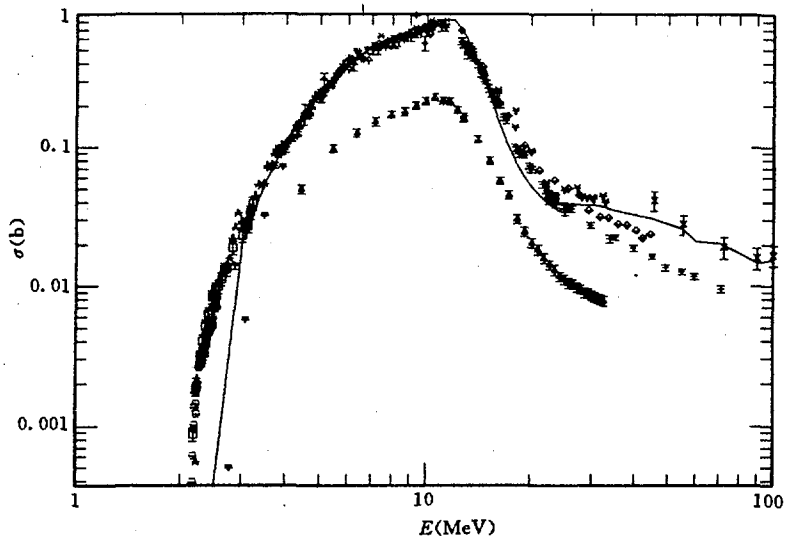

Fig. 8 Comparison of calculated $^{65}Cu(p,n)^{65}Zn$ reaction cross section by code ALICE91 with experimental data for E_p = 2.166 ~ 100 MeV

—— Alice91, □ M. E. Sevior(83), ◇ E. Gadioli(74),
▽ J.-P. Blaser(51), × H. A. Howe(58), ↑ J. Wing(62),
人 C. H. Johnson(60), ✱ G. Albouy(62), ▲ P. Kopecky(85),
○ C. H. Johnson(58), + R. Colle(74), * Dell, Shore, Jones and Chackett,
◇ L. F. Hansen(62), Y M. W. Greene,(72), — P. Pulfer(79).

2 Recommendation and Errors

2.1 The recommended values based on experimental data of $^{56}Fe(p,n)^{56}Co$ reaction cross sections were obtained by spline function code[38] with knot optimization, see Figs. 1~2.

2.2 With reference to CMUP2's calculation, the recommended data of $^{63}Cu(p,n)^{63}Zn$ reaction excitation functions were given from fitting experimental values, and shown in Figs. 3~4.

2.3 The higher group data of $^{65}Cu(p,n)^{65}Zn$ reaction cross sections were selected. The reasons are as follows:

(1) In the experiments of $^{65}Cu(p,n)^{65}Zn$ reaction excitation functions, M. E. Sevior[12], J. -P. Blaser[13], J. Wing[18], C. H. Johnson[19], R. Colle[22], H. A. Howe[23], G. A. Jones [24], K. F. Chackett[25] and L. F. Hansen[26] had also measured those of $^{63}Cu(p,n)^{63}Zn$ reaction, and E. Gadioli[6] also measured that of $^{56}Fe(p,n)^{56}Co$ reaction. All of them are in agreement and adopted as basic experimental data of $^{63}Cu(p,n)^{63}Zn$ and $^{56}Fe(p,n)^{56}Co$ reactions, respectively. Therefore, above-mentioned data for $^{65}Cu(p,n)^{65}Zn$ reaction should not be removed;

(2) ALICE91's calculated results prefer the higher group data.

The recommended values of $^{65}Cu(p,n)^{65}Zn$ reaction excitation functions were based on experimental data, except P. Kopecky's, see Figs. 5~6.

2.4 The smallest cited errors for $^{56}Fe(p,n)^{56}Co$ and $^{63}Cu(p,n)^{63}Zn$ reactions are about 5%, because almost all measurements had been done with accuracies of 7 ~ 12%; for $^{65}Cu(p,n)^{65}Zn$ reaction about 8%, due to big discrepancies among experimental data.

References

[1] S. Pearlstein, BNL-NCS-38404(1986)
[2] I. L. Jenkins et al., J. Inorg. Nucl. Chem. 32, 1419(1970)
[3] L. P. Remsberg et al., Phys. Rev. 130, 2069(1963)
[4] R. Michel et al., Nucl. Phys. A322, 40(1979)
[5] G. V. S. Rayudu, Can. J. Chem. 42, 1149(1964)
[6] E. Gadioli et al., Nuovo Cimento A22, 547(1974)
[7] S. Tanaka et al., J. Phys. Soc. Japan 14, 1269(1959)
[8] J. B. J. Read, J. Inorg. Nucl. Chem. 30, 2039(1968)
[9] P Dyer et al., Phys. Rev. C23,1865(1981)
[10] G. V. S. Rayudu, Inorg. Nucl. Chem. 30, 2311(1963)
[11] T. Asano et al., Phys. Rev. C28, 1840(1983)
[12] M. E. Sevior et al., Australian J. Phys. 36, 463(1983)

[13] J. −P. Blaser et al., Helvetica Physica Acta 24, 3(1951)
[14] J. W. Meadows, Phys. Rev. 91, 885(1953)
[15] M. Hille et al., Nucl. Phys. A198, 625(1972)
[16] R. M. Humes et al., Phys. Rev. 130, 1522(1963)
[17] D. J. Reuland et al., J. Inorg. Nucl. Chem. 31, 1915(1969)
[18] J. Wing et al., Phys. Rev. 128, 280(1962)
[19] C. H. Johnson et al., ORNL−2910(1960)
[20] S. N. Ghoshal, Phys. Rev. 80, 939(1950)
[21] H. Taketani et al., Phys. Rev. 125, 291(1962)
[22] R. Colle et al., Phys. Rev. C9, 1819(1974)
[23] H. A. Howe, Phys. Rev. 109, 2083(1958)
[24] G. A. Jones et al., TID−12696(1961)
[25] K. F. Chackett et al., Proc. Phys. Soc. 80, 738(1962)
[26] L. F. Hensen et al., Phys. Rev. 128, 291(1962)
[27] E. P. Steinberg et al., Phys. Rev. C7, 1410(1973)
[28] G. Albouy et al., J. Phys. Radium 23, 1000(1962)
[29] P. Koprcky, Intern. J. Applied Radiation & Isotopes 36, 657(1985)
[30] C. H. Johnson et al., Phys. Rev. 109, 1243(1958)
[31] G. F. Dell et al., Nucl. Phys. 64, 513(1965)
[32] B. W. Shore et al., Phys. Rev. 123, 276(1961)
[33] M. W. Greene et al., Intern. J. Applied Radiation & Isotopes 23, 342(1972)
[34] P. Pulfer, T. Pulfer 1979 in German
[35] Han Yinlu et al., INDC(CPR)−027 / L, p. 45, (1992)
[36] Cai Chonghai et al., INDC(CPR)−030 / L, p. 21, (1993)
[37] M. Blann et al., CODE ALICE / LIVERMORE 91
[38] Liu Tingjin et al., At. Energy Sci. & Technol. 1, 15(1990)

Revision on Recommended Data of ^{238}U for CENDL-2 in 1993 Version

Tang Guoyou Shi Zhaomin Shu Nengchuan
Zang Guohui Chen Jinxiang

(IHIP, Peking University)

The evaluation of neutron data of ^{238}U was revised in 1993. A great change of new version is that recommended data of a complete set were calculated by code FMT[1]. This program written by Zhang Jingshang is based on semi-classical theory of multi-step nuclear reaction processes. Some details of changes are as follows:

1. New files 6, 12, 13, 15 are included: They were taken from theoretical calculated data.
2. For neutron cross sections in range 50.0 keV to 20.0 MeV:

A) Total and partial inelastic scattering (MT = 51, 52, ···, 76, 91) data were got from theoretical calculation. Coupled-channel model code was used for calculating direct process of the first and second levels. It was completed by Shen Qingbiao[2]. Other levels were calculated by code DWUK4.

B) For (n,2n) reaction, the calculated data from code FMT were adopted.

The fission parameters used in this calculation were fission barrier *VF*, fission curvature parameter *HW* and coefficients of fission level density *CKF* as the following:

	1st fission	2nd fission	3rd fission	4th fission
VF	5.7534	5.3720	5.5324	6.4044
HW	0.4854	0.5525	0.6025	0.5600
CKF	9.1232	0.5339	3.5191	0.2837

Present recommended data for some reaction channels are compared with ENDF / B-6 and experimental data[3~8], see Figs. 1~6.

The comparisons of calculated neutron spectra at incident energies of 2.0, 14.2 and 18.0 MeV with experimental data[9~11] are shown in Figs. 7~9.

Acknowledgement

We thank Prof. Zhang Jingshang for giving us a great help in theoretical calculation.

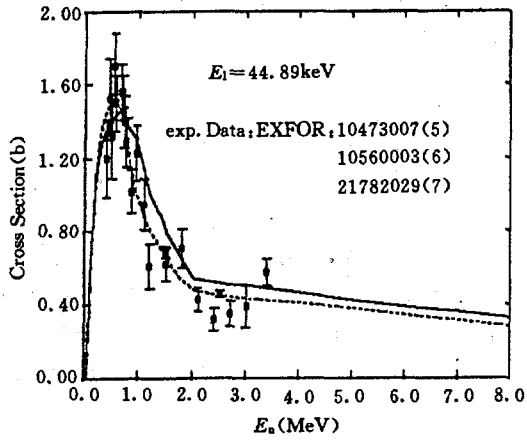

Fig. 1 Compared with ENDF / B-6 for E_l = 44.89 keV inelastic scattering
——— Present work, – – – ENDF / B-6.

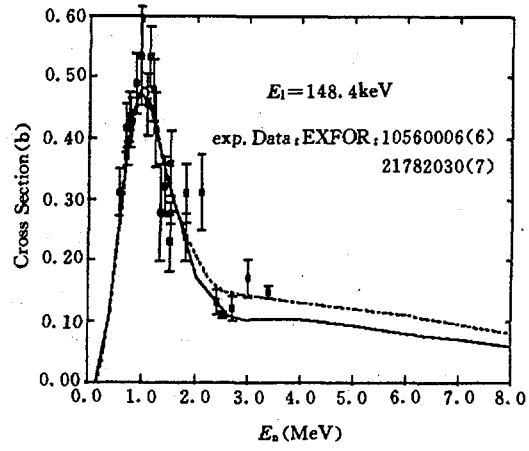

Fig. 2 The same as Fig. 1 but for E_l = 148.4 keV

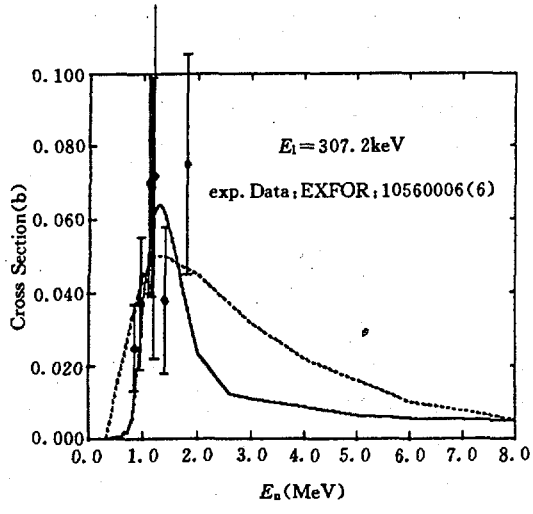

Fig. 3 The same as Fig. 1 but for E_l = 307.2 keV

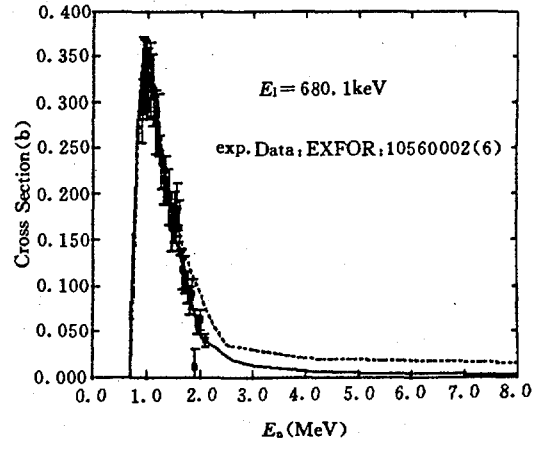

Fig. 4 The same as Fig. 1 but for E_l = 680.1 keV

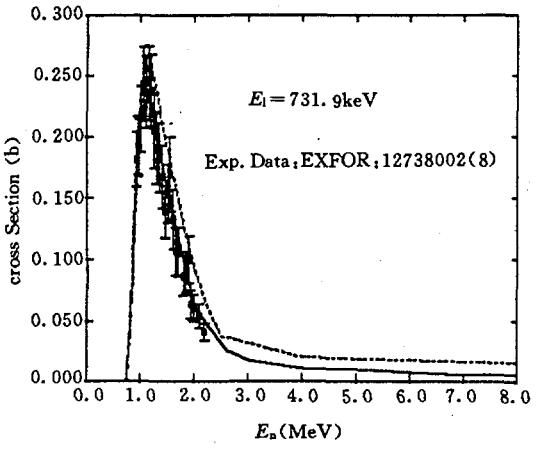

Fig. 5 The same as Fig. 1 but for E_l = 731.9 keV

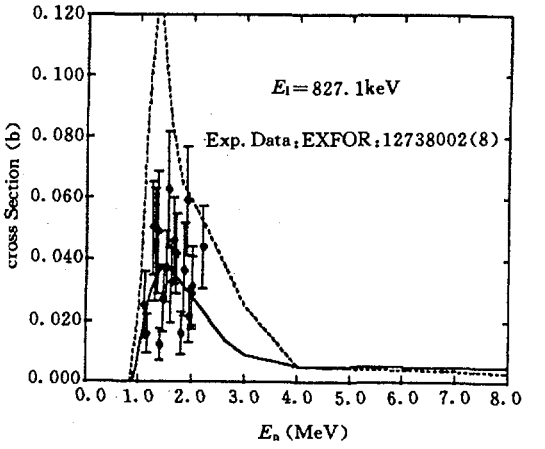

Fig. 6 The same as Fig. 1 but for E_l = 827.1 keV

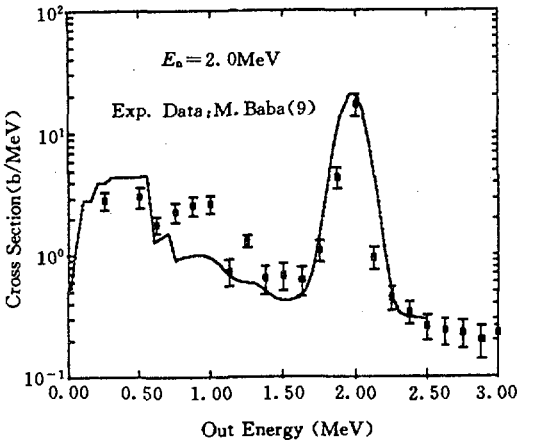

Fig. 7 Calculated secondary neutron spectrum compared with experimental data at E_n = 2.0 MeV

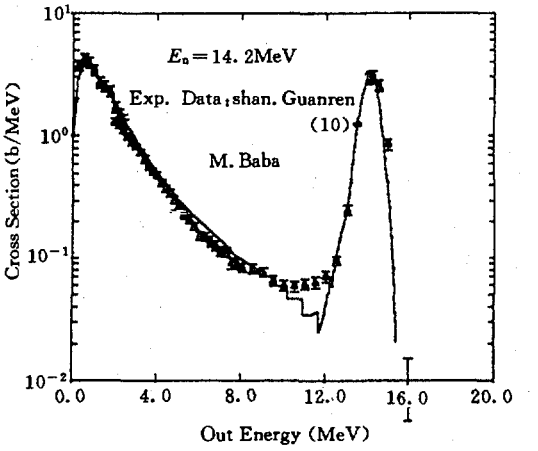

Fig. 8 Calculated secondary neutron spectrum compared with experimental data at E_n = 14.2 MeV

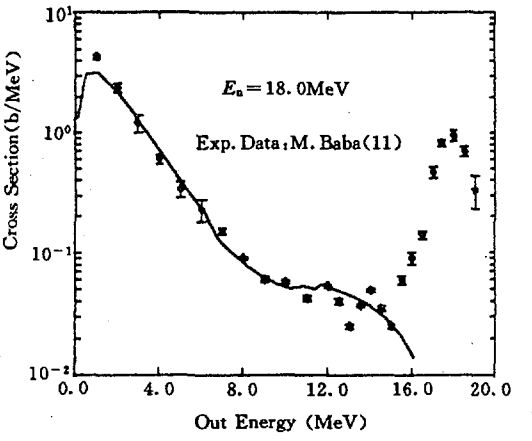

Fig. 9 Calculated secondary neutron spectrum compared with experimental data at E_n = 18.0 MeV

References

[1] Zhang Jingshang, INDC(CPR)–027 / L, p. 14 (1992)

[2] *Shen Qingbiao, INDC(CPR)–029 / L*, p. 35 (1992)

[3] M. Baba et al., JAERI–M–89–143 (1989)

[4] R. Batchelor et al., NP, 65, 236(1965)

[5] L. E. Beghian et al., NSE, 69, 191(1979)

[6] P. Guenther et al., ANL–NDM–16(1975)

[7] G. Haouat et al., NSE, 81(4) 491(1982)

[8] J. Q. Shao et al., NSE, 92, 350(1986)

[9] M. Baba et al., JAERI–M89–026 p. 87

[10] Shen Guanren et al., Proc. of Inter. Conf. on Nucl. Data for Sci. & Tech., Mito, Japan, p. 201, (1988)

[11] M. Baba et al., INDC(JPN)–153 / U, p. 109, (1991)

Neutron Data Analysis and Recommendation for ^{235}U

Yu Baosheng Cai Dunjiu

(Chinese Nuclear Data Center, IAE)

Introduction

A complete set of neutron nuclear data of ^{235}U has been recommended from 10^{-5} eV to 20 MeV energy range for CENDL–2. The recommended data of ^{235}U were mainly taken from ENDF / B–6, except the (n,2n), (n,3n) reaction cross sections and $\bar{\nu}$ values which were taken from our evaluation. The evaluated (n,2n), (n,3n) reaction cross sections and $\bar{\nu}$ values were obtained based on new experimental data and benchmark testing results. The comparison of our evaluated data with other evaluations has been performed.

1 Data Evaluation and Adjustment

1.1 ^{235}U(n,2n) and (n,3n) Reaction Cross Sections

For ^{235}U(n,2n) and (n,3n) reaction cross sections the experimental data could be found only at few energy points[1, 2] in CENDL–1, therefore all the recommended values were taken from model calculation. Recently, the experimental data from their threshold energies to 20 MeV were measured by Frehaut[3] using the large liquid scintillation method.

These experimental data[2~4] were collected and analysed, and then they were fitted with orthogonal polynomial method. The present fitting values were compared with the evaluated data from ENDF / B–6 and JENDL–3. The present fitting values are consistent with the experimental data very well among these evaluated data, therefore were adopted as recommended data of CENDL–2, see Fig. 1 and Fig. 2.

1.2 Evaluation of Nu–bar Values

The evaluation $\bar{\mu}$ for ^{235}U was obtained from a recent evaluation[5]. The $\bar{\nu}$ values was able to improve some benchmark testing results and adopted in ENDF / B–6.

To validate or improve the knowledge of the microscopic data, the integral experiments are an efficient tool. Integral qualification of nu-bar for ^{235}U were made by Tellier[6] using the well known tendency research method. Prompt neutron yields at neutron energies below 1 keV for ^{235}U show a flat shape. And all the evaluated libraries adopt a constant value below 1 keV. The application of the tendency values and the experimental ones suggests a minor modification of the initial neutron data. The optimum values of total nu-bar for ^{235}U which give the best agreement with the integral experiment were obtained by means of the effective multiplication coefficient method.

According to the results of the tendency research by Tellier[6] it was shown that the 2.434 values of total nu-bar was satisfactory to thermal neutron physicists. Therefore, the total nu-bar values for thermal neutron are complementary to the microscopic experiment. Based on the results as mentioned above at thermal neutron energies, the 2.432 value of total nu-bar from ENDF / B-6 should be revised. Thus, in present evaluation, the corrected total nu-bar values were adopted.

1.3 Scattering Angular Distribution

There are experimental data from 0.3 MeV to 5.5 MeV and 14.0 MeV. The experimental data were fitted by using Legendre polynomial and adjusted the optical model parameter so as to represent experimental data very well. Based on our evaluation, the Legendre polynomial coefficients from ENDF / B-6 were tested and compared with experimental data. And only at a few energies the differential cross sections calculated from Legendre coefficients were unreasonable in physics, the recommended values were corrected.

2 Data Treatment and Recommendation

In present evaluation, although the data taken basically from ENDF / B-6, but some cross sections and parameters were evaluated and modified. In order to meet self consistent condition in physics, the elastic scattering cross sections were obtained by subtracting the nonelastic cross section from the total cross section. The adjusted results shown that the cross sections were kept in their smooth and continuum.

Acknowledgments

The one of authors would like to thank Dr. H. Matsunobu for his helpful

discussion on the evaluation of ^{235}U in JAERI / NDC. They are also grateful to Dr. Liu Guisheng for his discussion on benchmark testing results, and Drs. Liang Qichang, Liu Tong for using their codes.

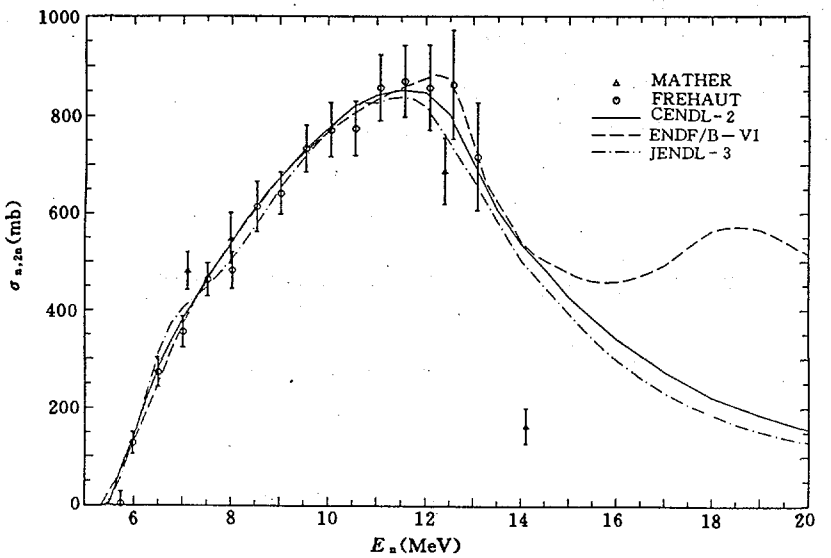

Fig. 1 Comparison among evaluated data with experimental data for $^{235}U(n,2n)$ reaction cross section

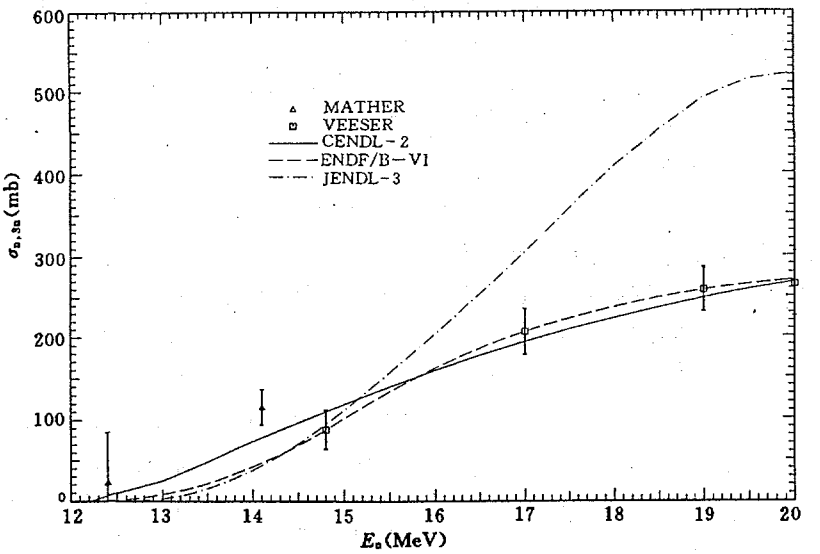

Fig. 2 Comparison among evaluated data with experimental data for $^{235}U(n,3n)$ reaction cross section

References

[1] N. M. Larson et al., Proc. of Conf. on Nucl. Data for Sci. and Tech., p. 573 (1988), Mito, Japan

[2] D. S. Mather, AWRE 072 / 72 (1972)

[3] J. Frehaut, Nucl. Sci. Eng., 74, 29(1990)

[4] L. R. Veeser, Phys. Rev. C, 16, 16(1977)

[5] R. Mcknight et al., INDC / P(90)–39, (1990)

[6] H. Tellier, INDC(NDS)–251 (1991)

Evaluation of $^{181}Ta(n,2n)^{180,180m}Ta$ Reaction Cross Sections

Cai Dunjiu Huang Xiaolong

(Chinese Nuclear Data Center, IAE)

Tantalum is an important material for fission and fusion reactors, and the nuclear data for Ta are very significant in nuclear technology applications, because it has high temperature melting point and high neutron multiplicity.

The excitation function of $^{181}Ta(n,2n)^{180}Ta$ reaction evaluated covers neutron energy range from threshold (7.6758 MeV) to 24 MeV. Three sets of measured data available[1~3] are collected and shown in table 2 and Fig. 2. The agreement among these values is satisfactory.

The $^{181}Ta(n,2n)^{180m}Ta$ reaction is suitable for measuring neutron spectra with $E_n \approx 9 \sim 20$ MeV, because it has large cross section, suitable half–life for measurement and smooth shaped excitation function with low threshold. However, since the γ–ray energies from ^{180m}Ta decay are very low, the activity measurements of them are difficult. Even very thin samples are used, the corrections of self–absorption of γ–ray in sample are also large. This makes the measured data scattered.

Seventeen sets of measured data available[4~18] are collected and listed in table 1, showing a huge spread from 867 mb[20] to 2740 mb[19] around 14 MeV. This is mainly due to determining the quantity of ^{180m}Ta product. Brzosko et

al.[17], Ryves et al.[8]and Lu Hanlin et al.[4, 5] have pointed out the influence of the decay scheme for ^{180m}Ta assumed in the measurement. Three different decay schemes, that is, Brown's[22], Gallagher's[21] and Ryves'[8] were used in the measurements. In order to examine the influence of the decay scheme on the cross section, we tried to normalize the cross sections of Lu Hanlin et al.[5], Ikeka et al.[7], Ryves et al.[8], Csikai[9], Bormann et al.[1], Brzosko et al.[17] and Prestwood et al.[18] using the decay scheme of Ryves[8], and the normalized data are given in table 1 and Fig. 1. It is obvious that the good agreement is obtained among the data sets (around 14 MeV) except the Brzosko's result which is higher than others (no matter if the measurements were performed by counting β or γ_c or both γ_a and γ_c radiation). Therefore, the decay scheme of Ryves is considered superior to the other two decay schemes of Brown et al.[22] and Gallagher et al.[21] which had been performed many years before β–ray spectrometers and NaI(Tl) crystals were used. We adopted the decay scheme of Ryves (see table 3) as a base for our evaluation. The other authors did not give the parameters used in data analysis (especially decay scheme data), so their data are not used in this evaluation.

Because there are some great gaps in the existing data on the ^{181}Ta(n,2n)^{180m}Ta reaction, it is not easy to recommend a best value for these cross sections. However, a better evaluated value may be obtained by fitting the measured data with theoretical calculation and systematic study in order to fill these gaps. Present evaluation is mainly based on the data of Lu [4~6] and Ryves[8], as well as the shape of Ikeda[7], Csikai[9] and Prestwood[18]. All the experimental results were adjusted by the unified nuclear decay data, the reference cross section and the dependence of cross section on energy taking from Ref. [4].

Because the careful investigation was made for the measured data of ^{181}Ta(n,2n)^{180,180m}Ta reaction, present evaluation shown in Fig. 1 appears to describe the cross section of ^{181}Ta(n,2n)^{180m}Ta reaction better, and quite differed from Bychkov's result[24]. It's also noticed that Yao's result[23] was improved by present evaluation.

The uncertainties and their correlations for measured quantities of the ^{181}Ta(n,2n)^{180,180m}Ta reactions among the various data sets were analyzed and considered. The correlation matrix for the evaluated data are given in table 4.a and table 4.b[25].

Table 1 Survey of measured cross sections for $^{181}Ta(n,2n)^{180m}Ta$ reaction

Year	Author	E_n (MeV)	Cross-section (mb)		Adjusted Factor			Method	
			Published	Adjusted	*F*1	*F*2	*F*3	Fluence	Activity
1989	Zhao Wenrong Lu Hanlin+	14.59 ± 0.2 (12.32~18.25)	1239 ± 30	1239	1	1	1	Al(n,α) AP	NaI(Tl) 80×Φ80mm Ge(Li) 136 cm³ Kx $\gamma_a+\gamma_c$
1987 1985	Lu Hanlin+	14.61 ± 0.31 (12.3~18.3)	1269 ± 46						
		8.5 ± 0.22	243 ± 18	262.5	1	1.0801	1		
1988	Y.Ikeda+	14.66 (13.33~14.92)	1307 ± 78	1499.3	1	0.9796	1.1710	Al(n, α)	Ge(Li)
1980	T.B.Ryves+	14.68	1307 ± 40	1290.4	1	0.9873	1	$^{56}Fe(n,p)$	Ge(Li) γ_c $4\pi\beta$ PC
1982	J.Csikai+	14.66 (13.5~14.78)	2154 ± 187	1563	1	1.0159	0.7143	Al(n,α)	NaI(Tl), β^- Ge(Li)
1970, 65		14.6 (13.56~14.71)			1	0.9795	?	$^{63}Cu(n,2n)$	NaI(Tl)
1979	S.C.Misra+	14 * .6	900 ± 47		1	1.0151	?	$^{63}Cu(n,2n)$	NaI(Tl) Kx $4\pi\beta-\gamma$
1978	N.Lakshmana-Das+	14.2	1096 ± 88	(1114)	0.9756	1.0416 0.9916	?	Al(n, α) $^{65}Cu(n,2n)$	Ge(Li) 35cm³ γ_a
1973	J.Anaminowicz+	14.60	1988 ± 173	(1941.3)	1	0.9765	?	$^{63}Cu(n,2n)$	NaI(Tl) $\gamma_a+\gamma_c$
1972	R.Mogharrab+	14.10	2074 ± 47		0.971	1.0066	?	Al(n, α)	PC(CH4) β^-
1968	H.K.Vonach+	14.6 (13.6~14.6)	1091 ± 33	(1080)	1	0.9897	?	Al(n,α)	NaI(Tl) 5×Φ5in PC(β^-)
1968	M.Bormann+	14.6 (12.96~18.25)	1157 ± 94	1335 1261.8	1	1 0.9452	1.1538	H(n,n) $^{63}Cu(n,2n)$	2πPC(β^-) NaI(Tl)
1967	J.S.Brzosko+	14.2 (12.52~17.88)	1930 ± 210	1542	0.9756	0.9942	0.8235	Al(n,α)	NaI(Tl) 5.1×Φ5.1cm Kx
1961	R.J.Prestwood+	14.68 ± 0.26 (12.13~19.76)	1087 ± 54	1261	1		1.1602	AP,Al(n,α) $^{238}U(n,f)$	PC(β^-)
1960	A.Poularikas+	14.8	2740 ± 30		1.02	0.9914	?	$^{63}Cu(n,2n)$	NaI(Tl) $\gamma_a+\gamma_c$
1953	E.B.Paul+	14.5	867 ± 217		0.9996		?	Al(n,α)	GM(β^-)

Note :

*F*1 Adjustment factor for neutron energy at 14.7 MeV.

*F*2 Adjustment factor for standard cross section.

*F*3 Adjustment factor for nuclear decay data.

Method of neutron fluence determination : AP Associated particle.

PT Proton recoil telescope.

Evaluated cross section for E_n = 14.7 MeV : 1265 ± 30 mb.

Table 2 Survey of measured cross section for $^{181}Ta(n,2n)^{180}Ta$ reaction

Year	Author	Lab.	E_n (MeV)	Cross-section(mb)		Adjusted Factor		Methods
				Published	Adjusted	*F*1	*F*2	
1989	A.Takahashi+	JPNOSA	14.1 ± 0.1	2100 ± 80	2039.1	0.971	1.0	TOF L-8.3M NE213 10× Φ25.4 cm 15°-160° H(n,n)
1980	J.Frehaut+	FRBRC	14.76 (8.44~14.76)	1856 ± 159	1796.5	1	0.9679	STANK(Gd) $\bar{\upsilon}_{cf252} = 3.732$ $^{238}U(n,f)$
1977	L.R.Veeser+	LAS	14.7 ± 0.15 (14.7~24.0)	2122 ± 115	2122	1	1	STANK(Gd) H(n,n)

Table 3 Decay scheme branching ratios for ^{180m}Ta

	Brown et al. (1951)	Gallagher et al. (1962)	Ryves (1980)
a(%)	11	3.2	3.5 ± 0.1
b(%)	10	9.8	14.7 ± 0.9
c(%)	79	27.0	24.3 ± 0.6
d(%)		60.0	57.5 ± 1.0*
α_a		3.467	3.412
α_c		4.767	4.685

* Primary value of Ryves is 57.6 ± 1.0

Table 4.a Covariance matrix for the evaluated cross section of $^{181}Ta(n,2n)^{180}Ta$ reaction

E_n	σ	St. error	Covariance Matrix								
MeV	mb	%									
8.44	281.5	15.0	1.0								
9.44	1114.8	9.5	0.88	1.0							
10.9	1668.3	6.0	0.78	0.81	1.0						
12.9	1930.1	6.0	0.65	0.71	0.72	1.0					
14.3	1985.9	5.5	0.52	0.62	0.62	0.70	1.0				
14.7	1969.2	4.6	0.03	0.01	0.02	0.03	0.21	1.0			
16.0	1816.1	7.8	0.02	0.03	0.02	0.03	0.03	0.61	1.0		
19.0	975.4	9.9	0.10	0.11	0.02	0.02	0.01	0.47	0.56	1.0	
23.0	454.0	20.0	0.05	0.08	0.09	0.03	0.02	0.55	0.59	0.75	1.0

Table 4.b Covariance matrix for the evaluated cross section of $^{181}Ta(n,2n)^{180m}Ta$ reaction

E_n	σ	St. error	Covariance Matrix									
MeV	mb	%										
8.5	271.5	10.0	1.0									
12.7	1304.2	4.0	0.22	1.0								
13.9	1320.1	4.0	0.24	0.70	1.0							
14.5	1293.8	2.5	0.21	0.60	0.73	1.0						
14.7	1270.6	2.5	0.20	0.57	0.68	0.68	1.0					
15.7	1152.3	3.0	0.20	0.55	0.65	0.63	0.68	1.0				
16.6	965.6	3.5	0.20	0.54	0.58	0.55	0.60	0.62	1.0			
17.8	659.3	4.2	0.22	0.60	0.63	0.59	0.60	0.64	0.70	1.0		
18.3	571.8	4.2	0.20	0.54	0.58	0.52	0.53	0.54	0.60	0.72	1.0	
19.8	398.4	9.0	0.20	0.54	0.57	0.52	0.52	0.53	0.56	0.68	0.68	1.0

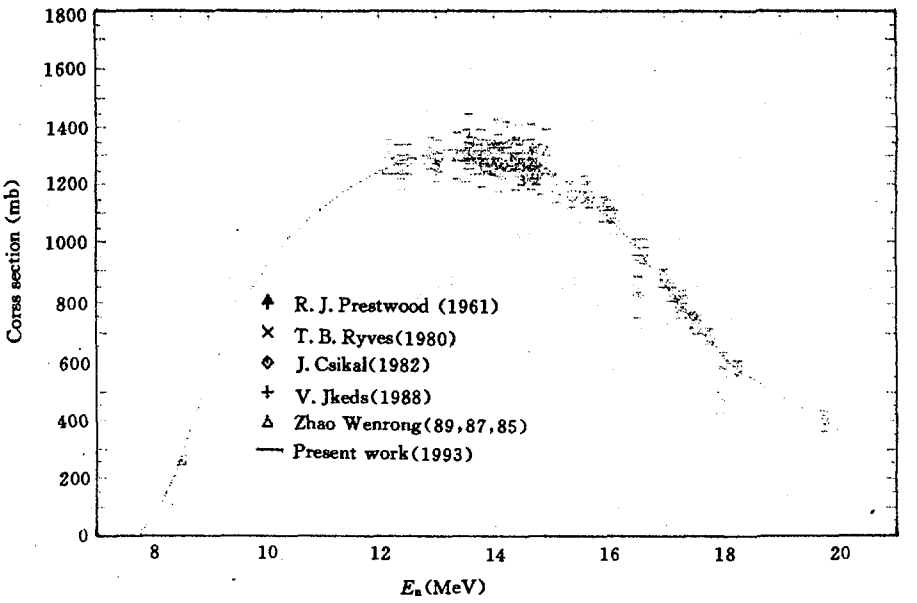

Fig. 1 Adjusted and evaluated cross section for $^{181}Ta(n,2n)^{180m}Ta$ reaction

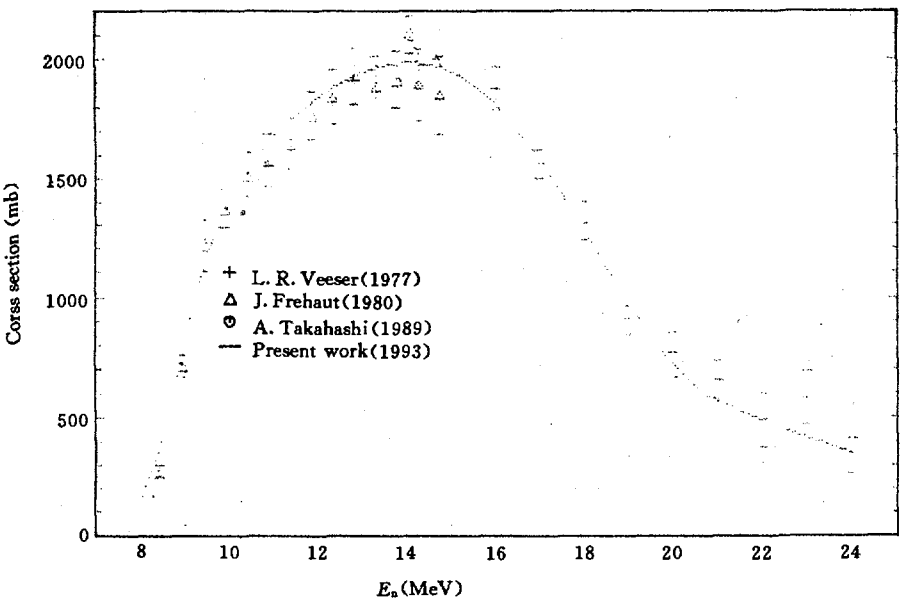

Fig. 2 Adjusted and evaluated cross section for $^{181}Ta(n,2n)^{180}Ta$ reaction

References

[1] A. Takahashi et al., INDC(JAP)–118 / L (1989)

[2] J. Frehaut et al., BNL–NCS–51245, 399 (1980)

[3] L. R. Veeser et al., Phys. Rev., C16, 1792 (1977)

[4] Zhao Wenrong et al., INDC(CPR)–16 (1989)

[5] Lu Hanlin et al., Nucl. Instrum. Methods, A255, 103 (1987); Nucl. sci. & Eng., 90, 304 (1985); Chin. J. Nucl. Phys., 4, 310 (1982)

[6] Lu Hanlin et al., Chin. J. Nucl. Phys., 7, 242 (1985)

[7] Y. Ikeda et al., JAERI–1312 (1988)

[8] T. B. Ryves et al., J. Phys. G6. 771(1980) and 763 (1980)

[9] J. Csikai, 82 Antwerp, 414 (1982)

[10] J. Csikai, EANDC–50, 2 (102),1965; 65 Antwerp, 537 (1965); Mag. Fiz. Foly., 16, 123(1968)

[11] S. C. Misra et al., J. Phys., G5, 855(1979)

[12] N. Lakshmana Das et al., J. Nuovo Cimento, 48A, 500(1978); Proc. Symp. on Nucl. Phys. and Solid State Phys., Calcutta, Dec.,22–26, 1975, CONF–751249, Vol. 31, p. 188

[13] J. Anaminowicz et al., Institute Badan Jadrowych Report IBJ 1464 / 1 / A, 14(1973)

[14] R. Mogharrab et al., Atomkernenergie, 19, 107(1972)

[15] H. K. Vonach et al., Proc. 2nd Conf. Neutron Cross–section Technology, Washington D. C., March 4~7, Vol. 2, p. 885, 1968

[16] M. Bormann et al., Nucl. Phys., A115, 309(1968)

[17] J. S. Brzosko et al., Nucl. Phys., A123, 6031969); INR–795 / I / PL (1967)

[18] R. J. Prestwood et al., Phys. Rev., 121, 1438(1961); LA–2493 (1960)

[19] A. Poularikas et al., J. Inorg. Nucl. Chem., 13, 196(1960)

[20] E. B. Paul et al., Can. J. Phys., 31, 267(1953)

[21] C. J. Gallagher et al., Nucl. Phys., 33, 285(1962)

[22] H.N.Brown et al., Phys.Rev., 84, 292 (1951)

[23] Yao Lishan et al., Journal of Lan Zhou University, 23 (1), 67(1987); HSJ–84159 (bp), 1984

[24] V. H. Bychkov et al., INDL / V, 1982

[25] Wang Zisheng et al., INDC(CPR)–024, 5(1991)

Investigation of Isomer Production Cross Sections from $^{180}Hf(n,2n)^{179m}Hf$ Reaction

Zhao Zhixiang

(Chinese Nuclear Data Center, IAE)

Introduction

Cross sections for producing isomeric state ($25/2^-$, 25.1d), through $^{180}Hf(n,2n)$ reaction, are useful in nuclear engineering applications. Unfortunately, only one measured data is available. In present work, the production cross sections of isomeric state with $J = 25/2^-$ and $T_{1/2} = 25.1d$ produced through $^{180}Hf(n,2n)$ reaction are evaluated on the basis of the limited measured data and theory calculated isomer ratio not only for $^{180}Hf(n,2n)$ but also for $^{179}Hf(n,n')$ reactions.

1 Evaluation of Isomer Ratio

The ^{179}Hf has two isomeric states. The first isomeric state is charactered by $J = 1/2^-$ and $T_{1/2} = 18.67s$ and denoted as m_1 state in this work. The second one, which is denoted by m_2, has rather large spin ($J = 25/2^-$) and long lifetime ($T_{1/2} = 25.1$ d). Both the $^{180}Hf(n,2n)$ and $^{179}Hf(n,n')$ reactions give the m_2 state of ^{179}Hf. If we define the isomer ratio as

$$R_i = \sigma_i(m_2) / \sigma_i(m_1 + m_2 + g) \tag{1}$$

where g represents the ground state and subscript "i" denotes the i–type reaction, the behavior of isomer ratio as a function of excitation energy from $^{180}Hf(n,2n)$ reaction should be similar to those from $^{179}Hf(n,n')$ reaction because of same γ–decay mode. Of course, the ratios from these two different reactions would differ by a common factor because the excitation cross section of the levels of ^{179}Hf by these two different reactions would differ. Moreover, excitation energy of ^{179}Hf by these two reaction at same incident neutron energy is different. Based on the analysis above, it is assumed that

$$R_{2n}(E_n - Q_{2n}) \approx \alpha R_{n'}(E_n) \tag{2}$$

where Q_{2n} means the reaction energy and α means a constant.

Chadwick and Young calculated R_{2n} as function of neutron energy for ^{180}Hf(n,2n)^{179m2}Hf below E_n = 14 MeV by using GNASH code[1]. To obtain R_{2n} up to 20 MeV, their calculation for ^{179}Hf(n,n')^{179m}Hf can be used according to the analysis above. The R_{2n} calculated by Chadwick and Young for ^{180}Hf(n,2n)^{179m2}Hf are shown in Fig. 1 in comparison with those calculated by using Eq. (1) from $R_{n'}$ of ^{179}Hf(n,n')^{179m2}Hf after normalized at a given energy by using α = 0.5725. It is found that the agreement between the R_{2n} from two different reactions is very well. Evaluated R_{2n} is obtained by eye-guide and also shown in Fig. 1.

2 Evaluation of Isomer Cross Section

In principle, multiplying the R_{2n} evaluated above by evaluated cross section of ^{180}Hf(n,2n)^{179}Hf reaction, $\sigma_{2n}(m_1+m_2+g)$, the isomer cross section would be given out for ^{180}Hf(n,2n)^{179m2}Hf. By using evaluated $\sigma(m_1+m_2+g)$ of ENDF / B-6[2] and of JENDL-3[3], very different results are obtained. Normalized these results to the only data measured by Patrick[4]

$$\sigma = 16.7 \pm 1.9 \quad \text{mb} \quad \text{at 14 MeV} \tag{3}$$

the discrepancy between the results based on ENDF / B-6 and JENDL-3 is greatly decreased (see Fig. 2) below E_n = 16 MeV. The differences above E_n = 16 MeV could be attributed to the fact that evaluated values of ENDF / B-6 for MT = 16 include not only the cross sections for (n,2n) reaction but also for (n,3n) reactions. So those isomer cross sections, calculated from the R_{2n} we evaluated and based on $\sigma(m_1+m_2+g)$ evaluated in JENDL-3 are recommended after normalizing to the measured data.

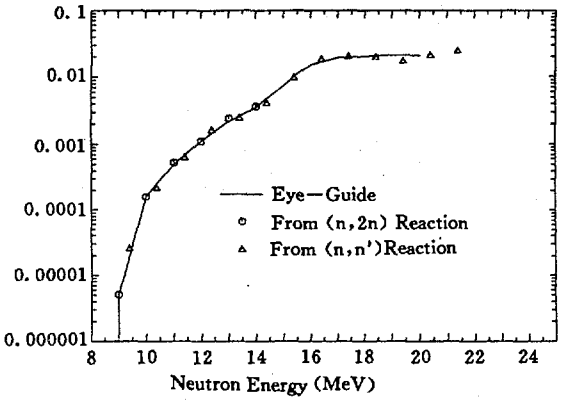

Fig. 1 Isomeric ratio of $^{180}Hf(n,2n)^{179m}Hf$

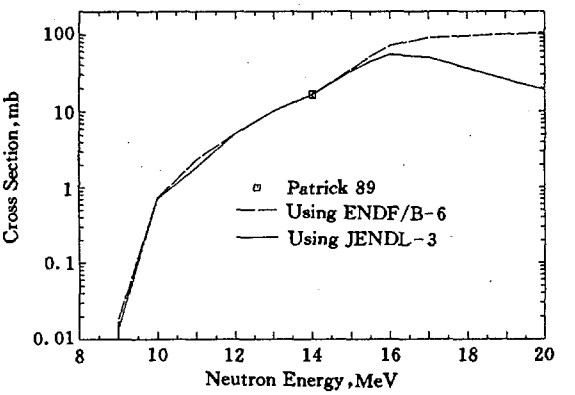

Fig. 2 Isomeric cross section of $^{180}Hf(n,2n)^{179m}Hf$

References

[1] M. B. Chadwick et al., LA-UR-91-3454 (1991)
[2] M. Drake et al., ENDF / B-6 Data Tape
[3] K. Hida et al., JAERI-1319, 1990
[4] B. H. Patrick et al., INDC(NDS)-232, 1990

IV PARAMETER AND PROGRAM LIBRARIES

The Sub–Library of Fission Barrier Parameters

Zhang Limin Su Zongdi Ge Zhigang

(Chinese Nuclear Data Center, IAE)

Abstract

The first edition of fission barrier parameters sub–library, constitutes one part of the Chinese Evaluated Nuclear Parameter Library (CENPL), including data file and management–retrieval code system, has been finished. The introduction for its contents and usage of the retrieval system is presented.

Introduction

The fission barrier is an important parameter to determine the fission character of a nucleus. In addition, an important trend in the evaluation of the neutron reaction data is the increasing use of nuclear reaction theory codes to compute the complete neutron data. The fission barrier parameters (FBP) are needed in the calculations of various cross sections and spectra for the fissile nuclides, even heavy nuclides at higher incident energies, and the requirement of the accuracy is ever higher in the practical calculation. Therefore FBP have played a special role both in fundamental nuclear physics and in the field of applications. Some valuable FBP obtained in the studies of various fission phenomena are being collected and compiled in a fission barriers parameter sub–library, which constitutes one part of Chinese Evaluated Nuclear Parameter Library (CENPL–FBP). The first edition of fission barrier parameters sub–library (FBP–1), which collected and compiled three sets of fission barrier parameters from J. E. Lynn[1] B. B. Back et al.[2, 3] and T. Ohsawa[4], has been finished. The management–retrieval code system of FBP–1 can retrieve the fission barrier parameters for a single nuclide (SN retrieval) and for the related

nuclides with the (n,f), (n,nf) and (n,2nf) reaction processes (NR retrieval), respectively, and can provide relevant information of selected FBP too.

In section 2, three sets of FBP selected in FBP–1 are introduced briefly. The data file and management–retrieval code system are described in section 3 and 4 respectively. Discussion is given in section 5.

1 Fission Barrier Parameters Selected in FBP–1

In FBP–1, three sets of the fission barrier parameters were collected and compiled, which were obtained by J. E. Lynn[1] (1974), B. B. Back et al.[2, 3] (1974) and T. Ohsawa[4] (1988) in different ways respectively. These parameters can provide user the full information of the fission barrier, such as the height and curvature of the fission barrier, the spectra and level density at saddle point, which would be adopted in the statistical theory calculation of nuclear reaction for fissionable nuclei. The fission barrier parameters and levels at saddle point obtained from Refs. [1～3] are introduced and reviewed briefly in this section.

Lynn calculated the neutron cross sections of actinide nuclei up to about 3 MeV incident neutron energy. His calculation was based on elementary Hauser–Feshbach theory, constant temperature level density with modifications for low excitation energies, the giant dipole resonance model in the radiative decay process, and a uniform picket–fence model with parameterization of the double–humped barrier in the fission process. Nearly all available relevant data on actinide nuclei from ^{229}Th to ^{253}Cf were analysed using the statistical theory mentioned above in his calculation. The recommended values of barrier parameter from analysis of fission data on the actinide nuclei were obtained. In Lynn's work, it was noted that the states density at barrier 1 is three to five times greater than the one associated with normal deformation, but the density at barrier 2 is much smaller than the one at barrier 1. In addition, there is an odd–even effect for the values of the "penetrability frequencies" $\hbar\omega_1$ and $\hbar\omega_2$.

B. B. Back et al. measured the fission probability distribution of (t,pf), (t,αf), (t,t'f), (p,p'f), (^{3}He,df) and (^{3}He,αf) reactions for doubly even nuclei of Th, U, Pu and Cm isotopes and (d,pf), (t,pf), (^{3}He,df), (^{3}He,αf), (t,αf) reactions for odd–A and doubly odd actinide nuclei of Th, Pa, U, Np, Pu, Am, Cm, ^{249}Bk and ^{249}Cf. These reactions are induced by direct reactions mechanism [2, 3]. The measured results were analyzed by a statistical model, in which resonant penetration of the double–humped fission barrier for doubly even nuclei was involved and a complete damping of the vibrational strength in both

wells for odd–A and doubly odd nuclei was assumed. In the calculation of the effective numbers of transition states at the two saddle points, there were two separate contributions when the decay involved an even–even or an odd–A nucleus. The first contribution came from states below 1 MeV using a discrete spectrum of levels, whereas the second contribution came from states above 1 MeV where a continuous level density was used. The continuous level densities were the same as used in the fission isomer calculations[5]. The barrier heights and curvatures were obtained from the analysis of the measured fission probability distributions for actinide nuclei. The most remarkable feature of these experimental barrier heights is the relative constancy of V_1 at $\approx 6 \pm 0.5$ MeV over the entire region from Th through Cf and the steady decrease of V_2 from $\approx$ 6.3 MeV in Th to $\approx$ 4 MeV for Cm isotopes. In Ref. [2], the comparisons with the barrier heights of various theoretical calculations for even–even nuclei indicate very good agreement for Pu and Cm isotopes, but systematic deviations of $\approx$ 2 MeV in Th region with uranium cases being intermediate.

T. Ohsawa[4] used a theoretical model calculation based on the double–humped barriers concept of fission to analyse the fission cross sections for 24 actinide nuclides ranging from ^{232}Pa to ^{253}Cf and recommended the fission barrier heights. The basic idea of Ohsawa's work is to try to reduce the number of adjustable parameters by making the best use of the physical available information from the present knowledge on the fission barriers. Firstly, the barrier curvature parameters ($\hbar\omega_1$ and $\hbar\omega_2$) can be determined by fission isomer half–lives[5] and fission probability data[2, 3]; Secondly, knowledge on the discrete transition states can be obtained from the channel analysis of the fission fragment angular distribution or from the theoretical estimation of quasi–particle levels at the saddle–point configurations; Third, continuum transition states can be represented by the level density formula with appropriate collective enhancement factors corresponding to the nuclear shape at the saddle–point. With all of these parameters fixed, the remaining adjustable parameters are only the heights of two barriers. The barrier heights obtained from fission cross section analysis are in better agreement with those recommended by Lynn[1] for lighter actinides, while it is worse for the second barrier of heavier actinides.

2 FBP–1 Data File

Contents:

FBP file consists of three sets of the fission barrier parameters, recom-

mended by Lynn[1] in 1974 for 50 actinide nuclei ranging from ^{229}Th to ^{255}Cf, by Back et al. for 46 actinide nuclei ranging from ^{229}Th to ^{253}Cf, by Ohsawa[4] in 1988 for 24 actinide nuclei ranging from ^{232}Pa to ^{253}Cf. The barrier curvature parameters were taken as three constants for odd–odd, odd–A and even–even nuclei respectively, which were determined by fission isomer half–lives and fission probability data.

Format:

Each record of the file contains Z, EL, A, V_1, dV_1, $h\omega_1$, $dh\omega_1$, V_2, dV_2, $h\omega_2$, $dh\omega_2$ and REF, they are charge number (column 1～3), element symbol (4～6), mass number (7～10), height of the first barrier (14～19), deviation of V_1 (20～23), curvature of the first barrier (27～32), deviation of $h\omega_1$ (33～36), height of the second barrier (40～45), deviation of V_2 (46～49), curvature of the second barrier (53～58), deviation of $h\omega_2$ (59～62) and reference (65～69), respectively.

3 FBP–1 Management–Retrieval Code System and Examples

When user runs " FBP ", some information and routine procedure for retrieval are shown on the screen at first. The retrieved parameters are put into the data file OUTFBP.DAT.

There are two ways for retrieving:

(1) for single nucleus (SN);

(2) for the related nuclei with (n,f), (n,nf) and (n,2nf) reaction processes in a neutron induced reaction (NR).

Retrieval steps are as follows with an example of ^{232}Pa:

(1) Choosing the retrieving way, SN or NR ?
SN (return)

(2) The charge number Z =
91 (return)

(3) The mass number A =
232 (return)

(4) Retrieving and showing retrieved parameters on screen:

Retrieving *FB* parameters for single nucleus (91, 232) in SN

V_1 (MeV)	$h\omega_1$ (MeV)	V_2 (MeV)	$h\omega_2$ (MeV)	Z A
6.3	0.65	6.25	0.45	L (91,232)
5.75	0.6	6.10	0.45	B (91,232)
6.20	0.6	6.14	0.42	O (91,232)

(5) Choosing the required parameters, L / B / O* / All or N (Not) ?
ALL (return)

(6) Printing the reference in the out data file , (Y or N) ?
N (return)

(7) Retrieving for other nucleus in this way , (Y or N) ?
N (return)
if Y, turn to the second step.

(8) Continue to retrieve , (Y or N) ?
if Y, turn to the first step;
if N, turn to next stop.

(9) Fortran stop

4 Discussion

The CENPL–FBP–1 has been set up at CNDC, and could provide to retrieve the fission barrier parameters for the nuclear data computation and some information for actinide nuclei by using the FBP–1 management–retrieval code system.

In order to obtain a overall understanding on the fission barrier parameters from different authors and their variation features with the increase of Z and A, the heights and curvatures of the double humped barrier for Th–Cf elements presented by Refs. [1～4] as mentioned in section 2 are plotted in Fig. 1.

---

* L, B, O mean Lynn, Back, Ohsawa parameters respectively.

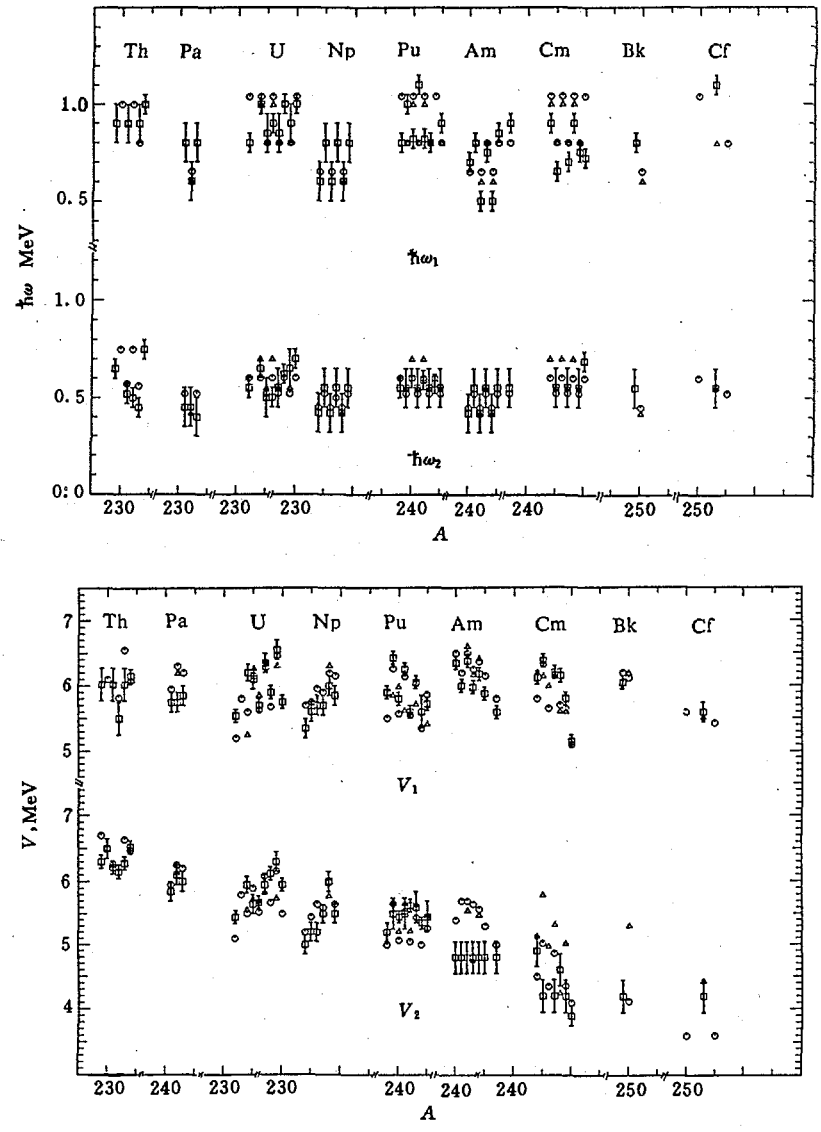

Fig. 1 Barrier heights and curvatures of Lynn, Back et al. and Ohsawa

⊙ J. E. Lynn, ⊕ B. B. Back et al., △ T. Ohsawa.

The following is noteworthy:

(1) The most feature of barrier heights is that the values of V_1 recommended by Lynn, Back et al. and Ohsawa are in 5.1～6.55 MeV in the entire ranging from Th to Cf, and V_2 present the decreased trend from $\approx$ 6.5 MeV for Th to $\approx$ 4 MeV for Cf; Three sets of V_2 values make more difference for heavier actinides Cm, Bk, and Cf.

(2) Most of $h\omega_1$ and $h\omega_2$ values are in 0.65~ 1.05 and 0.45~ 0.75 for the first and second barrier respectively, and there is definitely an odd–even effect.

(3) One of the essential quantities in the analysis of fission cross section is the barrier spectra (discrete transition states) and level density at saddle point, Since the loss of rotational invariance of nuclear shape at barrier deformations leads to the occurrence of some rotational degrees of freedom, it can be concluded that the level density at saddle point is enhanced compared with one at the normal excitation, a empirical enhancement factor of level density at saddle point is about three to five.

(4) These barrier parameters recommended by Lynn[1] and Ohsawa[4] depend on used model and other relative nuclear model parameters for the purpose of calculating cross sections from a statistical model. It may be seen that the parameters are somehow model dependent.

We will extend the CENPL–FBP to include more fission barrier parameters obtained from different ways and study systematical feature of fission barrier parameters to present systematics results in future.

Acknowledgement

This work is supported by IAEA under contract 7431 / RB.

References

[1] J. E. Lynn, AERE–R7468, 1974
[2] B. B. Back et al., Phys. Rev. C9, 1924(1974)
[3] B. B. Back et al., Phys. Rev. C10, 1948(1974)
[4] T. Ohsawa, IAEA–TECDOC–483, p. 134, 1988
[5] B. B. Back et al., Nucl. Phys., A165, 449(1971)

ERES — A PC Software for Nuclear Data Compilation in EXFOR Format

Li Shubing

(Nankai University, Tianjin)

Liang Qichang Liu Tingjin

(Chinese Nuclear Data Center, IAE)

Abstract

The major functions and implementation of the software ERES are introduced. The ERES is developed for nuclear data compilation in EXFOR format, running on IBM–PC / XT or IBM–PC / AT.

EXFOR (EXchange FORmat) is the format for the exchange of experimental neutron data accepted by four neutron data centers in the world.

Introduction

EXFOR (EXchange FORmat) is the international unified format for the exchange of experimental neutron data accepted by four neutron data centers in the world in 1970, now this EXFOR format was not only used for the exchange of experimental neutron data in the four centers with magnetic tape or diskette, but also used for the storage and retrieval system of experimental neutron data in some nuclear data centers. Four neutron nuclear data centers are responsible in the collection, compilation and dissemination of experimental neutron data in EXFOR in their responsibility area.

EXFOR–computerized exchange format is a convenient and flexible format for describing experimental numerical data and related bibliographic information which is necessary to understand the experimental nuclear data. EXFOR format has a set of strict syntax rules.

For the convenience of the compilation and exchange of experimental neutron data in the countries of the third world, a PC software system, so–called ERES(EXFOR Edit System), has been developed, the functions of ERES

includes EXFOR experimental neutron data editing, check and retrieval.

1 Summary of ERES

1.1 Description of EXFOR Format

EXFOR exchange magnetic tape contains a number of entries, each ENTRY is divided into several subentries, each SUBENTRY consists of three sections, i. e. bibliography or description information (BIB), COMMON data and DATA table.

Therefore, the format of EXFOR data tape can be shown as follows:

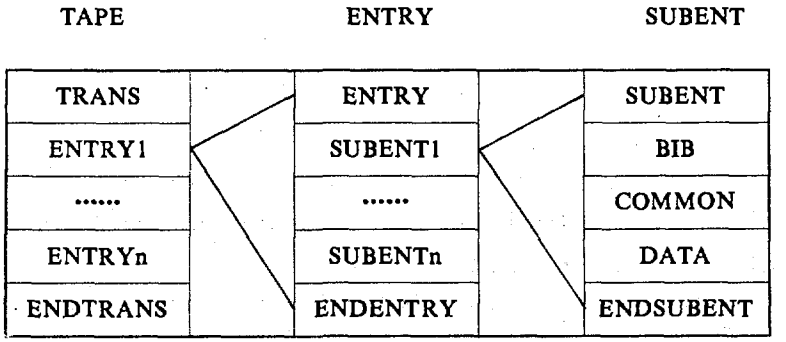

Each ENTRY, SUBENTRY and DATA item has certain syntax and physical significance, for the detail please refer to Ref. [1].

1.2 The Main Functions and Characteristics of ERES

The main functions of ERES are as follow:

. To compile experimental neutron data in EXFOR format with PC;

. To check the format correctness;

. To modify the errors;

. To generate a correct EXFOR entry;

. To retrieve the EXFOR data by ENTRY, SUBENTRY accession number or reaction type.

This ERES software system has some characteristics, such as excellent user interface, convenience of operation and good reliability etc.

For editing a new EXFOR data entry, the following input mode can be adopted:

RECORD : 1

1 ··· 10	11	12 ··· 22	23 ··· 33	34 ··· 44	45 ··· 55	56 ··· 66

According to the requirement of EXFOR format, each record is divided into seven fields, for the ENTRY, SUBENT number and date, they can be input in the beginning of corresponding field, the ERES can automatically justified right, for the statistic value, for example, N1, N2 in the record with EXFOR system identifier, they need not be input and can be automatically generated by ERES system.

The special keyword for EXFOR format includes system identifier and information keyword, such as ENTRY, SUBENT, REFERENCE and REACTION etc.. In order to raise the input speed and reduce the input errors, this software system provides an input mode of keyword abbreviation. In general, the abbreviation consists of a star symbol (*) and first two characters of the keyword, for example, when * ES is entered and press "RETURN" key, the ERES system can automatically convert it into ENDSUBENT. If incorrect abbreviation sign is entered, the arrow remains in original position, then the correct one can be entered again.

In order to help the users, the suspending service program for keyword abbreviation contrast table is written in assembly language. After starting the system, press two "SHIFT" keys simultaneously at any time for activation, the keyword abbreviation will be displayed on the screen, press any key, the screen return to the original state.

The functions of CHECK program in this system is quite complete, and basically achieve the requirements presented in Ref. [1]. This software has quite quick at operation, strong capability of toleration error and powerful protective measure, under any menu, type "0" (zero), return to main menu.

In ERES system, the master control program and editing, retrieval programs are written in FOXBASE+ , check program is written in IBM–PC FORTRAN, and input help program of keywords abbreviation is written in assembler.

1.3 Environment of ERES Operation

This software can be operated on the PC IBM / XT, IBM / AT or compatible ones, the required software and hardware environment are:

. 640 K bytes of RAM.

. CGA, EGA or VGA monitor.
. 2 M byte hard disk.
. one floppy disk driver 5 $\frac{1}{4}$ " , high density.
. DOS 3.0 or higher version.

2 General Design of ERES

2.1 The Design for Master Control Program of ERES

General control block diagram of ERES are as follows:

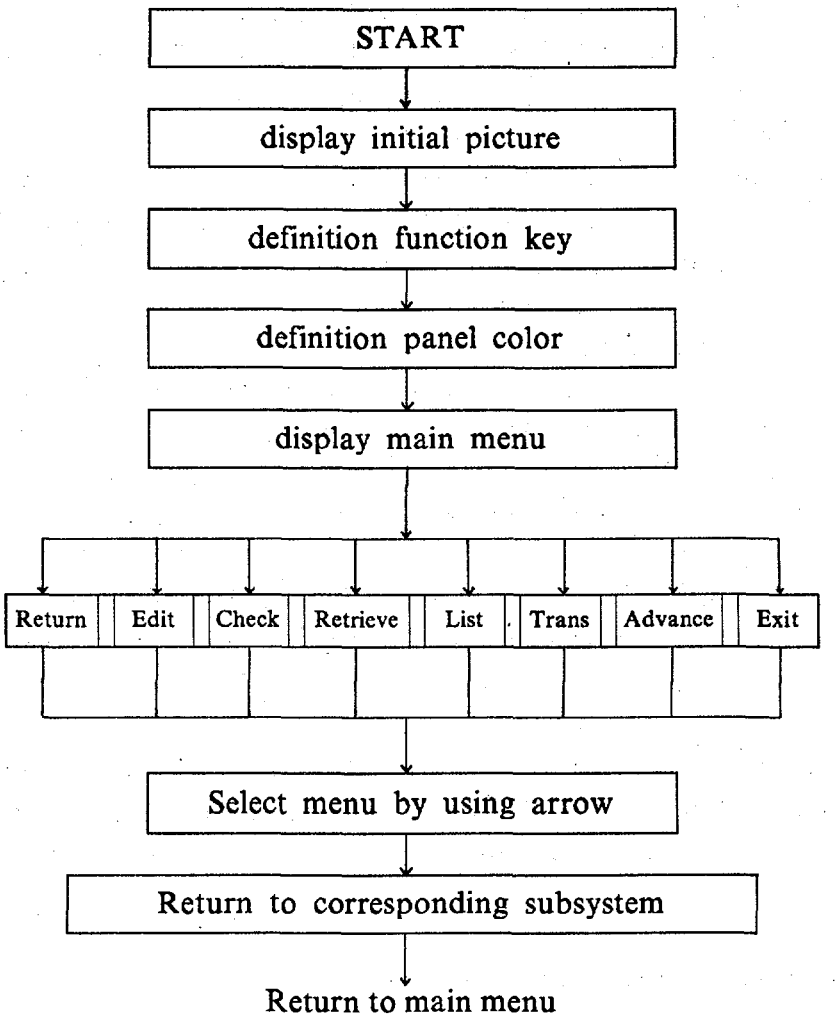

The significance of some major block in above block diagram:
. RETURN Come back FOXBASE+ system

. EDIT Edit subsystem

. CHECK Check subsystem, checking EXFOR data file and generating error message file; processing dictionaries and generating special dictionaries files for used in ERES system

. RETRIEVE Retrieval subsystem

. LIST Display, modify EXFOR data file and error information file with extension ".TXT".

. TRANSFER Convert the file type, i. e. the file with extension ".DBF" and ".TXT" can be converted each other

. ADVANCE Generating the necessary information for EXFOR data file

. EXIT Exit FOXBASE+ system, return to DOS

2.2 Major Module Analysis

According to the functions, ERES can be divided into three subsystem: EDIT, CHECK and RETRIEVE.

1) EDIT Subsystem

The functions of this subsystem includes INPUT, OUTPUT, MODIFY and MERGE etc..

(1) Data Input

ERES system provides an excellent environment for EXFOR data input, i. e. data can be input by using a convenience input mode, it can reduce the input errors, in the course of input process, press F10 key, input can be stopped and data file is saved in disk. Users can establish a new EXFOR data file, but also can add some records to existing EXFOR file by using this system.

When users input a file name for establishing a new file, system can check and show you whether this file exist, if it has existed, ERES will remind you whether the old file will be overlaid.

(2) Data Output

For an existed EXFOR data file, ERES system can output it in whole, part or by SUBENT number, users can select whether the output result goes to printer. If a file is selected which does not exist, the system can indicate the error and list all existed EXFOR files in current disk.

(3) Modify Data and Merge Files

For an existed EXFOR data file, it can be deleted, modified, inserted by using this system, there are two modification modes: man–machine interactive and full–screen editing, the EXFOR data file also can be deleted by SUBENT number.

Users can merge several EXFOR data files into one EXFOR transmission

tape and generate the necessary information by using this system.

2) Design of CHECK Program

The important part of ERES system is checking the correctness for a EXFOR data file, the CHECK program (about 7000 lines) is written in IBM–PC FORTRAN, it is similar to the compile system of high–level language, but hasn't the phase of generating object code. This program includes mainly the following parts:

(1) Morphology Analysis

The correctness of keywords and system identifiers can be checked. In many cases the table processing method were adopted.

(2) Syntax Analysis

According to the EXFOR format, the syntax correctness, for example, the correctness of preceding record and the following record for a system identifier can be checked.

(3) Code Check

If the keyword needs to have code, then the code can be analyzed and checked, the code also can be searched whether it exist in corresponding dictionary.

(4) Data Check

The DATA–HEADING and DATA–UNIT in the COMMON and DATA section and their match relation are checked.

(5) Errors Processing

When syntax errors were detected, this system can indicate the error information and its location, and save the error information into a corresponding file, and the influence from the errors can be limited into minimum.

Since there are many items to be checked, so the program is quite complex, for the convenience of test and maintenance, the program was divided into several module according to the functions.

3) Module Analysis

The structure of the module is shown in the following flow chart:

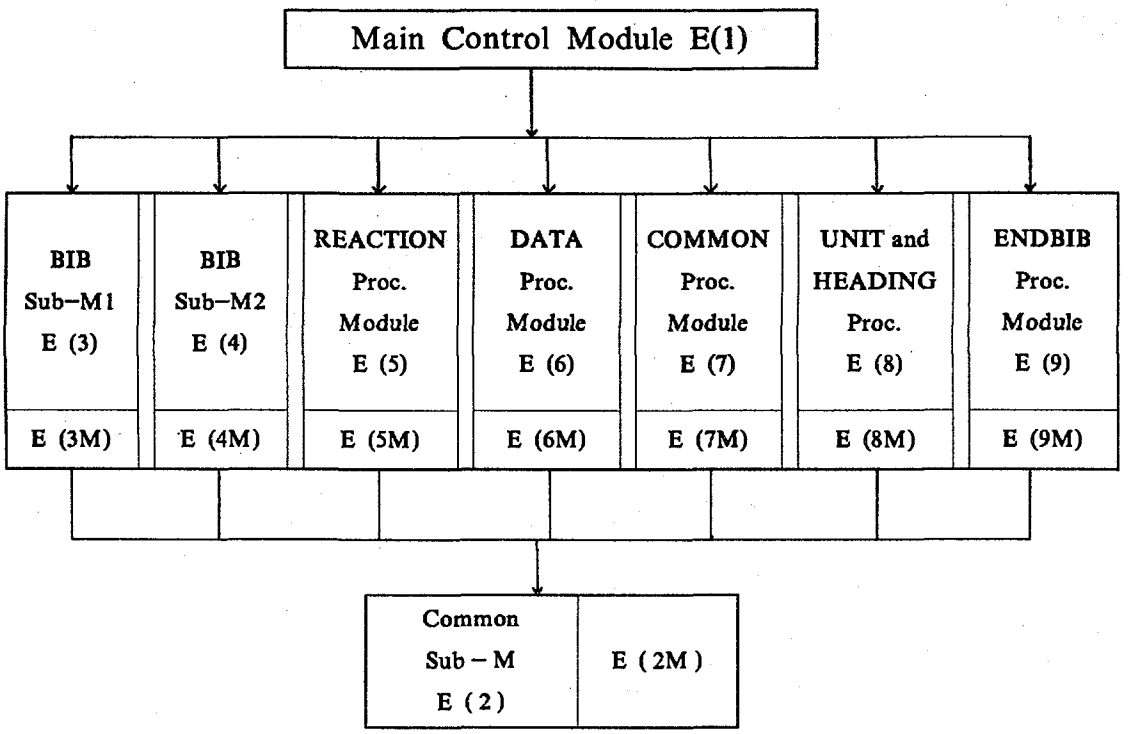

Where E(IM) I = 2, ···, 9 correspond to the test part of each module.

The steps of test are as follows:

. E(2) + E(2M)

. E(I) + E(IM) + E(2)

. $\sum E(i)$ I = 3, ···, 9, i = 1, ···, 9

Taking into account the convenient of test and maintenance, the compact degree of the program is enhanced and the coupling degree is decreased as much as possible in the design of the program.

4) Retrieval Sub–System

The system has many kinds of functions for EXFOR data retrieval. It can be done according to the number of ENTRY and SUBENTRY and also according to COMMON, DATA, BIB items etc. The retrieved data are stored in a file. If an ENTRY or SUBENTRY, which is not in the given file, is required, the system will give out an error message and list all ENTRY or SUBENTRY numbers, which can be selected as reference.

3 Some Technical Problems in the Program Design

3.1 Dictionary Processing

The all keyword and code descriptions used in the EXFOR system are included in the system dictionary. According to the features, the dictionary is divided into 40 sub–dictionaries.

The structure of each sub–dictionary is as follows:

The first record	DICTION No.
	Information
	.....
The last record	ENDDICTION

There are complete information and more description for the dictionary got from NDS / IAEA, so more hard disc space is needed. Therefore the dictionary is processed as follows to save disk space and to enhance the looking up speed.

1) Cut some information, which are not used in the program.

2) Arrange in alphabetical order for each sub–dictionary, produce a new dictionary DICT.TXT and a index file DICM.TXT, which is used to store the start position and the length. The record length of the dictionary DIC0.TXT is L and $L = \max \{ a_i : i = 1, 2, \cdots, N \}$, where a_i is the length of i–th sub–dictionary, and N is the total number of the sub–dictionaries.

In the check program , the files DIC0.TXT and DICM.TXT are opened in direct access mode, the statement for this is:

OPEN (2, FILE = 'DIC0.TXT', status = 'old', access = 'direct ', FORM = 'FORMATTED', RECL = 50)

(Where, RECL = 50 means that record length of DIC0.TXT is defined as 50).

Only 347 KB hard disc space is needed to store new dictionary DIC0.TXT, which save more than 500 KB comparing with original one.

In the check program, DIC0.TXT is put into a array, so that the number of access with hard disk can be decreased in the program running. For looking up some dictionary code, give out the code and the sub–dictionary number, which the code is in, first the start position and the length of this sub–dictionary are found, then it is looked up in a half and half way. In this method, only at most $1+\log_2 n$ times of comparisons need to be done for looking up one code (n is the dictionary length).

3.2 Character Processing

In the program, most of operations are processing characters, including taking sub–string, character string conjunction, merging, dividing and transforming between character string and numerical value.

Example 1: In the program, there are statements

```
CHARACTER STR1 * 4,STR2 * 5,STR3 * 10
STR3 = "ABCDEFGHI"
```

(1) Take sub–string

one way with character assignment statement is:

```
STR1 = STR3 (1:4)
STR2 = STR3 (5:9)
```

another way with READ statement is:

```
READ ( STR3, '(A4,A5)' ) STR1, STR2
```

The same results STR1 = "ABCD", STR2 = "EFGHI" are got in the two ways.

(2) Character string conjunction and merging

one way with character assignment statement is:

```
STR3 (1:4) = STR1
STR3 (5:10) = STR2
```

another way with WRITE statement is:

```
WRITE ( STR3, '(A4,A5)' ) STR1, STR2
```

The same results are got in the two ways, that is STR1 and STR2 are conjoined and stored in STR3.

(3) The exchange between character string and numeric

It is often needed in the analyzing EXFOR data to exchange between character string and numeric.

(3.1) Transform numeric to character string

Example 2:

```
REAL R1
CHARACTER STR * 10, CH * 2
R1 = 12.34
I = 56
WRITE ( STR, '(F10.2)' )R1
WRITE( CH, '(I2)' )I
```

After running, STR = "12.34", CH = "56"

(3.2) Transform character string to numeric

Example 3:

```
INTEGER YEAR, MONTH, DAY
REAL R1, R2
CHARACTER * 2 DATE * 6, STR1, STR2, STR3, STR * 8
```

DATE = "921020"

STR = "12.34"

READ (DATE, '(I2,I2,I2)') YEAR, MONTH, DAY

READ(STR, '(F8.2)') R1

After running,YEAR = 92, MONTH = 10, DAY = 20, R1 = 12.34

Note: when character data are transformed to numerical data, only the first character can be "+" or "−" in the character string, the others must be numbers 0～9. While numeric to character, the defined length of the character string must be larger than or equal to the length of numerical data to be transformed. Otherwise the error message will appear:

? Error: Operation error in run time

3.3 Reaction Check

Keyword REACTION is used to define the data under the data heading "DATA", "RATIO" and "SUM" etc. in DATA section.

In a "REACTION" section, there may be a single reaction unit or reaction unit combination (more than two reaction unit).

For example

① (51−SB−123 (N,G) 51−Sb−124−M1+M2 / T,,SIG / SUM / RAT)

② ((92−U−235(N,F),,SIG) / (79−AU−197(N,G)79−AU−198,,SIG))

1) Reaction Formula

To check "REACTION", it is expressed in BNF Backus Normal Form as follows:

<REACTION> = <REACTION unit> | <REACTION unit> <separation symbol> <REACTION unit>

<separation symbol> = + | − | x | /

<REACTION unit> = (reaction, quantity, data−type)

<reaction> = SF1(SF2,SF3)SF4

<quantity> = (SF5, SF6, SF7, SF8)

<data−type> = SF9

Therefore

<REACTION unit> = <SF1(SF2,SF3) SF4, SF5, SF6, SF7, SF8, SF9>

Where SF1 — target nuclide, SF2 — incident particle (more detail, see Ref. [1])

2) Reaction Processing

It is done in two steps to check the reaction in grammar. Firstly, the code is analyzed, check the parentheses, and find the start position of the reaction unit. Secondly, check each reaction unit in grammar. Here only explain how it works

for the first step.

From the reaction formula, the status transformation chart can be drawn, and the status matrix can be got, then the grammar checking program can be written from status matrix and transformation table.

From the reaction constitution elements, the input symbols can be divided into four types:

(— left parenthesis, reaction unit start mark.

) — right parenthesis, reaction unit end mark.

S — separation mark, + − × / =

A — reaction mark, numbers 0～9 and alphabets A～Z and comma etc..

The read marks are processed in the program as follows:

When left parenthesis "(" is met, the parentheses account number is added 1, and 1 is subtracted from it for right parenthesis ")". When the separation marks are met, they are treated differently: read next one if it is in reaction formula, change status if it is reaction combination separation mark, and write down its start position if it is the first reaction mark.

In summary, five kinds of status can be divided for reaction grammar analyzing :

S0 — start status.

S1 — a new reaction unit is met.

S2 — left parenthesis is met, and the reaction goes ahead one stage.

S3 — right parenthesis is met, the reaction comes back one stage

S4 — separation mark

S5 — the first letter in the A is met.

S0 and S1 are regarded as one status S1. A status matrix table is got, which describes the situation when the reaction status meets different reaction marks:

Status matrix table

Input Mark	Status				
	S1	S2	S3	S4	S5
(	S2	S2	S4	E	E
)	E	E	S5	S3	S5
S	E	E	S3	S4	S1
A	E	S3	S3	S4	E

Where E means that some status meets illegal mark. For example, S1 is

transformed to S2 if it meets "(", but which is wrong if it meets ")", this is error status E

	S1
(	S2
)	E

In order to process the transformation of status matrix table, five numbers are used, the meaning of them are as the following:

1. error processing
2. go ahead one stage
3. come back one stage
4. process for meeting
5. write down the start position, when the first mark of the reaction unit is met.

If the number in the parentheses counter is not zero at last, it means that the parentheses are not in pairs.

Go to table

	S1	S2	S3	S4	S5
(	2	2	1	1	1
)	1	1	3	1	3
S	1	1	1	1	4
A	1	5	1	1	1

It makes the program structure tight and the level clear to process reaction formula by using status matrix method.

References

[1] V. Mclane, EXFOR system manual, BNL, New York, 1988

[2] F. L. Bauer et al., Compiler construction: A Advanced Course, Springer–Verlag, New York, 1974

[3] T. G. Lewis, Software Engineering, Prentice–Hall, London, 1979

[4] A. Balfour et al., Programming in Standard FORTRAN 77, Heinemann Educational Books, London, 1979

A Code for Processing and Plotting Data and Intercomparison of Evaluated Data for ^{63}Cu

Liu Tong Zhao Zhixiang

(Chinese Nuclear Data Center, IAE)

Introduction

In the course of evaluation, evaluators usually need to compare various evaluated, experimental and theoretical calculated data. So, a code for processing and plotting would be very useful in doing the comparison. During the intercomparison of evaluations of ^{63}Cu, MAINPLT code has been developed. This code has several small part, each part is controlled by a command, several command forms a paragraph, one or several paragraph forms a input card. This code is very convenient to the users and easy to learn. MAINPLT can read, process and plot the data in the following format : EXFOR format, ENDF / B format, free format and the format user defined himself.

1 The Major Function of MAINPLT

1.1 Input Data

MAINPLT code can read the data in the following format.

1) ENDF / B format (Only for MF = 3 and MF = 4).
2) EXFOR format, according to given entry and subentry number and given the format of the data.
3) "Column data" (see example).

1.2 Output Data

1) Output data according to the format defined by user.
2) Plot line, symbol, symbol with error bar.

1.3 Data Process

1) Do the four fundamental operations of arithmetic between data and data or data and constant.

2) Do the functional operations. The functions are : SQRT, SIN, COS, SIND, COSD, TAN, LOG, LOG10, EXP, ASIN, ACOS, ASIND, ACOSD, ATAN, SINH, COSH, TANH, ABS.

3) Do the interpolation.

4) Delete some extra experimental data according to the user's requirement, when the experimental data are too dense to plot.

2 A Simple Example for the Use of MAINPLT

Before running the MAINPLT code, user must write an input card. The input card control the code. For example, comparing the elastic scattering cross section of JENDL–3 library with the experimental data, the following input card must be written at first:

	Input card	Comments
XUNIT	MeV	X–axis unit
YUNIT	CROSS SECTION (b)	Y–axis unit
OPENINPUT	CU63.J3	open JENDL–3 file
READENDFB	0 3 2	read MF = 3 MT = 2
PROGRAM	C1 = C1 / 1000000.	change unit from eV to MeV
LINE	0 | C1 | C2 |	draw line
LINENOTE	0 | JENDL–3 |	note in the picture
C–ARRAY		restore array
OPENINPUT	CU63.ELA	open experimental data file
COLUMN	3	tell the code read three column
READDATA		read data
SYMBE	0 | C1 | C2 | C3 | C3 |	draw symbol point with error bar
SYMBNOTE	0 | S. M. EL–KADI(82) |	note in the picture
NOTEBT	Example of MAINPLT	note at the bottom of picture

The file of CU63. ELA contains the experimental data of S. M. EL–KADI[1], This kind of data is called "Column data".

CU63. ELA file

N

X(1) Y(1) DY(1)
X(2) Y(2) DY(2)
.....
X(N) Y(N) DY(N)

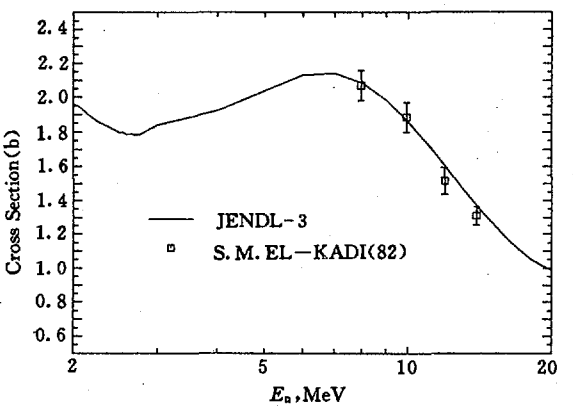

Fig. 1 Example of MAINPLT

After writing the input card, user can run the MAINPLT code and get the picture. The picture for the example above is shown in Fig. 1. If a VT240 series terminal (VT240, VT340, •••) is available, the position of the note can be easily adjusted by using the arrow keys.

MAINPLT is written in FORTRAN–77 language. It can be used on Micro–VAX–II and on PC (supported by NDP 2.1). This code is independent with the plotting device, the user can connect with the device himself by editing a small code. The code and the user's manual can be obtained from the authors.

3 Intercomparison of ^{63}Cu

There are two sets of evaluated neutron data for ^{63}Cu, JENDL–3 and ENDF / B–6. During the comparison, all the pictures are drawn by MAINPLT.

3.1 Total Cross Section

The evaluated data of ENDF / B–6 for total cross section is based on the experimental data of Pandey[2] from 99.5 keV to 1.12 MeV. From 1.12 MeV to 4 MeV natural copper data of Perey[3] were adopted. The JENDL–3 is based on the natural copper data measured by Whalen[4] and Igarasi[5] from 153 keV to 3 MeV. The comparison is shown in Fig. 2.

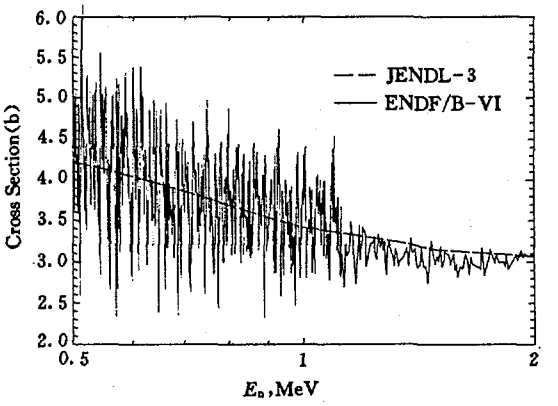

Fig. 2 Comparison of evaluated total neutron cross section for ^{63}Cu

3.2 (n,2n) Cross Section

There are about forty sets of experimental data for (n,2n) cross section. Only the data measured after 1960 are plotted. The average value at 14.5 MeV is also shown in Fig. 4. From Fig. 4, it can be found that large discrepancy exists among the measured data, and the data of ENDF / B–6 is consistent with the latest measured data of Ryves[6] well.

3.3 (n,γ) Cross Section

There are some experimental data for (n,γ) cross section below 4 MeV, but in the high energy region, only one set of data measured by Perkin[7] is available. The data of ENDF / B–6 are more consistent with the measured one than those of JENDL–3.

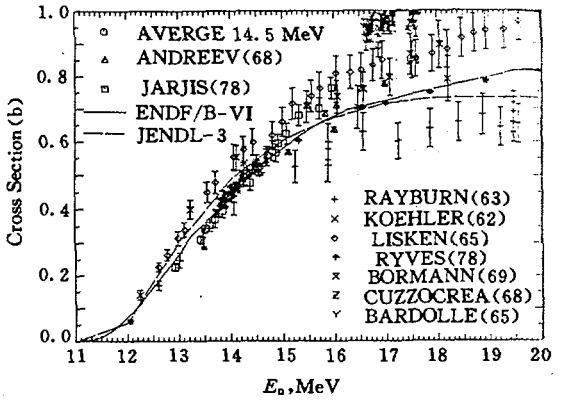

Fig. 3 Comparison of evaluated and measured cross section for $^{63}Cu(n,2n)$ reaction

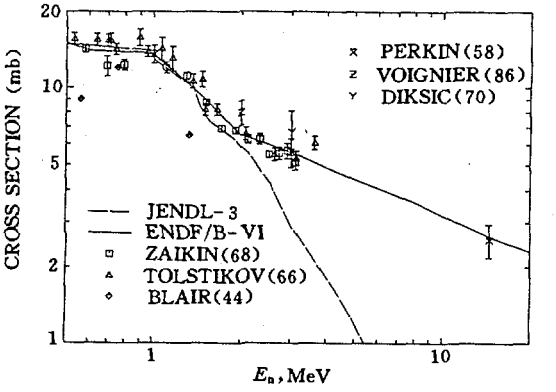

Fig. 4 Comparison of evaluated and measured cross section for $^{63}Cu(n,\gamma)$ reaction

Acknowledgment

The authors would like to thank Zhang Jin for using his unpublished plotting library.

References

[1] S. M. EL-KADI et al., J. Nucl. Phys. A390, 509(1982)
[2] M. S. Pandey et al., Phys. Rev., C15, 600(1977)
[3] Hetrick and Perey, Private Communication, 1977
[4] J. F. Whalen et al., ANL-7710, 12(1971)
[5] S. Igarasi, J. Nucl. Sci. Technol., 12, 67(1975)
[6] T. B. Ryves, K. J. Zieba, J. Met., 14, 3, 127(1978)
[7] J. L. Perkin et al., J. Proc. Phys. Soc. 72, 505(1958)

V ATOMIC AND MOLECULAR DATA

Evaluation on Physical Sputtering Data for Light Projectile

Yao Jinzhang Yu Hongwei

(Chinese Nuclear Data Center, IAE)

Introduction

Ion–induced sputtering of solid is important in several fields of science and technology such as plasma–surface interaction in fusion device, ion implantation, thin film synthesis, and surface analysis.

The purpose of the present paper is to describe the relation between the ion–induced sputtering yield of monatomic solids and the energy of the incident ion for various ion–target combinations

The most widely used empirical formula for the sputtering yield was given by Bohdansky[1]. This formula describes the yield for all projectile–target combinations from threshold energy to about 100 keV. For light ion sputtering under the normal incidence, the formula is

$$Y(E,0)=\frac{0.042}{U_s}\left(\frac{R_p}{R}\right)\alpha\, S_n(E)\left(1-\left(\frac{E_{th}}{E}\right)^{2/3}\right)\left(1-\frac{E_{th}}{E}\right)^2$$

where

$$S_n(E)=8.478\,\frac{Z_1Z_2}{\left(Z_1^{2/3}+Z_2^{2/3}\right)^{1/2}}\,\frac{M_1}{M_1+M_2}\,\frac{M_1}{M_1+M_2}\,S_n(\varepsilon)$$

$$S_n(\varepsilon)=\frac{3.441\varepsilon^{1/2}\ln(\varepsilon+2.718)}{1+6.355\varepsilon^{1/2}+\varepsilon(6.882\varepsilon^{1/2}-1.708)}$$

ε is the reduced energy defined by

$$\varepsilon=\frac{0.03255}{Z_1Z_2(Z_1^{2/3}+Z_2^{2/3})}\frac{M_2}{M_1+M_2}E\ (\text{eV})$$

U_s is binding energy of solid surface

$$\frac{R}{R_p}=K\frac{M_1}{M_2}+1,\quad K \text{ is adjustable parameters}$$

$$\alpha\begin{cases}=0.3\left(\frac{M_2}{M_1}\right)^{2/3} & \text{for } 0.5<\frac{M_2}{M_1}<10\\ \approx 0.2 & \text{for } \frac{M_1}{M_2}<0.5\end{cases}$$

$$E_{th}=\frac{U_s}{\gamma(1-\gamma)},\quad \text{and}\quad \gamma=\frac{4M_1M_2}{(M_1+M_2)^2}$$

The sputtering yield for oblique incidence is especially important at limiter plates and at parts which are close to the main plasma, where the magnetic field lines cross these parts at oblique angels.

$$Y(E,\theta)=(\cos\theta)^{-f}\exp\{f(1-(\cos\theta)^{-1})\sin\eta\}Y(E,0)$$

where

$$f=U_s^{1/2}\left(0.94-1.33\times10^{-3}\frac{M_2}{M_1}\right)$$

$$\eta=a_L n^{1/3}\left(2\varepsilon\left(\frac{U_s}{\gamma E}\right)^{1/2}\right)^{-1/2}$$

$$a_L=0.468503\,(Z_1^{2/3}+Z_2^{2/3})^{-1/2}$$

n is atomic density of the target.

Results and Discussion

Figs. 1, 2 show both experimental data points and the calculated values of the energy dependence of sputtering yield. The solid lines indicate the calculation of bipartition model of PANDA–SP code by Luo Zhengming et al.. For comparison with Monte Carlo calculation, the computational results of TRIM–SP code[2] are also presented. The dot dash lines illustrate the calculations of empirical formula as mentioned above. We give data on sputtering of Nickel and Carbon solid surfaces with projectiles of Hydrogen, Deuterium Helium and Tritium ions at normal incidence, and meanwhile, we also present data at oblique incidence. The results are reasonably in agreement with values measured and calculated by TRIM–SP and Luo's PANDA–SP codes within error bars.

In many cases the accuracy of the empirical formula is better than 30 % but in special cases differences of more than 50 % are possible. The experimental data have an accuracy of about ± 30 % but the reproducibility is sometimes not better than a factor of two.

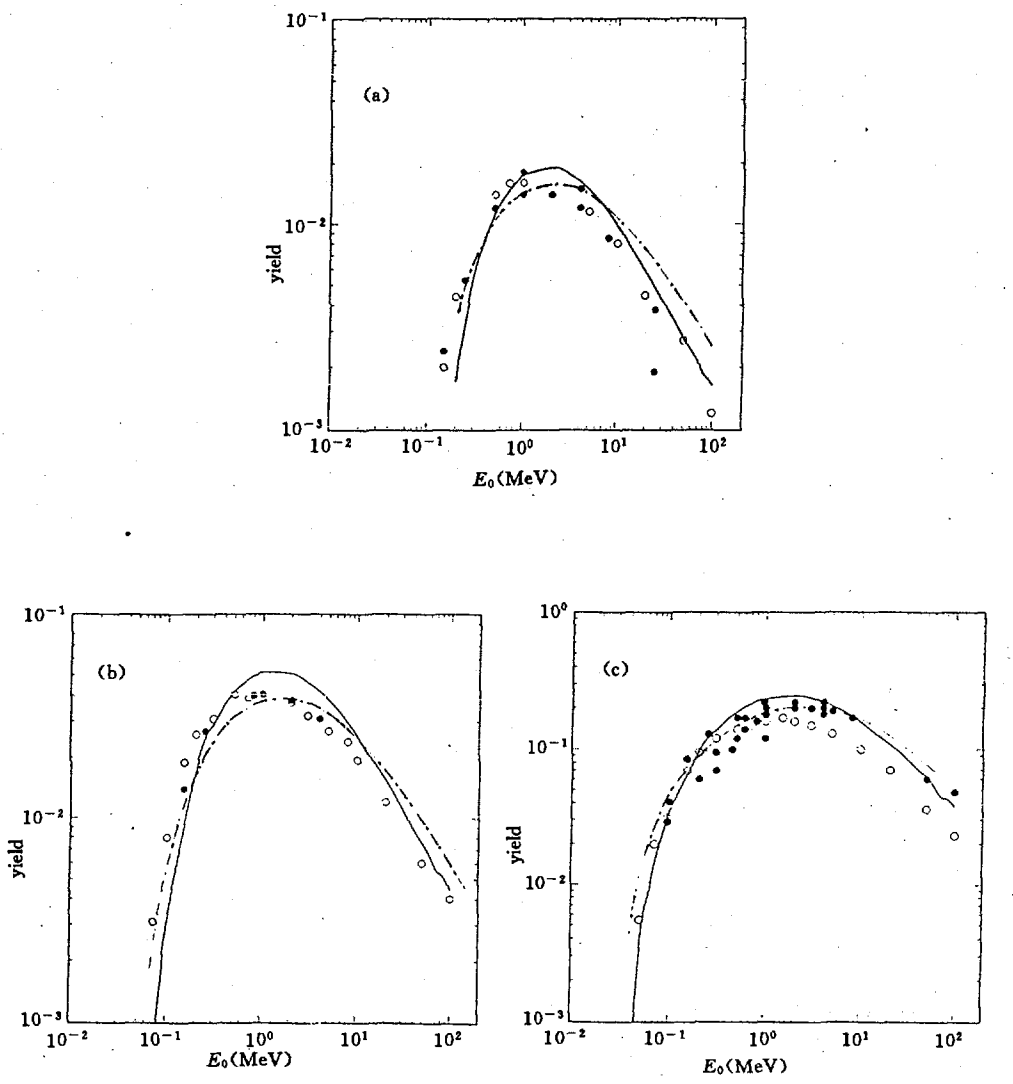

Fig. 1 Sputtering yields of Ni surface by some projectiles at normal incidence

a) H+, b) D+, c) ^{4}He

● exp., ○ Monte Carlo, —— Luo, —·—·· present work.

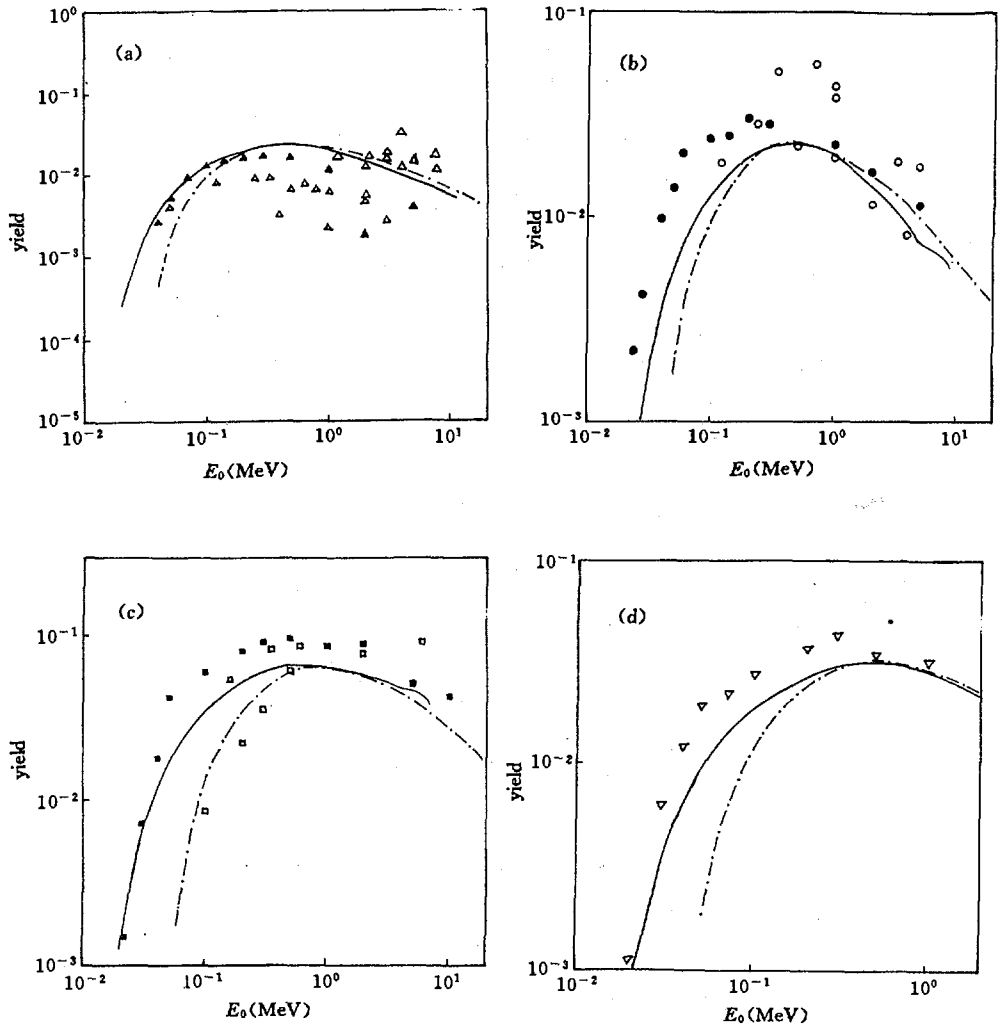

Fig. 2 Sputtering yields of C surface by some projectiles at normal incidence

a) H+, b) D+, c) ^{4}He, d) T+

△ exp., ▲ Monte Carlo, —— Luo, —·—·· present work.

References

[1] J. Bohdansky, Nucl. Instrum. Methods in Phys. Res., B2, 587(1984)

[2] J. P. Biersack et al., Appl. Phys., 34, 73(1984)

Particle Reflection from Solid Surfaces

Fang Shaohong Yao Jinzhang

(Chinese Nuclear Data Center, IAE)

Abstract

With our particular interest in fusion related applications, we will restrict our discussions to scattering of light ions (H^+, D^+, T^+, $^3He^+$ and $^4He^+$) and some impurities on candidate plasma facing component materials. The information on H^+ and D^+ projectiles has been illustrated in reference[1]. In the present paper, we will emphasize on that T^+, $^3He^+$ and $^4He^+$ particles project into surfaces of 12 elemental targets under incident angle region of $0 < \alpha < 60$ degrees. Impact energies will range from 10 eV to one hundred keV.

Introduction

Reflection is described in terms of the particle reflection coefficient R_n, being the ratio of the number of projectiles reflected to the number of projectile incident, and also the energy reflection coefficient R_e, being the ratio of energy carried away by the reflected projectiles to the energy carried by the incident projectiles. We will demonstrate that how R_n and R_e vary with incident energy and seek systematic behaviours as a function of projectile–target combination. The most previously published data on particle reflection from surfaces are involved in the projectiles incident normally onto a surface.

It has long been recognized that particle and energy reflection coefficients are decreased monotonically as projectile energy increase and approach to unity at very low incident energy. Recently, W. Eckstein[2] indicated that the reflection coefficients decrease again when the kinetic energy approaches to the strength of chemical binding forces to surface atoms. The calculated results[3] using a PANDA–U(PU) code to take account of surface binding energy E_s show that the reflection coefficients decrease again when the incident energy less than 100 eV. We illustrate the same tendency calculated by our empirical formula which is modified to the formula described by R. Ito et al.[4] as follows:

$$R_e = \frac{\frac{0.705}{f}}{1+\left(\frac{\varepsilon}{0.047}\right)^{0.597}+\left(\frac{\varepsilon}{0.619}\right)^{1.5}} - e^{-\pi(M_1+M_2)\varepsilon} \tag{1}$$

$$R_n = \frac{R_e}{\gamma_e}$$

where

$$\gamma_e = \frac{1}{1+\left(\frac{\varepsilon}{0.133}\right)^{0.285}} + \frac{0.530}{1+\left(\frac{\varepsilon}{85}\right)^{-1.46}} \tag{2}$$

$$f = Z_1^{2/3} M_1^{-1/2} \left(\frac{M_1+M_2}{M_2}\right)^{\frac{(2\varepsilon-3)}{(\varepsilon+1)}} \frac{\rho_a}{\rho_t} \tag{3}$$

$$\frac{\rho_a}{\rho_t} = \frac{\frac{2\varepsilon}{\rho_n} + \left(\frac{1}{S_L}+\frac{1}{4S_B}\right)^{-1}}{S_a} \tag{4}$$

$$\rho_n = \frac{\{\Gamma(0,(C-1)\ln(B\varepsilon)) - \Gamma(0,-2\ln(B\varepsilon))\}}{AB} \tag{5}$$

$$\Gamma(v,x) = \int_x^\infty e^{-t} t^{(v-1)}\, dt \tag{6}$$

$$A = 0.56258, \quad B = 1.1776, \quad C = 0.62680$$

$$S_a = 0.0793\ Z_1^{2/3}\ M_1^{-3/2}\ M_2 \varepsilon^{1/2}$$

$$S_L = D\left(\frac{M_1+M_2}{M_2\xi}\right)^{3/2} S_a \tag{7}$$

$$\xi = \left(Z_1^{2/3}+Z_2^{2/3}\right)^{1/2} Z_2^{-1/3}$$

Where ε is the reduced energy and D is the correction factor for the low

energy electronic stopping cross section.

$$\varepsilon = \frac{0.03255}{Z_1 Z_2 (Z_1^{2/3} + Z_2^{2/3})} \frac{M_2}{M_1 + M_2} E \ (\text{eV})$$

$$D = 0.2617 \ (1 + Z_2^{2/3})^{3/2} \ Z_2^{-1} \ A_1$$

$$S_B = 61.47 \ Z_1 \ Z_2^{-1} \ (Z_1^{2/3} + Z_2^{2/3})^{1/2} (M_1 + M_2) M_1^{-1}$$

$$\times \frac{\ln \left(\frac{\varepsilon_B}{(1-\beta^2)} + 1 + \frac{G}{\varepsilon_B} \right) - \beta^2}{I_0 \varepsilon_B} \tag{8}$$

$$\varepsilon_B = 2 m_e c^2 \frac{\beta^2}{Z_2 I_0}$$

$$I_0 = \begin{cases} 12 + 7 \ Z_2^{-1} & \text{for } Z_2 < 13 \\ 9.76 + 58.5 \ Z_2^{-1.19} & \text{for } Z_2 \geqslant 13 \end{cases}$$

$$G = \begin{cases} 100 \ \dfrac{Z_1}{Z_2} & \text{for } Z_1 < 3 \\ 5 & \text{for } Z_1 \geqslant 3 \end{cases}$$

Where $m_e c^2$ is the rest energy of the electron, $Z_2 I_0$ is the mean excitation energy of target atoms and β is the ratio of the projectile velocity to the velocity of light.

For the dependence of reflection coefficients on the angle of incidence, the following formula is given

$$R(\alpha) = R(o) + \frac{(1 - R(o))}{(1 + a_1 \ \cot^{2a_2} \alpha)} \tag{9}$$

Where $R(o)$ is reflection coefficients of normal incidence of projectiles.

$$a_1 = 7.38\ \varepsilon^{0.359},\quad a_2 = \frac{0.836}{\varepsilon^{0.087}}\quad \text{for}\quad R_n$$

$$a_1 = 17.9\ \varepsilon^{0.435},\quad a_2 = \frac{0.771}{\varepsilon^{0.014}}\quad \text{for}\quad R_e$$

Results and Discussion

Figs. 1, 2 show the results of projectiles H^+ and D^+ $^3He^+$, $^4He^+$ on surfaces of Carbon, Iron and Gold targets. PP indicates the calculation values using PANDA–P(PP) code which based on a bipartition model solution of the Botzmann transport equation. PU represents results calculated by a revision of PP taking into account surface binding energy of target (it is 7.4 eV for Carbon, 5.2 eV for Iron and 3.8 eV for Gold). RC shows the results of reflection coefficients calculated using modified empirical formula above.Some measured results from various laboratories[4] are also given with symbols. We can find that particle reflection coefficients are high at low energy and decrease monotonically as projectile energy increases in range of 100 eV to 100 keV. However, the reflection coefficients decrease again when the incident energy approaches the surface binding energy of solid. There is some uncertainty as to how one should describe reflection at vanishingly low energy. At low energy stripping is very inefficient so that the lowest energy recoils is not detected. Experimental studies are largely confined to energy between 1 and 10 keV where beams are easy to be prepared, reflected species is easy to be detected. Their accuracy is quoted as 10 to 30 %. It is probably up to 50 % under the bad conditions. Monte Carlo simulations generally have an inherent statistical accuracy of 10 %; the results may be altered by as much as 30 % through the choice of potentials and other relevant parameters. The extensive calculations of Luo's bipartition model code often agree with Monte Carlo such as TRIM[5] and MARLOW[6] codes simulations. Our calculation values using modified semiempirical formula are in good agreement with experimental values and also agree with the extensive calculations of PU code within the region of errors for projectile energy from 100 eV to 10 keV. Figs. 3, 4 represent the relations of reflection coefficients to incident energies for the combinations of $^3He^+$ with nickel and $^4He^+$ with molybdenum under incident angels of 0, 15, 30, 45 and 60 degs.. The uppermost line is for 60 degrees and the others follow in descending order. There is some experimental points at normal incident angles and only a few results measured under the others. The recommended line is also used for

cases where are no experimental values, as for example is almost always the case for T^+ projectile as shown in Figs. 5, 6.

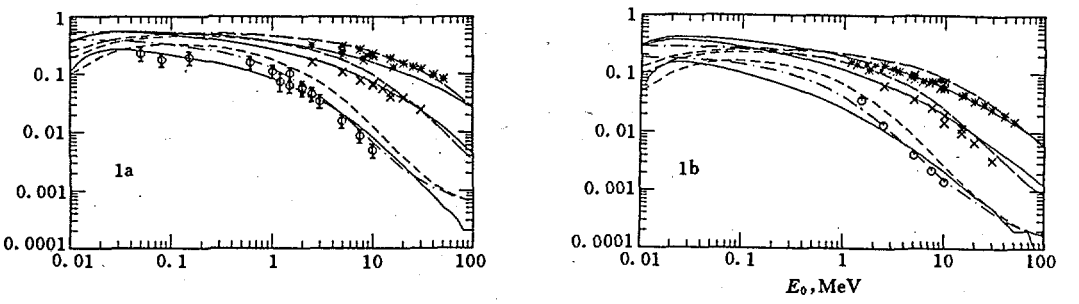

Fig. 1–1 Reflection coefficients for H^+ on C, Fe and Au solid surfaces at normal incidence

1a) R_n, 1b) R_e, —·—·· PP, – – · PU, ——— RC

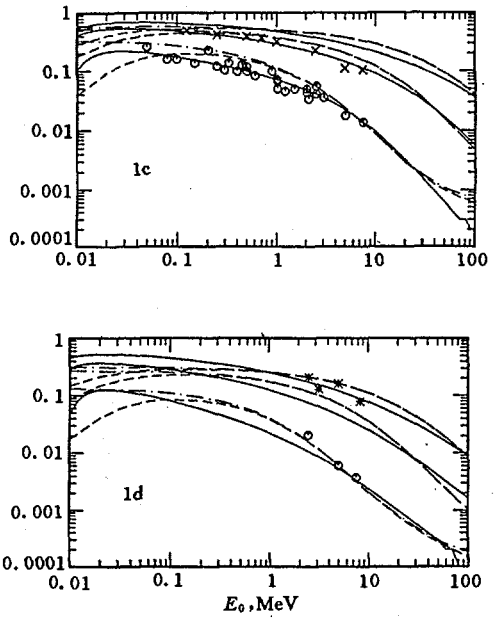

Fig. 1–2 Reflection coefficients for D^+ on C, Fe and Au solid surfaces at normal incidence

1c) R_n, 1d) R_e, ○ D–C, × D–Fe, * D–Au

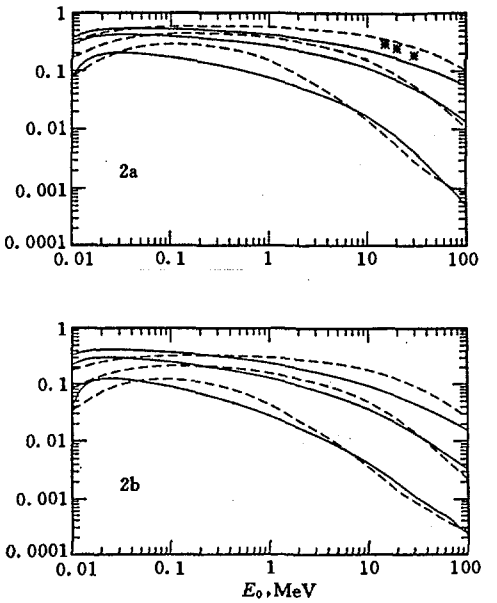

Fig. 2–1 Reflection coefficients for $^3He^+$ on C, Fe and Au solid surfaces at normal incidence

2a) R_n, 2b) R_e, – – – · PU, ——— RC

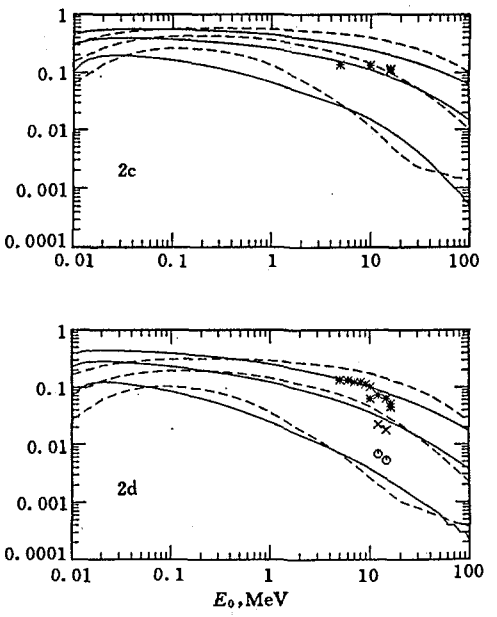

Fig. 2–2 Reflection coefficients for $^4He^+$ on C, Fe and Au solid surfaces at normal incidence

2c) R_n, 2d) R_e, ○ ^{4}He–C, × ^{4}He–Fe, * ^{4}He–Au

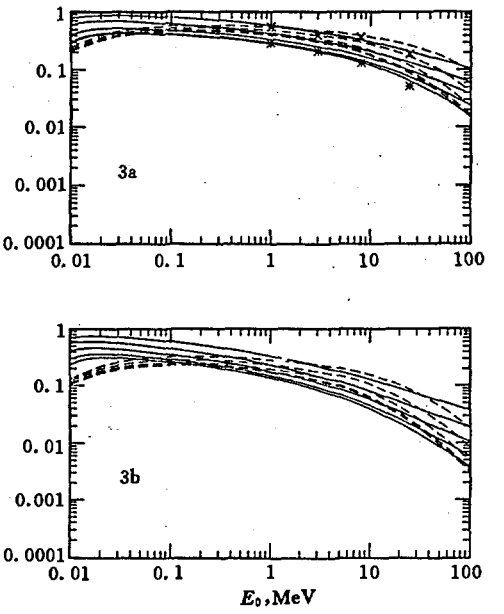

Fig. 3 Reflection for $^3He^+$ on Ni solid surface

3a) R_n, 3b) R_e, – – – · PU, ——— RC

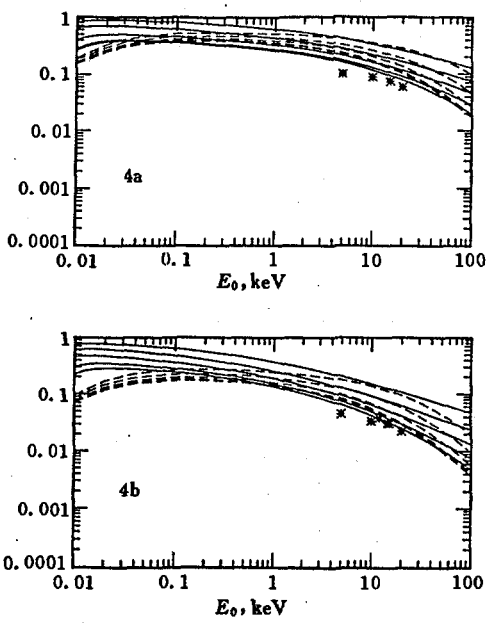

Fig. 4 Reflection for $^4He^+$ on Mo solid surface

4a) R_n, 4b) R_e, × 60–Exp, * 0–Exp

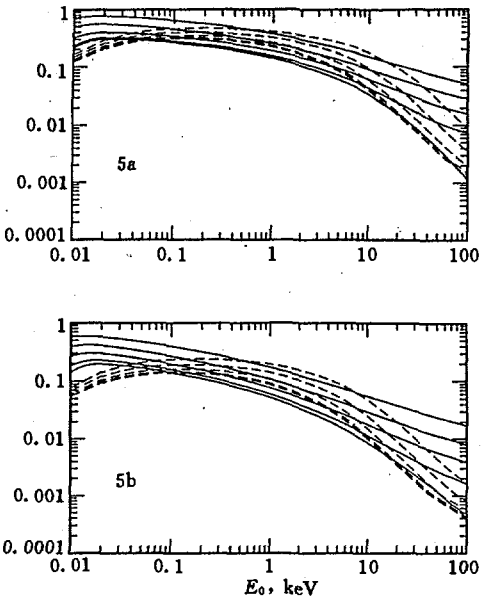

Fig. 5 Reflection for T^+ on Si solid surface

5a) R_n, 5b) R_e, – – – · PU

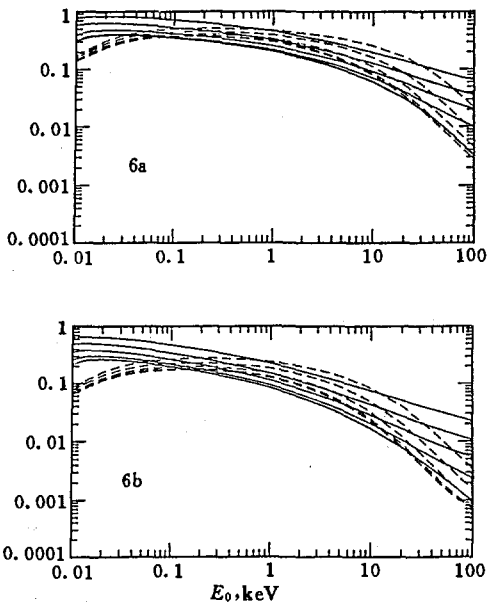

Fig. 6 Reflection for T^+ on Ti solid surface

6a) R_n, 6b) R_e, ——— RC

References

[1] Yao Jinzhang et al., Communication of Nuclear Data Progress, 8, 70(1992)

[2] W. Eckstein, Supplement to the Journal of Nuclear Fusion, Vol. 1, 17(1991)

[3] Luo Zhengming , Nucl. Instr. & Methods in Phys. Res., B48, 444(1990)

[4] R, Ito et al., IPPJ–AM–41 (1985)

[5] W. Eckstein et al., Max–Planck–Institute fur Plasmaphysik Garching, Report IPP 9 / 32 (1979)

[6] W. Eckstein et al., Z. Phys. A. Atom and Nuclei, 310, 1(1983)

VI DATA PROCESSING

Dimension and Deriving Manner for Derived Quantities

Zhao Zhixiang

(Chinese Nuclear Data Center, IAE)

Introduction

Most physical quantities we are interested in are derived from some directly measured physical quantities. In the field of modern nuclear data reduction, further study to derived quantities is still needed. An evidence for this is so called PPP phenomenon[1]. In the author's early papers on PPP[2~4], it was demonstrated that PPP phenomenon can be attributed as the inconsistencies in generating derived quantities and their covariance matrix , and that this inconsistencies can be eliminated by an iterating process.

Some more general problems, which are independent of PPP, will be discussed in this paper. The problem concerned can be described as follows:

Let us assume that we have N_i directly measured data for physical quantity X_i,

$$X_i^* = (X_i^*(1) , \cdots , X_i^*(N_i))^T \tag{1}$$

The directly measured data vector for m physical quantities can be written as

$$D=\begin{bmatrix} X_1^* \\ \cdot \\ \cdot \\ \cdot \\ X_m^* \end{bmatrix} \tag{2}$$

The dimension of vector D is

$$\dim\ D=\sum_{i=1}^{m}N_i \tag{3}$$

If we are interested in physical quantity, Y, which is derived from

$$Y=f(\ X_1\ ,\ \cdots\ ,\ X_m\ ) \tag{4}$$

now, to be sure that the information involved in D are neither overlap nor missing, what the dimension for derived vector

$$G=(\ Y_1\ ,\ \cdots\ ,\ Y_n\ ) \tag{5}$$

should be and what is the limitation on deriving manner? For obtaining the estimates of derived quantities through combination and fitting, it is rather significant to answer the questions above.

During the discussion of PPP, several authors have noted impact of the dimension of derived quantities on least-square results[5~6]. S. Chiba proposed "dimension conservation"[5]. Present paper will demonstrate that "dimension conservation" is right only when we are interested in all of physical quantities of $Y, X_1\ ,\ \cdots\ ,\ X_m$. If we are interested only in Y, the dimension of derived quantities should be less than those of directly measured data when $m>1$.

1 Dimension of Derived Quantities

Using directly measured data D defined by Eq. (2) and relationship of Eq. (4), the greatest number of derived quantities for Y is given by

$$n_0=\prod_{i=1}^{m}N_i \tag{6}$$

But these derived quantities may not be independent each other. It means that some of derived quantities could be represented by the others. In this case, the

covariance matrix for derived quantities generated based on the law of error propagation must be singular so that the least–square method can not be used to combine or fit these derived data. For instance, the directly measured data and relationship between directly measured and derived data are as follows

$$Y = a + C \tag{7}$$

$$D = (a_1^* , a_2^* , C_1^* , C_2^*)^T \tag{8}$$

If we denote derived data by

$$Y_{ij} = a_i^* + C_j^* \tag{9}$$

we have four derived data for Y: Y_{11}, Y_{12}, Y_{21}, Y_{22}, but these four derived quantities are not independent of each other because of

$$Y_{22} = Y_{21} - Y_{11} + Y_{12} \tag{10}$$

It is easy to prove that the covariance matrix V_G for

$$G = (Y_{11} , Y_{12} , Y_{21} , Y_{22} ,)^T \tag{11}$$

must be singular, so that the least–square estimate for Y can not be obtained based on G and V_G generated in the manner above.

On the other hand, only using Y_{11} and Y_{12} will also give a wrong estimate for Y because of the information of a_2^* missing. It will be demonstrated in the following that under the condition "the information involved in D are neither overlap nor missing", the dimension of derived quantity vector G should be

$$n = \dim G = \sum_{i=1}^{m} N_i - (m - 1) \tag{12}$$

There is a non–linear transformation relation between G and D. To determine uniquely D, $\sum N_i$ independent equations are needed. Among them, (m–1) equations must be generated based on

$$\begin{aligned} X_1(j_1) &= X_1^*(j_1) \\ &\vdots \\ &\vdots \\ &\vdots \end{aligned} \tag{13}$$

$$X_m(j_m)=X_m^*(j_m)$$

Therefore only n equations are independent in n_0 equations given by Eq. (4).

On the other hand, the condition that the information in D is neither overlap nor missing requires that any $X_i^*(j)$ appear at least once in deriving process and keep the information between any pair of $X_i^*(k_i)$ and $X_j^*(k_j)$ no missing.

Assuming that

$$N_1 \geqslant N_2 \geqslant \cdots \geqslant N_m \tag{14}$$

the condition "any $X_i^*(j)$ appears at least once" requires N_1 derived quantities, another ($N_2 - 1$) derived quantities needed to make sure no information missing between $X_2^*(j)$ and other $X_1^*(j')$, $\cdots$. So the dimension of derived quantities should be given by Eq. (12).

It must be pointed out that the dimension given by Eq. (12) is right only when we are interested only in Y. If we are interested in all of physical quantities concerned (Y, X_1, $\cdots$, X_m), D should be uniquely determined from derived data and relationship between D and G. In this case, the dimension of G should be equal to one of D, $\sum N_i$.

2 Deriving Manner of Derived Quantities

In fact, only satisfying Eq. (12) for the dimension of G is not sufficient because the case of "part of information overlap and another part of information missing" may exists. On the other hand, there may be a lot of deriving manners under the condition "information neither overlap nor missing". For the example given by Eqs. (7~8), right dimension should be $n = 3$ and four deriving manners of (Y_{11}, Y_{12}, Y_{21}),(Y_{11}, Y_{12}, Y_{22}), (Y_{11}, Y_{21}, Y_{22}) and (Y_{12}, Y_{21}, Y_{22}) are all correct.

In the following, we will give a deriving manner which is only one of many correct manners as mentioned above.

Written the quantity derived from $X_1^*(j_1),\cdots, X_m^*(j_m)$ ($j_k = 1, 2, \cdots, N_k$), through Eq. (4) as ($j_1 \quad j_2 \quad \cdots \quad j_m$), the following deriving manner is correct:

$$\begin{array}{l}(1 \quad 1\cdots1 \quad 1),(1 \quad 1\cdots1 \quad 2),\cdots,(1 \quad 1\cdots1 \quad N_1)\\(1 \quad 1\cdots2 \quad 1),(1 \quad 1\cdots3 \quad 1),\cdots,(1 \quad 1\cdots N_2 \quad 1)\\ \vdots \\ (2 \quad 1\cdots1 \quad 1),(3 \quad 1\cdots1 \quad 1),\cdots,(N_m \quad 1\cdots1 \quad 1)\end{array} \tag{15}$$

3 Computational Example

Let us see the example S. Chiba has used in his paper[5].
We have independent measured data

$$a_1^* = 2.5 \pm 0.15;\ a_2^* = 2.0 \pm 0.09\cdot\ C_1^* = 1.0 \pm 0.3;\ C_2^* = 1.0 \pm 0.134 \tag{16}$$

and relationship

$$Y_{ij} = a_i^* - C_j^* \tag{17}$$

If we are only interested in Y, four derived quantities for Y and its covariance matrix can be obtained as follows

$$G^{\mathrm{T}} = (\ Y_{11}\quad Y_{12}\quad Y_{21}\quad Y_{22}\ ) = (\ 1.5\quad 1.5\quad 1.0\quad 1.0\ ) \tag{18}$$

$$V_G = \begin{bmatrix} 0.1125 & 0.0225 & 0.09 & 0 \\ 0.0225 & 0.040456 & 0 & 0.017956 \\ 0.09 & 0 & 0.0981 & 0.0081 \\ 0 & 0.017956 & 0.0081 & 0.026056 \end{bmatrix} \tag{19}$$

It is easy to prove $|\ V_G\ | = 0$, so V_G is a singular matrix. In the 4–dimensional derived quantity space, it is impossible to obtain least–square estimate of Y based on G and V_G.

In this example, $N_1 = N_2 = 2$ so that right dimension for derived quantities should be $n = 3$. We have four deriving manners which are completely equivalent each other:

$$G_1 = \begin{bmatrix} Y_{12} \\ Y_{21} \\ Y_{22} \end{bmatrix};\ G_2 = \begin{bmatrix} Y_{11} \\ Y_{21} \\ Y_{22} \end{bmatrix};\ G_3 = \begin{bmatrix} Y_{11} \\ Y_{12} \\ Y_{22} \end{bmatrix};\ G_4 = \begin{bmatrix} Y_{11} \\ Y_{12} \\ Y_{21} \end{bmatrix} \tag{20}$$

In 3–dimensional derived quantity space, the least–square estimates for Y based on these four deriving manners are exactly consistent:

$$\hat{Y} = 1.132 \pm 0.145 \tag{21}$$

4 Discussion

To obtain correct least–square result in derived quantity space, one must pay attention to inconsistencies problem to avoid PPP phenomenon in generating derived quantities and their covariance matrix. The situation is complicated by the problems of dimension and deriving manner for derived quantities. As the author pointed out[2~4], it would be better to solve least–square equation in data space if possible to avoid any mistakes in deriving process. For the example given by Eqs. (16~ 17), it is very convenient to obtain the correct result in data space. Due to that directly measured data are independent each other, the least–square estimates for a and C can be given by weighted averaging:

$$\hat{a} = 2.132 \pm 0.07717$$

$$\hat{C} = 1.0 \pm 0.1223$$

so estimate for $\hat{Y}$ is

$$\hat{Y} = \hat{a} - \hat{C} = 1.132$$

$$\sigma^2(\hat{Y}) = \sigma^2(\hat{a}) + \sigma^2(\hat{C}) = 0.145^2$$

in consistent with those of Eq. (21).

References

[1] R. W. Peelle, Informal Memorandum, Oct. 13,1987 ORNL, USA

[2] Zhao Zhixiang et al., ORNL / TM–12106 (1992)

[3] Zhao Zhixiang et al., Proc. of Conf. on Evaluation Methodology, BNL(1992) (to be published)

[4] Zhao Zhixiang, Chinese Nucl. Sci. and Eng., to be published

[5] S. Chiba, Proc. of NEANSC Specialist' Meeting on Evaluation and Processing of Covariance Data, ORNL(1992), USA (to b published)

[6] R. L. Perel et al., Proc. of Conf. on Evaluation Methodology, BNL(1992), USA (to be published)

Evaluation of Correlative Nuclear Data at Certain Energy Point

Zhang Jianhua (HIP. Beijing)

Liu Tingjin (CNDC, IAE)

A method to process correlative nuclear data at certain energy point is presented. The corresponding processing code has also been developed. Using the code, the effects of the correlation have been discussed in detail for the cases of the two and three data.

Introduction

The processing of nuclear parameter at a certain energy is a problem often met by nuclear data evaluators. The essential objective of this processing is to estimate the combination–mean of the physical quantity measured by different groups which is considered to represent the estimation of the unknown true value. In nuclear data evaluation, a highly accurate datum at an energy is significant for the determination of the absolute position of the evaluated curve of the whole energy range. However, the traditional method of the treatment to the problem is quite rough, and is applicable only to the case of independent nuclear data and make senses at the extreme cases [1]. Therefore it is essential to develop a method of high accuracy to deal with the problem.

There, generally, exists difference among different measured values. Two factors contribute to the difference [2]. The first one results from the existence of the statistical errors which come from the limitation of the data samples. The second one originates from the correlative errors and the possibility existing negligence errors which have the properties of the systematic errors but are neglected by the experimenters when reporting their errors. It is the second factor that are much more difficult to dispose and are often treated simply as the statistical errors by most evaluators. This lead to seriously damage to the accuracy of the evaluated data.

In this paper, starting from the most general cases, we develop a method to deal with not only the statistical errors, but also the systematical errors and the possibility existed negligence errors. Throughout the section I, a statistical

model is presented for isolating the possibility existing negligence error, adjusting the original data and estimating the combination–mean of the correlative data. The corresponding code has also been developed. Using the code, in section II, the physical behavior of the experimental correlation is studied.

1 Statistical Model[1, 2]

Suppose a nuclear parameter y, e. g. cross section, fission product yield, has n measured values by n laboratories,

$$\vec{Y}' = (y'_1, y'_2, \cdots, y'_n)^{\mathrm{T}} \tag{1.1}$$

the covariance matrix of $\vec{y}'$ is

$$V = \begin{bmatrix} \mathrm{cov}(y'_1, y'_1) & \mathrm{cov}(y'_1, y'_2) & \cdots & \mathrm{cov}(y'_1, y'_n) \\ \cdots & \cdots & \cdots & \cdots \\ \mathrm{cov}(y'_n, y'_1) & \mathrm{cov}(y'_n, y'_2) & \cdots & \mathrm{cov}(y'_n, y'_n) \end{bmatrix} \tag{1.2}$$

Denotes the common genuine value of the n measurements by

$$\hat{Y}^{\mathrm{T}} = (y_1, y_2, \cdots, y_n) \tag{1.3}$$

Obviously the freedom degree of the problem is $n-1$.

Usually, the n measured values are inconsistent with each other within the reported errors, therefore, there must exist negligence errors for at least one of data. Denotes the negligence errors of the n measured data by

$$\vec{G}^{\mathrm{T}} = (g_1, g_2, \cdots, g_n) \tag{1.4}$$

evidently, the likelihood function can be written as

$$X^2(\vec{Y}' \mid \hat{Y}, \vec{G}) = (\vec{Y}' - \vec{G} - \hat{Y})^{\mathrm{T}} V^{-1} (\vec{Y}' - \vec{G} - \hat{Y}) \tag{1.5}$$

As for the uncertainty of the negligence errors, its prior distribution function can rationally be assumed as (here only the exponent part of the multi–dimension normal distribution is explicitly written out, the same bellow)

$$X^2 (\vec{G} \mid \lambda) = \lambda \vec{G}^T \times V_g^{-1} \times \vec{G} \tag{1.6}$$

where V_g means the covariance matrix of the negligence errors, and λ is a Lagranger multiplier which represents the overall credibility of the n groups. When $\lambda \to \infty$, then $g_i \to 0$, there exist no negligence errors; when $\lambda \to 0$, then g_i become large.

Following the certainty–assumption of $\hat{Y}$, we have

$$X^2 (\hat{Y}) = 0 \tag{1.7}$$

From Eqs. (1.5), (1.6) and (1.7), following the Bayes Theorem,

$$X^2 (\vec{G} \mid \vec{Y}', \lambda) = [\vec{G} - (V_1^{-1} + \lambda V_g^{-1})^{-1} V_1^{-1} \times \vec{Y}']^T \times (V_1^{-1} + \lambda V_g^{-1}) [\vec{G} - (V_1^{-1} + \lambda V_g^{-1})^{-1} V_1^{-1} \times \vec{Y}'] \tag{1.8}$$

and the posterior probability function of $\vec{Y}'$ is

$$X^2 (\vec{Y}' \mid \lambda) = \vec{Y}'^T V_1^{-1} (V_1^{-1} + \lambda V_1^{-1})^{-1} \lambda V_g^{-1} \vec{Y}' \tag{1.9}$$

here

$$V_1^{-1} = V^{-1} - \frac{V^{-1} \times U \times V^{-1}}{\vec{e} \times V^{-1} \times \vec{e}} \tag{1.10}$$

and

$$U = \vec{e}^T \times \vec{e}, \qquad \vec{e}^T = (1, 1, \cdots, 1)$$

Setting $X^2 (\vec{Y}' \mid \lambda)$ equal to its most probable value $n-1$

$$X^2 (\vec{Y}' \mid \lambda) = n - 1 \tag{1.11}$$

and following the Maximum Likelihood Principal, the negligence errors and their covariance matrix for the given data can be got from (1.11):

$$\vec{G}_0 = (V_1^{-1} + \lambda V_g^{-1})^{-1} V_1^{-1} \vec{Y}' \tag{1.12}$$

$$V_g^{-1} = V_1^{-1} + \lambda V_g^{-1} \tag{1.13}$$

Having $\hat{Y}$ in Eq. (1.5) substituted by $\vec{Y}$, the adjusted measured value, Eq. (1.5) will become the likelihood function of $\vec{Y}$. Combining this equation with that of (1.12) and (1.13), and using Bayes Theorem, we can get

$$X^2(\vec{Y}) = [\vec{Y} - (\vec{Y}' - \vec{G}_0)]^T (V + V_g^{-1})^{-1} [\vec{Y} - (\vec{Y}' - \vec{G}_0)] \tag{1.14}$$

From Eq. (1.14), the best estimate of the adjusted data can be obtained:

$$\vec{Y} = \vec{Y}' - \vec{G}_0 \tag{1.15}$$

$$V_a = V + V_g \tag{1.16}$$

Making minimum of the following residual function

$$(\vec{Y} - Y_e\ \vec{e})\ V_a^{-1}\ (\vec{Y} - Y_e\ \vec{e}) \quad \rightarrow \min \tag{1.17}$$

the best estimate of the desired parameter come to be obtained as

$$y_e = \frac{\vec{e}^T\ V_a^{-1}}{\vec{e}^T\ V_a^{-1}\ \vec{e}} \times \vec{Y} \tag{1.18}$$

$$\Delta y_e = \sqrt{\frac{1}{\vec{e}^T\ V_a^{-1}\ \vec{e}}} \tag{1.19}$$

2 Practical Code

Based on the formulas in the former section, a computer code has been developed. The consistency of the original data is firstly tested in the program. If the input data satisfy the following condition:

$$\vec{Y}'^T \left[V^{-1} - \frac{V^{-1}\ U\ V^{-1}}{\vec{e}^T\ V^{-1}\ \vec{e}} \right] \leqslant n - 1 \tag{2.1}$$

then they are considered consistent with each other, and the combination–mean is obtained by Eqs. (1.18) and (1.19) with the original data. If Eq. (2.1) is not satisfied, then it is considered that there exist negligence errors . Searching for the root of λ of Eq. (1.11) in the domain of [0, 10000]. If there exists no root in

the range, then the negligence errors are considered too small to be adjusted, and the combination–mean is carried out with the original data with Eq. (1.18) and (1.19). If there exists a root in the region, then the negligence error is extracted and removed from the original data in accordance with Eq. (1.15) and (1.16) and at last, the combination–mean is obtained by Eq. (1.18) and (1.19) with the adjusted data.

3 Calculation and Discussion

3.1 Two–Dimension Case

We take two measured data for the resonance energy of ^{12}C for calculation and discussion[3]. The measured values of the two groups are

$$y_1 \pm s_1 = 2078.31 \pm 0.4108 \quad \text{keV} \tag{3.1}$$

$$y_2 \pm s_2 = 2079.20 \pm 1.1743 \quad \text{keV} \tag{3.2}$$

The effect of the correlation to the combination–mean is illustrated in (Fig. 1).

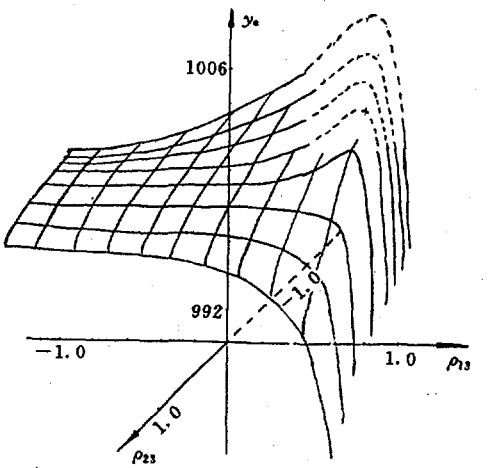

Fig. 1 Effects of correlation in the two dimensional data case

The combination–mean via correlation features the following characteristics:

1) When $\rho < 0$, it is demonstrated that the combination–mean appears

between the two experimental points. Physically, from the definition of the correlation coefficient, it can be inferred that when there exists negative correlation between the two measurements, the two experimental measurements tend to appear on the different sides of the unknown true value. In other words, it is reasonable for the combination–mean which represents the true value to stay between the two experimental points.

2) When $\rho = 0$, the correlative data degenerate into independent ones. This combination–mean coincides with that obtained with the methods of the simple weighted–mean.This also demonstrates the widely applied method of weighted–mean applicable only to the case of independent data.

3) When $\rho > 0$, positive correlation exists between the data.

(1) When $\rho = 0.4568$, the covariance matrix becomes

$$V = \begin{bmatrix} 0.1688 & 0.2204 \\ 0.2204 & 1.3779 \end{bmatrix} \tag{3.3}$$

which is the same with that of F. G. Perey[3]. This combination–mean comes the same with that of F. G. Perey's. It is necessary to notice that in Perey's calculation, negligence errors hadn't been taken into account, while in the present case, it is found that the negligence errors are too small to do any adjustment.

(2) When $\rho > 0.3498$, from Fig. 1, it can be seen that the combination–mean begins to appear out of the range of (y_1, y_2).

Assuming $y_2 > y_1$ analytically we have

$$y_e = y_1 + \frac{(y_2 - y_1)(1 - \rho s_2 / s_1)}{1 + s_2^2 / s_1^2 - 2\rho s_2 / s_1} \tag{3.4}$$

or

$$y_e = y_2 + \frac{(y_2 - y_1)(\rho s_1 / s_2 - 1)}{1 + s_1^2 / s_2^2 - 2\rho s_1 / s_2} \tag{3.5}$$

when

$$\rho s_2 / s_1 > 1 \quad \text{or} \quad \rho s_1 / s_2 > 1 \tag{3.6}$$

it can be separately obtained that

$$y_e < y_1 \qquad \text{or} \qquad y_e > y_2 \tag{3.7}$$

There exists divergence of views on the above results. Some evaluators insist that the correlation between the two measurements is determined by the condition that there must exist some common factors (common sample or common neutron resource etc.) shared by both micro–measuring experiment systems, and from this viewpoints, it can inferred that the condition (3.6) can never be realized. However, from our experience, those conditions on the measurement correlation are too strong, although sharing common factors between the two measurements leads to correlation, this is only a special case, more generally, if there exist correlative factors in the two micro–measuring experiment systems (e. g. samples made from the same company or apparatus calibrated to the same standard etc.), this will bring about the correlation between the two measurements, and the former is only an extreme case of our latter one. From our viewpoints, we have found that the condition (3.6) can be realized, and there no special limitation on these equations.

Physically, if there exists positive correlation between the measured values, they will tend to appear at the same side of the true value. When the correlation is weak, the statistical errors dominate, and the combination–mean can still stay between y_1 and y_2. With the increase of the correlation, the correlative errors begin to prevail, and it becomes reasonable for the combination–mean to stay out of the range (y_1, y_2). Though there are two sides of the range, it is rational to deduce that the datum with smaller errors should more approach the genuine value, so this combination–mean is reasonable.

3.2 Three Dimension Case

For three dimension case, it is very difficult to discuss the effect of the correlation analytically. Here the effects of the correlation to the combination–mean is discussed numerically. The following three groups of data are taken for calculation:

$$y_1 \pm s_1 = 995.0 \pm 8.0$$
$$y_2 \pm s_2 = 1000.0 \pm 5.0$$
$$y_3 \pm s_3 = 1005.0 \pm 10.0$$

The effect of the correlation to the combination–mean is shown in Fig. 2 and

Fig. 3.

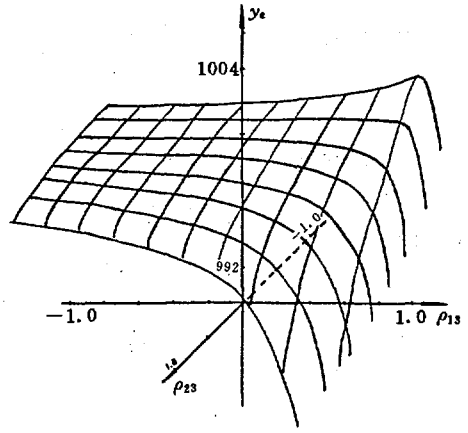

Fig. 2 Effects of correlation in three dimensional data case ($\rho_{12} = -0.2$)

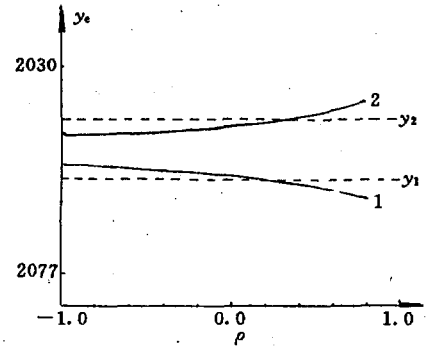

Fig. 3 Effects of correlation in three dimensional data case ($\rho_{12} = 0.6$)

From the calculation, it can be concluded:

1) Given a smaller ρ_{12} (−0.2 as in Fig. 2), when ρ_{23} approaches 0.0, ρ_{13} affects the combination–mean in the same way as that of the two dimension case; when ρ_{23} becomes large, the effect of ρ_{13} to the combination–mean shows some difference with that of the two dimension case, this is induced by the fact that this resultant combination–mean is now determined by both ρ_{13} and ρ_{23}, not only by ρ_{13}.

2) Given a larger ρ_{12}, (0.6 as in Fig. 3), no matter what value ρ_{23} may be, the effect of ρ_{13} to the combination–mean shows less resemblance of the two dimensional data cases as that when ρ_{12} is small, this difference is mainly contributed by the strong correlation of ρ_{12}, and the combination is no longer determined by one correlation, but by the three correlation comprehensively.

References

[1] Liu Tingjin et al., Nuclear Technique (in Chinese), 10, 7(1986)

[2] Yung An Chao, Nucl. Sci. & Eng., 72, 1, 1(1979), Yung An Chao, Nucl. Sci., & Eng., 75, 1, 60(1980)

[3] F. G. Perey, Conf. on Neutron Phys. & Nucl. Data, Harwell, p. 104(1978)

Uncertainty Files for Neutron Cross Sections and Elastic Angular Scattering Distributions on ^{56}Fe

Zhao Zhixiang Liu Tong

(Chinese Nuclear Data Center, IAE)

Introduction

The covariance information of nuclear data for structural material Fe is significant in neutronics calculation for fusion reactors. Based on a consistent theory calculation by means of UNF code[1], a evaluation of neutron induced reaction data on ^{56}Fe, including cross section, angular distribution, double differential cross section and gamma ray production data, has been completed. The evaluations on covariance files for the data above are going on and some of the evaluation methods and results are reported in this paper.

1 Evaluation Method

In present work, five methods are used to evaluate the uncertainty files for cross sections and angular distributions.

1.1 Group Averaging

For the reaction with plenty of measured cross section data,group averaging is used to generate the covariance matrix of cross sections.Firstly, the covariance matrix of measured data is carefully evaluated.Then, according to incident energy, the measured data are divided into different energy bin. In each bin, there are at least one measured data.The least squares methods is used to give the averaged cross section vector G and its covariance matrix V_G as follows:

$$G = (F^T V^{-1} F)^{-1} F^T V^{-1} G^* \tag{1}$$

$$V_G = (F^T V^{-1} F)^{-1} \tag{2}$$

where averaged cross section vector G and measured data vector G^* are defined by

$$G = (g_1 \ g_2 \ \cdots \ g_m)^T \tag{3}$$

$$G^* = \begin{bmatrix} g_1^* \\ g_2^* \\ \cdots \\ g_m^* \end{bmatrix} \tag{4}$$

where g_i and g_i^* represent the averaged cross section to be determined and measured data vector in i–th energy bin, respectively, and

$$g_i^* = (g_i^*(1) \ g_i^*(2) \ \cdots \ g_i^*(K_i))^T \tag{5}$$

The matrix V denotes ($N \times N$) covariance matrix of measured data vector G^*,

$$N = \sum_{i=1}^{m} K_i \tag{6}$$

and F is so–called sensitivity matrix

$$F = \begin{bmatrix} E_1 & O & \cdots & O \\ O & E_2 & \cdots & O \\ \cdots & \cdots & \cdots & \cdots \\ O & O & \cdots & E_m \end{bmatrix} \tag{7}$$

where O is null matrix and E_i consists of K_i units

$$E_i = (1 \quad 1 \quad \cdots \quad 1)^T \tag{8}$$

In the procedure above, what we are interested is only V_G not G. In fact, evaluated cross sections are given by least squares fitting or by UNF calculation

to make sure smooth cross section obtained.

1.2 Least Squares Fitting

This method is only used to generate the covariance matrix of Legendre coefficients for elastic scattering angular distributions.

1.3 Based on Differences among Several Evaluated Libraries

For many reaction channels, there is no or only few measured data available. In these cases, a method suggested by Vonach[2] is used to generate the covariance matrix for these cross sections. The basic idea of this method was described by Vonach[2].

For ^{56}Fe, four evaluations, including ENDF/B–6, JENDL–3, BROND–2 and this work, are used to carry out the comparison. It is found that the differences among these evaluations are generally systematical, especially for inelastic cross sections of discrete levels. So correlation function suggested by Vonach is not used in this work. Defined relative difference by

$$\delta_j^i(E_n) = (\sigma_0^i(E_n) - \sigma_j^i(E_n)) / \sigma_0^i(E_n) \tag{9}$$

where i denotes the type of cross section and j characters a given evaluation. The subscript 0 represents this evaluation. The covariance file for σ_0^i is estimated based on the magnitude of δ^i in LB=1 sub–subsection and the energy grid is determined according to the change of the sign of δ^i. In this work, the evaluation with the maximum δ is removed, so the "bands" defined by the maximum and minimum of other three evaluations is considered having 68% confidence level.

1.4 Bayesian Approach

For several reaction cross sections, the evaluation given by other evaluator is adopted in this work. In this case, the uncertainty files given by the original authors are also adopted. Of course, if updating is done with newly measured data by means of Bayesian approach, GLUCS code[3] could be used to give updated cross sections and its covariance file.

1.5 Internal and External Errors

So–called "internal error" of evaluated cross sections is estimated by analysing experimental error of the measured data used in the evaluation, especially for long–range component. And "external error" is estimated based on scatter of measured data around the evaluated one. The larger one between internal and external errors is adopted in this work.

2 Results

2.1 Total, Inelastic to First Excited Level and Capture Cross Sections

Evaluated cross sections of ENDF / B–6 are adopted in this evaluation. So uncertainty files of ENDF / B–6 for these cross sections are also adopted.

2.2 Elastic and Non–elastic Cross Sections

"NC type" sub–subsections are used based on the following relations:

$$\sigma_{non} = \sigma_{inl} + \sigma_{n2n} + \sigma_{np} + \sigma_{n\alpha} + \sigma_{nd} + \sigma_{nt} + \sigma_{nnp} + \sigma_{nn\alpha} + \sigma_{n\gamma} \quad (10)$$

$$\sigma_{el} = \sigma_{t} - \sigma_{non} \quad (11)$$

2.3 Inelastic Cross Sections

For total inelastic cross sections (MT = 4), uncertainty file is given based on the differences among four evaluations.

For the cross sections of discrete (MT = 52 ~ 75) and continuum levels (MT = 91), uncertainty files are mainly given based on the differences among four evaluations. But for 10 discrete levels, the contribution from direct interaction is taken into account by means of a DWUCK calculation. For these levels, the contribution from direct interaction is dominant above 10 MeV and uncertainties of cross sections above 10 MeV are derived from the uncertainties of the deformed parameters used in DWUCK calculation.

2.4 (n,2n) Cross Section

The uncertainties of (n,2n) cross sections are obtained based on the experimental error of the data available below 15 MeV, and above 15 MeV based on differences among four evaluations after normalized to our evaluation.

2.5 (n,nα) Cross Section

No measured data is available so the uncertainties for this cross section are obtained based on differences among four evaluations.

2.6 (n,np), (n,d) and (n,t) Cross Sections

Only few measured data are available for these cross sections:

$\sigma_{nd} = 8 \pm 3$ mb at 14.8 MeV (Grimes et al.[4])

$\sigma_{nt} = 45 \pm 12$ μb at 14.6 MeV (Qaim et al.,[5])

and by subtracting σ_{np} of this work from the proton emission cross section measured by Grimes[4]:

$$\sigma_{nnp} = 68 \pm 22 \text{ mb at } 14.8 \text{ MeV}$$

Our evaluation is consistent with data above very well. The errors of these measured data are taken as long–range components. The short range components are obtained based on differences among four evaluations after normalized other three evaluations to ours.

2.7 (n,p) Cross Section

Group averaging method is used to obtained covariance matrix for (n,p) cross sections. The correlations among different data sets due to the use of same reference cross sections and decay data are considered.

2.8 (n,α) Cross Section

The covariance matrix for (n,α) cross sections is obtained based on the differences among four evaluations.

2.9 Legendre Coefficients of Elastic Angular Distribution

By means of least square code SPF[6], covariance matrix for Legendre coefficients of elastic scattering angular distributions are obtained. The covariance matrix only for a_1, a_2, a_3 and a_4 is got although the order of fitting Legendre polynomial could be up to 20 for obtaining good fitting. It seems to be needed to do further investigation on impact of this truncation.

3 Concluding Remark

The comparisons between our results and other evaluations for uncertainty files are carried out. Usually, the agreements is good in the case of plenty measured data available as a basis of the evaluation. ^{56}Fe(n,p) cross section is a typical example. Otherwise, uncertainty files given by different evaluators by means of different methods have large discrepancies.

References

[1] Zhang Jinshang, Nucl. Sci. & Eng., 114, 55(1993)

[2] H. Vonach, S. Tagesen, M. Wagner and A. Pavlik, EFF–DOC–85, 1992

[3] D. M. Hetrick and C. Y. Fu, ORNL / TM–7341, 1980

[4] R. C. Haight and S. M. Grimes, BNL–NCS–51245, Vol. I, p. 245, 1980

[5] S. M. Qaim and G. Stoecklin, Nucl. Phys., A257, 233, 1976

[6] Zhang Jin, private communication

Some Problems on Covariance Evaluation

— A Letter to a Foreign Colleague

Zhou Delin

1 Probability of Confidence of the Covariance Evaluations

1.1 Is it needed to give the probability of confidence and / or the meaning explicitly of the various covariance matrices given and generated by the various evaluators? Actually, different covariance will be given by different evaluators even based on the same body of experimental data and their uncertainty information. For example, could we say that some covariances generated by the evaluators subjectively are actually "the uncertainty of one measurement" or roughly the so–called "forecast error"? We may notice that in a simplest case of one parameter evaluation for example, " the forecast error" will be approximately $\sqrt{N}$ times larger than the uncertainty of the average of N independent measurements with equal weight for this parameter. We may also find that for some evaluations the uncertainties given by some evaluators are 2

or 3 times the standard deviation, for example, 2 or 3 times the covariances obtained by using the least squares or Bayesian approach, but by some other evaluators, these covariances are adopted directly for the evaluations.

Obviously, in any case, the complete experimental covariance information is always vital to the data and covariance evaluation subjectively or objectively. It seems to be also necessary to have a position in the format to indicate that what do the evaluated covariances mean, if we couldn't have a standard way to estimate the covariances for the evaluations.

1.2 How About the Confidence Interval of a Model Theory Predictions?

For model theory calculation, perhaps there are two ways to estimate the uncertainties (covariance) of the parameters then via error propagation to estimate the covariance of the predictions:

(i) From the covariance of the measured data via error propagation via fitting the calculation to the measured data (multi–measurement usually). In this case, the consistency (the "external error") of the data set should be checked and considered.

(ii) From systematics of the parameters

For these two cases, considering the model dependence of the parameters, it seems to be more reasonable to adopt the "forecast error" for the parameters to be used to estimate the covariance of model theory predictions.

1.3 Confidence Region of Curve Fitting

We may also notice that some problems exist in the confidence of an evaluated excitation function obtained from a curve fitting with some polynomials by using least squares or Bayesian approach. In this case the confidence region of the "fitted curve" depends on the number of parameters. So it seems to be necessary to give the "number of parameters" in the format explicitly. Or should we avoid combining the multi–measurement of an excitation function with mathematical polynomials (except Legendre polynomials for angular distribution) as far as possible? Especially, we should notice that it will be difficult to obtain an objective combination strictly for the multi–measurement of multi–parameter via curve fitting with some mathematical polynomials.

2 Format for the Experimental Evaluation Results of the Data and Covariance for the Files of Particle and γ Emission Concerned

The data and covariance of angle and energy distribution of particle emission as well as the gamma production data are usually obtained by model theory calculation fitting the measured data mainly around 14 MeV. But the data around 14 MeV are also most important for use. It will be valuable to adopt the experimental evaluation including covariance evaluation for this and other possible energies (e. g., around 9 and 18 MeV) in the data files. We have tried to generate the covariances of DDX(cosx,E') for the reactions related to neutron emission, i. e., (n,2n), (n,n'), (n,np) and (n,nα) reactions. The only experimental data available for experimental evaluation are the DDX of neutron emission. In these data, neutrons emitted from four reactions are included. Fitting the measured DDX(cosx,E') with Legendre polynomials by using Bayesian approach, the model theory calculation results of the $F_l(E')$ coefficients for DDX(cosx,E') for various reactions are adopted as a prior parameters, then the posterior parameters are obtained. For convenient, the fittings are carried out in L. S. and in equidistant E'. Generally speaking, the $F_l(E')$'s for various reactions are correlated. Fortunately, in most cases, the DDX data are dominated by (n,2n) (at low energy part) or by (n,n') (at high energy part) reaction only.

A comprehensive (simultaneous) evaluations of the reaction cross sections at these energies have also been carried out. For the large size of the DDX data of particles emission, it is difficult to include them to the simultaneous evaluations. The correlations among the cross sections of the main reactions will exist.

Then, how about the format to adopt these experimental evaluation results of the data and covariance at 14 MeV and other energies in the files? Or these data can only be used as a reference, or a check, or a "benchmark" for model theory calculation?

3 Could We Generate an " External Covariance" for a Multi–Parameter Evaluation from Multi–Measurement?

Obviously it is valuable to have an "external covariance" for the combination of multi–measurement of multi–parameter, just like the "external error" for the single parameter estimation. But how to estimate it?

A simple way is: to estimate the external variance for the parameters X and Y separately and suppose that the " external ρ" between X and Y is the same as the "internal ρ". It should be more reasonable to estimate the variances from measured data χ^*, y^* directely (i. e., the sum of $\sum(x_i^* - \hat{x})^2 / N(N-1)$ and $\sum(y_i^* - \hat{y})^2 / N(N-1)$) and to

estimate the covariance from the smoothed measured data x_s, y_s (i. e., the sum of $\sum(x_{si} - \hat{x}) (y_{si} - \hat{y}) / N(N-1)$).

4 Constant ρ or Constant Relative Correlated Error?

For simplifying the combination of correlative data, in many cases it seems to be more reasonable and more feasible to adopt a constant relative correlated error than that to adopt a constant ρ for generating the covariance matrix for multi–parameter measurements.

Actually, in the covariance generation for EDX evaluation for example, the larger uncertainties at large output energy (E') region of the measured data most probably come from larger uncorrelated error, but not correlated error. Actually, in the EDX evaluation for structural material, it will be difficult to avoid PPP in the combination of derived quantities to suppose a constant ρ.

CINDA INDEX

Nuclide	Quantity	Energy (eV)		Lab	Type	Documentation			
		Min	Max			Ref	Vol	Page	Date
^{16}O	(n,x)	5.0+6	2.0+7	ZHN	Theo	Jour CNDP	10	28	Dec 93
^{54}Fe	(d,α)	6.4+6	1.6+7	NRS	Expt	Jour CNDP	10	1	Dec 93
	(d,2n)	8.9+6	1.6+7	NRS	Expt	Jour CNDP	10	1	Dec 93
^{56}Fe	(p,n)	5.4+6	1.2+9	AEP	Eval	Jour CNDP	10	60	Dec 93
^{58}Ni	(d,α)	5.4+6	1.5+7	NRS	Expt	Jour CNDP	10	1	Dec 93
	(d,αn)	5.4+6	1.5+7	NRS	Expt	Jour CNDP	10	1	Dec 93
	(d,x)	5.4+6	1.5+7	NRS	Expt	Jour CNDP	10	1	Dec 93
	(n,α)		5.1+6	BJG	Expt	Jour CNDP	10	14	Dec 93
^{63}Cu	(p,n)	4.2+6	1.2+10	AEP	Eval	Jour CNDP	10	60	Dec 93
^{65}Cu	(p,n)	2.2+6	1.8+9	AEP	Eval	Jour CNDP	10	60	Dec 93
^{180}Hf	(n,2n)	8.0+6	2.0+7	AEP	Eval	Jour CNDP	10	85	Dec 93
^{181}Ta	(n,2n)	7.7+6	2.4+7	AEP	Eval	Jour CNDP	10	78	Dec 93
^{182}W	(d,2n)	1.0+7	1.6+7	NRS	Expt	Jour CNDP	10	1	Dec 93
^{184}W	(d,2n)	7.7+6	1.6+7	NRS	Expt	Jour CNDP	10	1	Dec 93
^{186}W	(d,p)	6.3+6	1.6+7	NRS	Expt	Jour CNDP	10	1	Dec 93
	(d,2n)	7.0+6	1.6+7	NRS	Expt	Jour CNDP	10	1	Dec 93
^{189}W	(d,2n)	8.4+6	1.6+7	NRS	Expt	Jour CNDP	10	1	Dec 93
^{235}U	Evaluation	1.0−5	2.0+7	AEP	Eval	Jour CNDP	10	75	Dec 93
^{238}U	Evaluation	1.0−5	2.0+7	BJG	Eval	Jour CNDP	10	71	Dec 93

Author, Comments
Liu Jianfeng+, SIG, DA, DE
Tao Zhenlan+, GE-LI, ACTIV, SIG
Tao Zhenlan+, GE-LI, ACTIV, SIG
Zhuang Youxiang, SIG
Tao Zhenlan+, GE-LI, ACTIV, SIG
Tao Zhenlan+, GE-LI, ACTIV, SIG
Tao Zhenlan+, GE-LI, ACTIV, SIG
Tang Guoyou+, DA
Zhuang Youxiang, SIG
Zhuang Youxiang, SIG
Zhao Zhixiang, SIG
Cai Dunjiu+, SIG
Tao Zhenlan+, GE-LI, ACTIV, SIG
Tao Zhenlan+, GE-LI, ACTIV, SIG
Tao Zhenlan+, GE-LI, ACTIV, SIG
Tao Zhenlan+, GE-LI, ACTIV, SIG
Tao Zhenlan+, GE-LI, ACTIV, SIG
Yu Baosheng+, FOR CENDL-2
Tang Guoyou+, FOR CENDL-2

核 数 据 进 展 通 讯（第 10 期）
原子能出版社出版
（北京 2108 信箱）
中国核数据中心排版
核科学技术情报研究所印刷
☆
开本 787×1092 1/16 · 印张 15 · 字数 130 千字
1993 年 12 月北京第一版 · 1993 年 12 月北京第一次印刷
ISBN 7－5022－1096－2
TL · 670

COMMUNICATION OF NUCLEAR DATA PROGRESS

ISBN 7-5022-1096-2
TL · 670